RICE UNIVERSITY

The $Ca^{40}(p,\gamma)Sc^{41}$ Reaction

by

Dave Harper Youngblood

A THESIS SUBMITTED
IN PARTIAL FULFILLMENT OF THE
REQUIREMENTS FOR THE DEGREE OF

DOCTOR OF PHILOSOPHY

Thesis Director's signature:

G. M. Glass

Houston, Texas

May 1965

TABLE OF CONTENTS

INTRODUCTION

The nuclei Ca^{41} and Sc^{41}, formed by the addition of one nucleon to the doubly magic nucleus Ca^{40}, have been the subject of much investigation in the recent past. On first examination these nuclei might be thought describable as a single nucleon in various excited levels outside of the tightly bound core. The levels expected are the $p_{3/2}$, $p_{1/2}$, $f_{5/2}$ and $d_{5/2}$ orbitals. However these nuclei depart very much from this simple picture as shown by the investigations of their energy levels through the $Ca^{40}(d,p)Ca^{41}$ reaction[1] and $Ca^{40}(p,p)Ca^{40}$[2] which revealed approximately 100 states below 6 MeV. Of these only 2 carry any substantial fraction of the single particle strength. To account for this large number of levels requires consideration of the possible states available by excitations of the core. While the $Ca^{40}(p,p)Ca^{40}$ and $Ca^{40}(d,p)Ca^{41}$ reactions make possible ℓ value assignments, J value assignments needed to determine the origin of the states are not possible.

In order to locate new levels in Sc^{41} not seen in $Ca^{40}(p,p)Ca^{40}$ due to low penetrability, particularly for higher ℓ values, and to gain information about the states observed in the (p,p), the $Ca^{40}(p,\gamma)Sc^{41}$ reaction was studied. In studying this reaction we have chosen to investigate only those capture resonances which are characterized by gamma decay directly to the $f_{7/2}$ ground state. These states should be those formed by protons of angular momentum $\ell \geq 2$. Lower ℓ's are unlikely due to the high gamma ray multipolarity required for transitions to the ground state. Since gamma decay is competing with much faster

particle emission, states characterized by small proton widths would be expected to be observed in this experiment.

From an experimental point of view also there are several features which make an investigation of this type appealing. Only a single value of channel spin, 1/2, is possible, simplifying analysis procedures greatly and removing some possible ambiguities in determinations of spins and parities of levels formed in Sc^{41}. Furthermore, at proton energies of 3.43, 3.82, and 4.00 MeV, inelastic scattering, leaving Ca^{40} in its 3.35, 3.73, and 3.90 MeV excited states is energetically possible, but does not occur noticeably for about 1 MeV about the thresholds and then only weakly. No other competing processes can occur below 5.3 Mev where the $Ca^{40}(p,\alpha\gamma)K^{37}$ reaction becomes possible.

The $Ca^{40}(p,\gamma)Sc^{41}$ reaction has been observed only twice previously. Once by W. M. Martin[3] who bombarded Ca^{40} with 25 MeV protons for a half life measurement of the Sc^{41} beta decay, and by J. W. Butler[4], who obtained an excitation function from 600 keV to 1900 keV observing four states attributable to Sc^{41}. In the present work the radiative capture of protons by Ca^{40} has been investigated in two stages. The first stage consisted of the location of levels in the range of bombarding energy between 600 keV and 5.2 MeV (corresponding to a range of excitation in Sc^{41} from 1.7 to 6.0 MeV) by measuring the positron activity of Sc^{41}. Since all excited states of Sc^{41} are proton unstable, the occurrence of this activity can be taken as the signature of those capture states having transitions directly to the ground state. Forty-six resonances found in the excitation function were identified with states of Sc^{41} by

measuring the associated β spectra. $g\Gamma_{\gamma g.s.}$ for these states was determined, assuming negligible population of the ground state via cascading through intermediate excited states. In the second stage of this investigation, the angular distributions of the gamma decay of 16 capture resonances located below E_p = 4.1 MeV to the $f_{7/2}$ ground state of Sc^{41} were measured. This permitted J assignments to 8 of the states, and limited the range of possible J values on the others.

A comparison of these results with the $Ca^{40}(p,p)Ca^{40}$ results is made. Seventeen levels are observed which are common to both reactions. In addition the strength in the radiative capture channel of corresponding levels may be used to obtain J values on some of the states observed in the elastic scattering measurements. A comparison of levels of the mirror nuclei Sc^{41} and Ca^{41} below an excitation energy of 5 MeV is presented.

Direct capture from continuum states, expected by the most favored transition, E1, was investigated using the techniques necessary for the measurements in the first stage of this experiment. For our specific case capture of ℓ = 2 protons is possible with a subsequent E1 transition to the ground state of Sc^{41}. This capture apparently occurs primarily in the region just outside the nucleus and the cross section depends on the magnitude of the Sc^{41} ground state wave function in this region.

As a direct consequence of the measurements in the first stage of this experiment the lifetime of the $3/2^-$ first excited state, of considerable interest due to its expected single particle character, was determined.

Until about 4 years ago the half life of the positron decay of Sc^{41} was in error by 30% and the mass of Sc^{41} was incorrect by 600 keV. The $Ca^{40}(p, \gamma)Sc^{41}$ reaction provided a unique means of obtaining Sc^{41} positron activity free from contaminants of similar half life and end point energy. Advantage was taken of this to obtain an accurate value for the Sc^{41} half life. The mass of Sc^{41} was also obtained by measuring the Q value for the $Ca^{40}(p, \gamma)Sc^{41}$ reaction at two of the stronger low lying capture states.

CHAPTER I

Location of Resonances, Determination of $g\Gamma_\gamma$ and Γ

1. Introduction

The study of the $Ca^{40}(p, \gamma)Sc^{41}$ reaction was made using the 5.5 MeV Van de Graaff accelerator of the Bonner Nuclear Laboratories. The measurements were carried out in the range of bombarding energies from 0.60 to 5.2 MeV. In order to enhance the sensitivity for detecting weak capture resonances, advantage was taken of the fact that Sc^{41} is radioactive, decaying with a half life of 0.6 seconds by the emission of positrons of 5.5 MeV maximum energy. The positrons were detected with high efficiency by employing a plastic scintillator subtending a solid angle of approximately 2π. Because of the high energy of the positrons, this radiation was detected with a minimum of interference from extraneous activities produced by target contaminants. Furthermore the beta activity was counted only while the beam was electrostatically deflected off the target to avoid prompt radiation. Further reduction of background was achieved by detecting the positrons with two nested plastic scintillators operating in coincidence. The beta detector was designed to serve also as a spectrometer of low resolving power, so that an energy spectrum of the beta radiation could be taken at each capture resonance. In this manner the identification of each resonance with a state in Sc^{41} could be confirmed. Absolute positron yields for each resonance were obtained after measuring the efficiency of the beta detector. The integrated cross sections and the radiative widths, aside

from a statistical factor, for the direct ground state transitions were determined. Contributions to the positron yield from cascade processes were expected to be negligible for most of the states, since all excited states of Sc^{41} are above the threshold for proton emission. Thus each gamma transition in a cascade is competing with much faster particle emission.

2. Experimental Apparatus and Procedure

The target chamber used in the measurements was located 5 meters from the 90° analyzing magnet of the accelerator. The beam path through the analyzing magnet was defined by tantalum slits at the entrance and exit of the magnet, and by the slits used for the regulation of the accelerator voltage located 3 meters from the output of the magnet. Upon suitable adjustment of these slits, a beam spread of .03% of the beam energy was achieved, and the beam energy could be reproduced to within approximately 1 keV during a given run.

a. Target Chamber

Due to the sensitivity of this experiment to the presence of contaminants in the target, especially the affinity of calcium for oxygen, an evaporation "in place" was necessary to avoid exposure of the target to the atmosphere during transfer from an evaporator.

The design of the target chamber is shown in Figure 1. The chamber is made of a brass cylinder of 3" inner diameter and 8" long and is joined to the beam tube so that its axis is vertical. These dimensions were chosen for the chamber so that it could accommodate retractable evaporation electrodes. The target was located at the end of a 1" O.D. lead-lined aluminum tube, into which the beam entered after traversing the chamber. The tube was insulated from the rest of the system by a polyethelyne insulator to allow integration of the beam flux. The target was located in this manner to accommodate the use of a high efficiency detector to be described later. A screw-on cap pressed the target

FIGURE 1

Schematic of chamber, detectors, and beam tube arrangement. At top, left, the evaporator (E) positioned for evaporation is seen through the window (W) of the chamber. The target extension tube (T) is insulated from the rest of the system by a polyethylene insulator (I). At top, right, the detectors (A) are shown in normal operating position with respect to the target. At bottom, the beam deflection and slit system is shown. Note that the beam tube is tilted slightly so that only deflected beam reaches the target. The undeflected beam is caught on the top of the slit (S_c). S_E are the regulating slits, D the deflector plates, Q a viewing quartz, P an oil diffusion pump, S_1, S_2, S_3 collimating slits and T is the target.

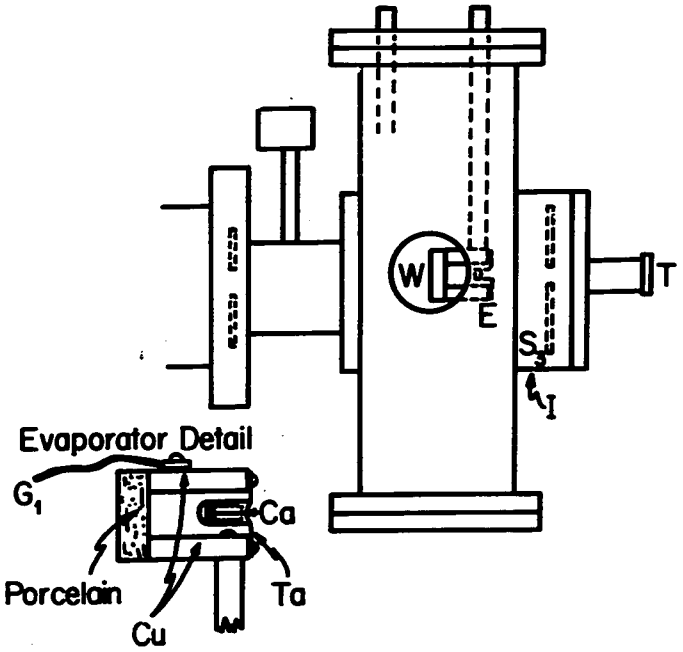
W
E
T
S
I
Evaporator Detail
G1
Ca
Porcelain
Ta
Cu

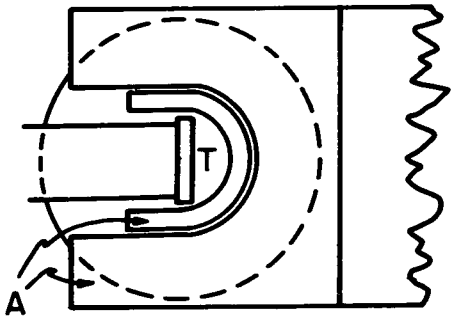
T
A

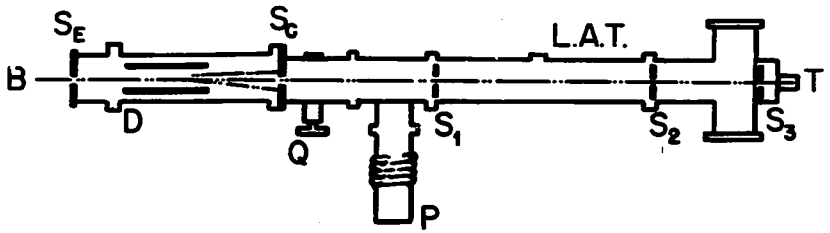
SE
SC
L.A.T.
B
T
D
Q
S1
S2
S3
P

backing (in the form of a 3/4" disc of 2 ml. gold) against a silicone "O" ring serving as a vacuum seal at the back of the target holder. The target backing stopped the protons, but transmitted the positrons with negligible energy loss.

Immediately before entering the chamber the beam passed through a section of the beam tube 30" long encased in a liquid nitrogen bath which served to reduce build up of contaminants on the target. The system was pumped by an oil diffusion pump placed before the liquid air trap.

The arrangement of the deflector plates, beam catching and defining slits are shown in Figure 1. The size and path of the beam after passing through the regulation slits was determined by additional sets of slits placed after the deflector plates. The beam tube after the deflector plates was tilted and the beam deflected slightly at all times to prevent any neutral beam from striking the target.

b. Target Preparation

Targets were prepared in situ by evaporation of 99.5% pure calcium metal onto 100 mg/cm^2 thick gold blanks located in the end of the target holder. The calcium metal, in lump form, was scraped to remove surface oxidation before placement in the evaporators. The evaporators, made from 5 mil tantalum, were shaped so that the evaporated calcium was deposited primarily on the surfaces in the forward direction. An evaporator is shown schematically in Figure 1. The retractable rod on which they were mounted served as one of the conductors, while a bus wire to the chamber side served as the other conductor. The progress of the

evaporation could be observed through the glass viewing port and the lucite end plate.

Provision was made for two evaporators, placed 2 cm. apart, in order to prepare targets of varying thickness. While in the retracted position, the evaporators were outgassed by evaporating a small amount of calcium. The evaporator was then positioned in front of the target and the target thickness controlled by the length of evaporation time and the number of evaporators used. Using this procedure calcium targets varying in thickness up to 50 keV at 1.84 MeV were produced. Targets prepared in this manner had an oxygen content of less than 2%, as determined by a proton elastic scattering measurement to be discussed later.

c. The Detection System

The beta radiation from the source was detected by a set of nested plastic scintillators arranged as shown in Figure 1, to subtend a solid angle at the target approaching 2π steradians. Positrons having an energy of about 5.5 MeV - corresponding to the endpoint energy of the Sc^{41} spectrum - sustained an energy loss of 900 keV in traversing the thin forward detector, and were absorbed by the thick detector behind. The thin detector, machined from Pilot B, is a portion of a cylinder 4" high with an inside diameter of 7/8" and a wall thickness of 3/16". The thick detector, a 3" cylinder of Pilot B, then "wraps around" the thin detector and is of sufficient thickness to stop 5.5 MeV betas and may be used to obtain low resolution energy spectra of the detected betas.

Each scintillator is optically coupled to Dumont 6363 phototubes selected for high signal to noise ratio. This was of special importance for the thin detector due to the low light output expected.

The outputs of the detectors, after suitable amplification and pulse height selection were routed into Cosmic model 901 coincidence equipment set to operate at a resolving time of 60 nanoseconds. Parallel outputs, after amplification, were routed into the two inputs of a Nuclear Data 1024 channel analyzer operating in the multiplex mode and gated by the coincidence output. In this manner pulse height information about the signals in coincidence from the different detectors is stored in different portions of the memory. A block diagram of the electronics is shown in Figure 2.

Crude beta spectra taken on each resonance were compared with a Sc^{41} spectrum stored in the other half of the memory in order to identify the resonance with a state in Sc^{41}. The energy calibration of the spectrometer was carried out utilizing the method outlined by Cramer[5] for a spectrometer of a similar type, using both the end point energies of beta calibration spectra and the high energy edge of compton recoil electron spectra given by gamma ray sources. Figure 3 shows the pulse height spectrum obtained in both detectors from a Sc^{41} source, the beta spectrum in the thick detector for a Ce^{144}-Pr^{144} source (E^{β}_{max} = 2.98MeV), and a typical spectrum taken at high bombarding energy where a contaminant beta (attributed to Al^{25}, E^{β}_{max} = 3.25 MeV) is observed superimposed on the Sc^{41} spectrum. Also shown in the figure is the delay curve for the coincidence apparatus, with the region of operation indicated.

FIGURE 2

Block diagram of electronics for positron measurements.

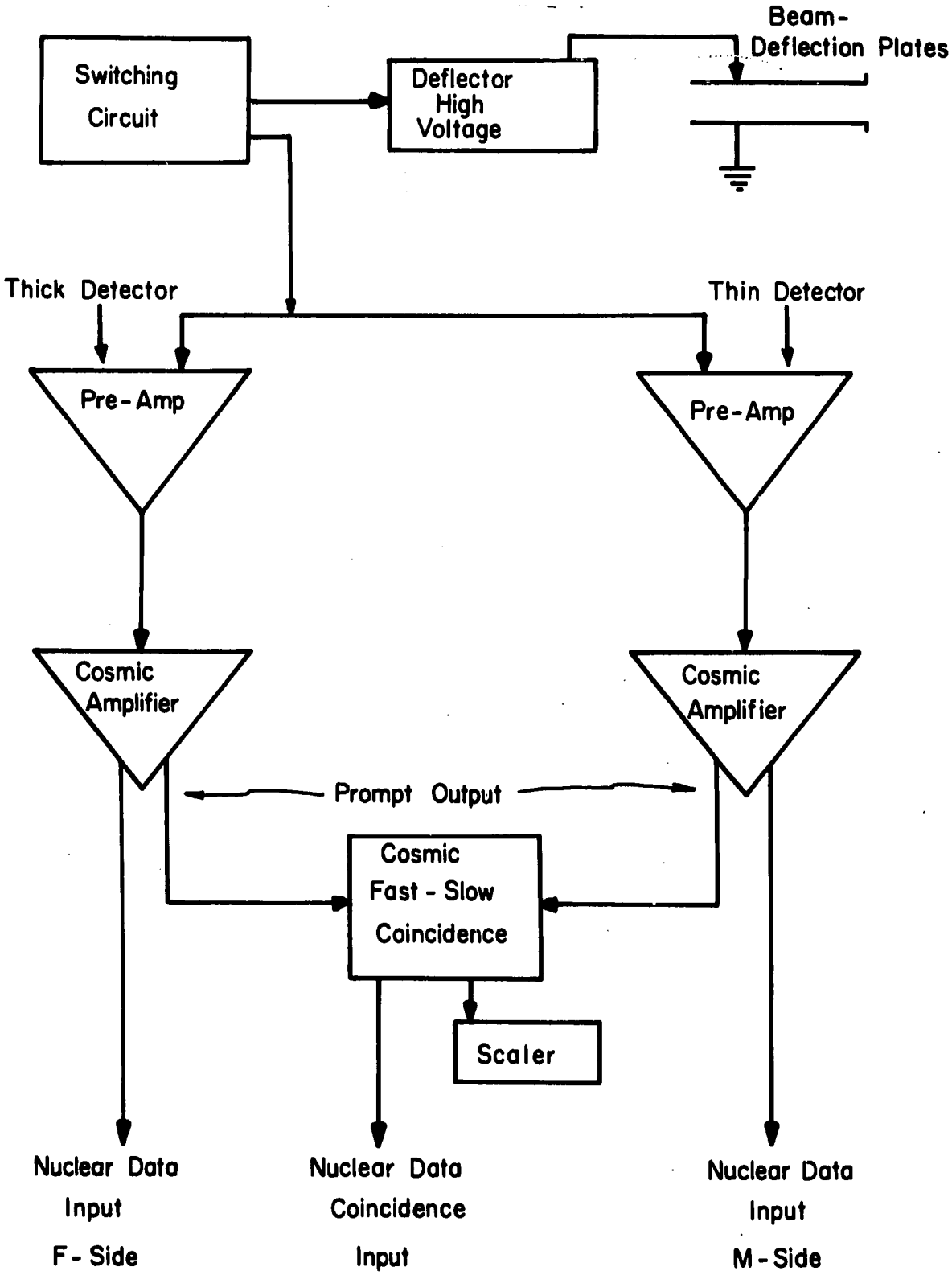
Beam-
Deflection Plates
Switching
Circuit
Deflector
High
Voltage
Thick Detector
Thin Detector
Pre-Amp
Pre-Amp
Cosmic
Amplifier
Cosmic
Amplifier
Prompt Output
Cosmic
Fast - Slow
Coincidence
Scaler
Nuclear Data
Input
F - Side
Nuclear Data
Coincidence
Input
Nuclear Data
Input
M - Side

FIGURE 3

Top: A Sc^{41} coincidence spectrum for both detectors is shown. The window positions indicated are typical.

Bottom, left: A delay curve measured with the Sc^{41} positrons is shown.

Bottom, right: A spectrum taken at higher bombarding energies where a contaminant beta crept into the window is shown.

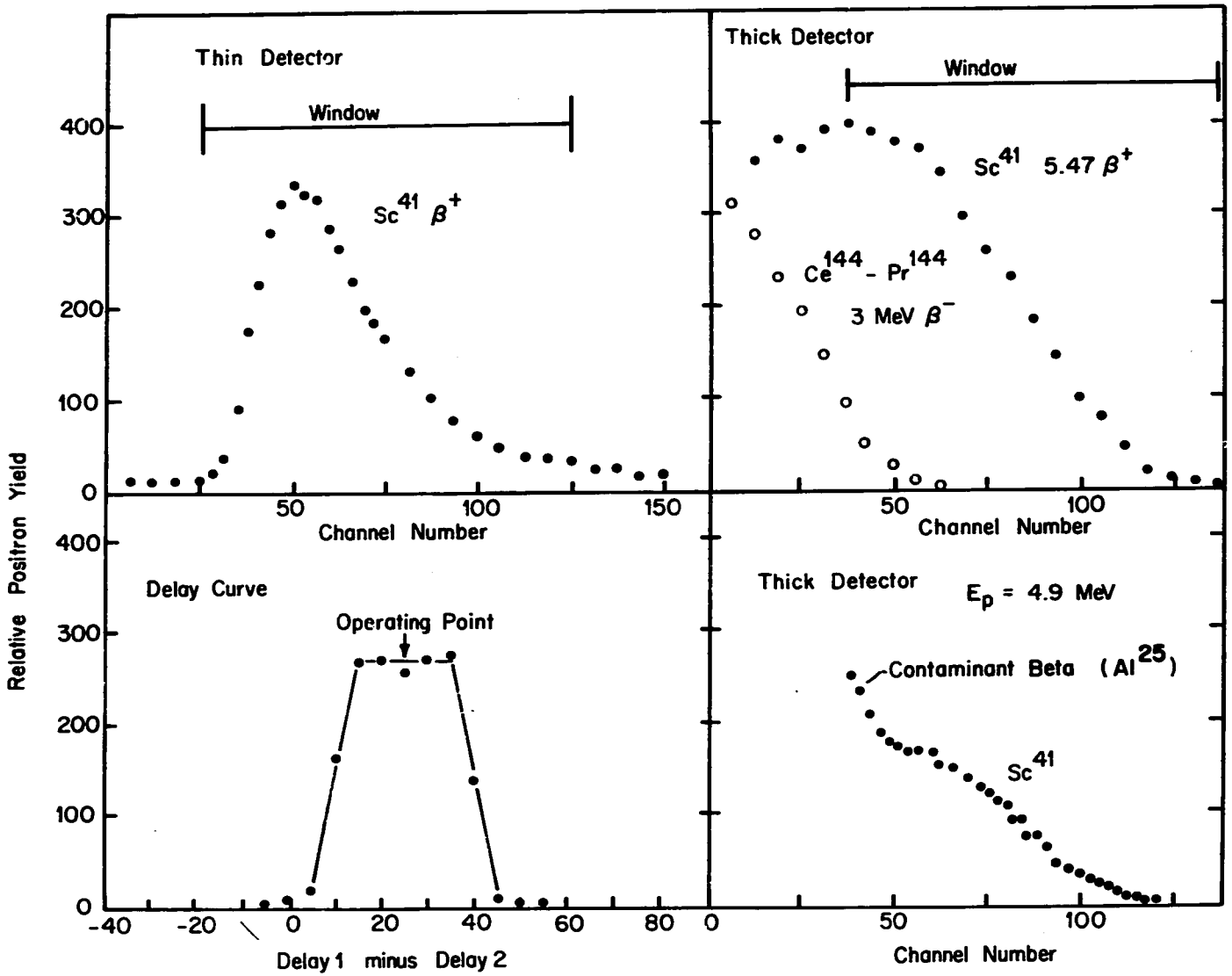
Thin Detector
Window
Sc41 β+
Thick Detector
Window
Sc41 5.47 β+
Ce144 - Pr144
3 MeV β−
Relative Positron Yield
Channel Number
Delay Curve
Operating Point
Delay 1 minus Delay 2
Thick Detector
Ep = 4.9 MeV
Contaminant Beta (Al25)
Sc41
Channel Number

Optimum signal to noise was obtained by setting pulse height windows to pass to the coincidence circuit from the thick detector only pulses corresponding to betas leaving the target with between 1.5 and 5.5 MeV, and from the thin detector those pulses lying in the immediate neighborhood of the peak in the distribution. A continuous monitor of the window settings was maintained with the Nuclear Data 1024 channel analyzer. The output pulses from the coincidence circuit were counted on a scaler for a fixed amount of beam charge collected to obtain the positron yield curves.

d. The Beam Pulsing

As already mentioned, measurements of the positron flux were made while the beam was deflected off the target. The phasing of beam current on target with respect to the counting intervals is illustrated in the figure below which diagrams the over-all cycle of operation.

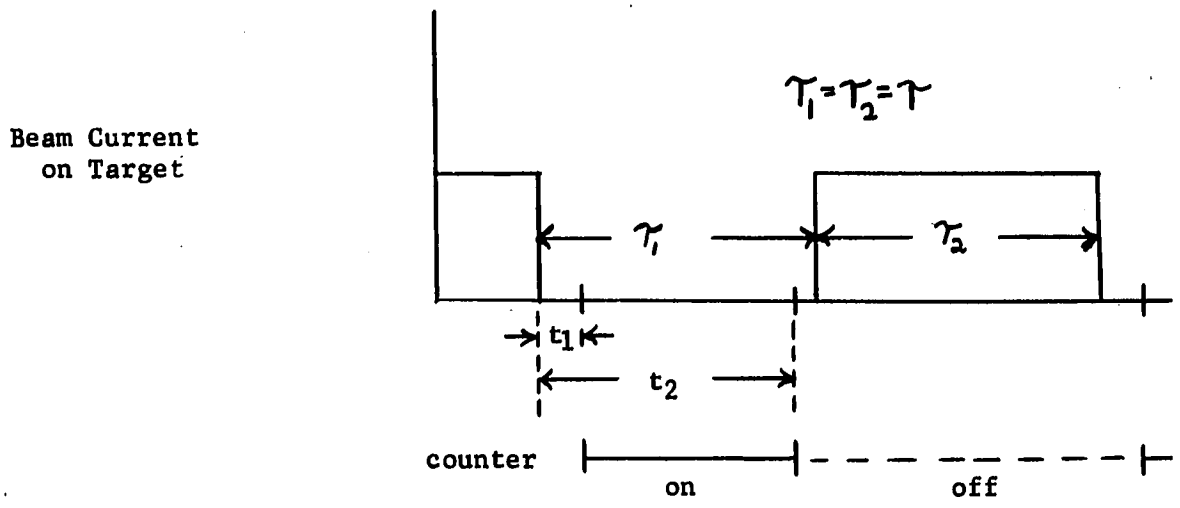

The detectors were turned on at a time t_1 after the beam was deflected off the target and turned off at a time (t_2-t_1) later, before the beam was back on the target. The pulsing period of the beam, 2τ, was about 200 milliseconds in the present work, chosen to maximize the observed yield of positrons for a given data accumulation period. The time t_1 was about 5 milliseconds and (t_2-t_1) was adjusted so that the counter was turned on about 2 milliseconds before the beam again struck the target. While the beam was on the target, the counter was paralyzed by applying a negative voltage to the focusing electrode of the photomultiplier tubes[6] on a signal from the switching circuit. When operating with a pulsed beam, corrections to account for the nuclei decaying while the detectors are turned off must be made to determine absolute beta flux. This is of importance only for the absolute calibration of the detector system, to be described later. Other measurements involved only relative yields and thus only the stability of each of the above-mentioned periods was of importance.

In order to determine the absolute beta flux, the total number of Sc^{41} nuclei decaying must be obtained from the observed yield. The relation between the number of Sc^{41} nuclei formed (N_f) and the number of betas observed (Y_{obs}) is given by[7]:

$$N_f = \frac{\tau\lambda(1-e^{-2\lambda\tau})\, f(\Omega,\varepsilon)\, Y_{obs}}{(1-e^{-\lambda\tau})(e^{-\lambda t_1}-e^{-\lambda t_2})}$$

where λ is the decay constant of the Sc^{41} radiation, and $f(\Omega, \varepsilon)$ is the efficiency function determined as described later.

e. Switching Circuit

A block diagram of the beam pulsing electronics is shown in Figure 2. All components are standard except the switching unit. The switching unit supplies the control signals to switch the high voltage which deflects the beam and to control the detectors. The unit consists of a transistorized pulser designed especially for this application where maximum stability in all timing functions is required.

The circuit diagram is shown in Figure 4. Basically the pulser consists of a 2-transistor multivibrator which provides the basic switching signal to pulse the beam. The pulsing period (2τ) is controlled by R_1 and the symmetry (τ_2/τ_1) by R_2. This is followed by a one-shot multivibrator whose time constant, adjustable by R_3, determines the length of time the beam is off before the detectors are turned on (t_1). This in turn triggers a second one-shot whose time constant, adjustable by R_4, determines the length of time the detectors are on (t_2-t_1). The power supply for the pulser is regulated with a zener diode in a conventional manner. The beam and detector switching signals are sent through transistor squaring circuits and then into tubes to obtain proper voltage for driving the appropriate systems. The high voltage power supply, switch tube, and photomultiplier preamplifiers are as described by Cramer[5].

FIGURE 4

Circuit diagram of switching circuit.

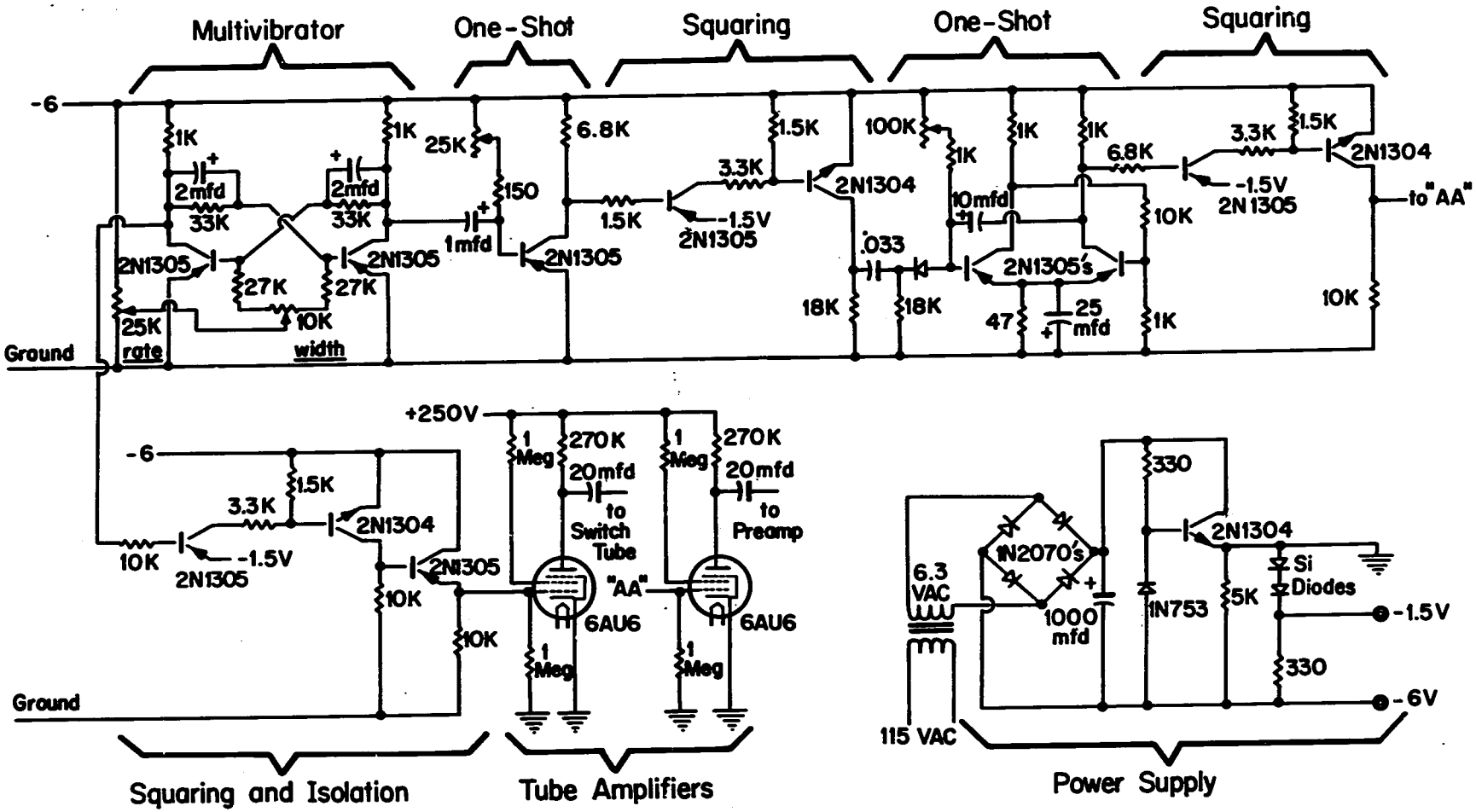
Multivibrator
One-Shot
Squaring
One-Shot
Squaring
-6
1K
2mfd
33K
2N1305
27K
25K
rate
10K
width
1K
2mfd
33K
2N1305
27K
Ground
25K
150
1mfd
6.8K
1.5K
2N1305
3.3K
1.5K
2N1304
-1.5V
2N1305
100K
1K
10mfd
.033
2N1305's
18K
18K
47
25
mfd
1K
1K
6.8K
10K
3.3K
1.5K
2N1304
-1.5V
2N1305
to "AA"
10K
-6
1.5K
3.3K
2N1304
10K
-1.5V
2N1305
2N1305
10K
10K
Ground
+250V
1
Meg
270K
20mfd
to
Switch
Tube
"AA"
6AU6
1
Meg
1
Meg
270K
20mfd
to
Preamp
6AU6
1
Meg
330
2N1304
6.3
VAC
1N2070's
1000
mfd
1N753
5K
Si
Diodes
-1.5V
330
-6V
115 VAC
Squaring and Isolation
Tube Amplifiers
Power Supply

The values τ, t_2, t_1, needed accurately for the determination of the absolute efficiency of the detector system, to be discussed later in this paper, were measured by counting pulses from a 100 kc crystal controlled pulse source gated by the appropriate signals. The values obtained were τ = 105.36±.26 ms, t_1 = 5.37±.03 ms, t_2 = 97.74±.49 ms with the uncertainty attributable to drifts in the apparatus over a period of 4 days. For all measurements other than the absolute calibration, only the stability of the pulser was important.

f. Calibration of the Proton Energy Scale

The proton bombarding energy was determined from the frequency of a nuclear magnetic resonance magnetometer having its probe located in the field of the 90° analyzing magnet of the accelerator[8]. The frequency scale of the magnetometer was calibrated in terms of energy by measuring the thresholds for the reactions[9]

$$Li^7(p,n)Be^7,\ E_{thr} = 1.8807 \pm 0.0004\ \text{MeV},$$

and

$$C^{13}(p,n)N^{13},\ E_{thr} = 3.2358 \pm 0.0011\ \text{MeV}.$$

Freshly prepared targets of Li^7 and C^{13} were used. The threshold frequencies were determined using standard experimental procedures[10]. Repeated determinations of these frequencies for the two reactions fell, during a given run, within a frequency interval corresponding to ±0.5 keV.

In addition a value of 4.238 ± .004 MeV was observed for the $F^{19}(p,n)$ threshold agreeing within the combined errors with the accepted value of 4.233 ± .003 MeV. Other measurements at this laboratory have been in wide disagreement about magnet saturation effects for proton energy determinations in the region from 4 to 5 MeV, but all show it to be less than 5 keV at 5 MeV, and thus the effect was ignored. The energies of 5 prominent resonance spaced over the energy range investigated were then carefully determined to serve as secondary energy standards for future runs.

g. Detector Calibration

In order to determine the integrated cross sections, and hence radiative widths of the states of Sc^{41} observed with the $Ca^{40}(p,\gamma)Sc^{41}$ reaction, the absolute yield of positrons must be known. Thus the efficiency of the beta detector system must be determined for the Sc^{41} beta source. This was done in a separate series of measurements.

Strong sources of isolated Sc^{41} activity suitable for use in an absolute calibration measurement cannot be made. As a practicable alternative, the calibration was carried out with a source of F^{20} activity. Sources of this activity yielding a high flux of betas could easily be made by means of the $F^{19}(d,p)F^{20}$ reaction, free of interference by betas from extraneous sources decaying with similar half lives and end point energies. The end point energy (5.41 MeV) is very near to that of Sc^{41}. This latter fact has the importance that although it is a β^- rather than a β^+, only small corrections to the results are necessary to make then applicable to the case of Sc^{41}. The procedure followed

in the calibration was as follows:

1.) The total flux of betas from a F^{20} source produced by a (d,p) reaction was determined by measuring the yield of betas with a beta spectrometer subtending a known solid angle at the source. This measurement yielded the total number of betas emitted per unit charge delivered to the target for a given deuteron bombarding energy and target thickness for well defined conditions of measurement.

2.) The coincidence beta spectrometer was then positioned at a convenient distance from the source and the yield of betas measured under conditions otherwise identical to (1) except that the beam current was reduced by a factor of 100 to avoid counting rate dependent gain shifts. Appropriate bias levels were set so that only electrons with energies greater than 3 MeV were detected. For these bias conditions the number of counts obtained per unit charge, when compared to the total flux determined in (1) per unit charge, leads to the counter efficiency for detecting F^{20} betas.

3.) The fluorine target was removed from the chamber and replaced by a thick calcium target, the counter position remaining unchanged. A $Ca^{40}(p,\gamma)Sc^{41}$ resonance, chosen for its high yield and isolation in energy was then run and its yield compared to (2) for a calibration of the efficiency for detecting the Sc^{41} positrons. This resonance served subsequently as the standard of reference, in terms of which absolute yields of the other resonances were determined. Corrections to this calibration were made to take into account the slight difference in energy of the Sc^{41} decay, and the fact that positrons were emitted.

These steps in the calibration procedure will now be discussed in greater detail.

The calibration of the F^{20} source was carried out using a well-collimated large volume, plastic scintillator beta spectrometer, which was designed specifically for applications involving short-lived high energy beta emitters produced in situ by bombarding suitable target materials. The spectrometer has been discussed fully elsewhere[5], but briefly described it consists of a cylinder of plastic-organic scintillator 7.5 cm. in diameter and 9 cm. long, joined to a Dumont type 6363 photomultiplier tube. The scintillator, located 30 cm. from the target and subtending a solid angle of about 10^{-2} steradians, is shielded from all betas except those admitted through an entrance aperture by a housing made of aluminum and lead. The accepted beam of betas is restricted to a narrow cone coaxial with the scintillator to insure that virtually the total energy of the incident particles is absorbed within the scintillator. Spectra are recorded with a multichannel pulse-height analyzer which is calibrated in terms of energy by means of the end points of several known beta spectra and the edges of Compton recoil electron distributions from standard gamma rays. The relationship between pulse-height and energy is linear up to 13 MeV, and end point energies can be measured to an accuracy of 1-2%.

The source of F^{20} was produced by bombarding a PbF_2 target with 2 MeV deuterons. The target was evaporated on a gold foil 100 mg/cm^2 thick and mounted at the end of the beam tube about 30 cm. from the spectrometer. A pulsed beam technique as described earlier was used for this measurement.

The calibration of the source was accomplished by measuring the yield of F^{20} betas in the solid angle defined by the spectrometer for a given charge of deuterons delivered to the target. The spectrum of F^{20} betas was accumulated in 256 channels of a Nuclear data 1024 channel analyzer. Below an electron energy of 2 MeV the spectrum was distorted by the 1.6 MeV gamma ray associated with the beta decay.

A second spectrum, taken immediately after the first but with a polyethylene plug inserted in the collimator of the spectrometer in order to stop the betas was utilized as a background spectrum.

A 2" NaI crystal scintillation spectrometer placed at 90° to the beam direction served to interrelate the yield of the 1.6 MeV gamma ray for the primary and background spectra. This spectrum was accumulated in the 2nd quarter of the memory of the analyzer. Polyethylene absorbers of the same thickness were placed in front of both detectors for the background measurement to equalize the gamma attenuation. Calibration of the F^{20} source consists of determining the total number of betas per unit charge emitted by the source, from the knowledge of the number counted for the solid angle subtended by the spectrometer. Ordinarily the number emitted could be obtained by directly integrating the experimental spectrum. However in this case the portion of the spectrum below 2 MeV was distorted by imperfect subtraction of the 1.6 MeV gamma ray associated with the F^{20} beta decay. Accordingly, the following procedure was used to determine the total flux of betas from the information contained in the undistorted part of the spectrum.

A fermi plot of the data in the region of the spectrum above 3 MeV was made by plotting $(N(E)/f(Z,E))^{1/2}$ versus E where N(E) is the number of electrons measured at energy E and f(Z,E) is the tabulated fermi function. A straight line, least square fitted to the data points is shown in Figure 5 and can be represented by the equation:

$$(N(E)/f(Z,E))^{1/2} = k(E-E_o)$$

where E_o is the end point energy of the spectrum. The value of E_o obtained in this way, 5.4 MeV, is in satisfactory agreement with other determinations. The constant, k, also given by the fit may then be used to obtain the number of betas emitted by integrating the theoretical spectrum[11]:

$$Y = \int_o^{E_o} N(E)\, dE = k^2 \int_o^{E_o} f(Z,E)\, (E-E_o)^2\, dE$$

The yield thus obtained is uncertain to about $\pm 7\%$ due to variations in k possible by fitting different regions of the spectrum, as well as changing the energy calibration of the spectrometer within reasonable limits. The uncertainty due to this procedure is the largest of any in this measurement. The experimental F^{20} spectrum, as well as that calculated using the value of k obtained as above is shown in Figure 5.

The fermi function, f(Z,E), used for the calculations was obtained from the NBS "Tables for the Analysis of Beta Spectra"[11]*.

* This function, defined on page 21 of the NBS tables[16], is multiplied here by $e/\hbar$ to make it appropriate for energy rather than momentum distributions.

FIGURE 5

Top: Fermi plot of F^{20} spectrum taken during calibration with least square fit.

Bottom: F^{20} beta spectrum with the spectrum calculated using k obtained from the Fermi plot shown.

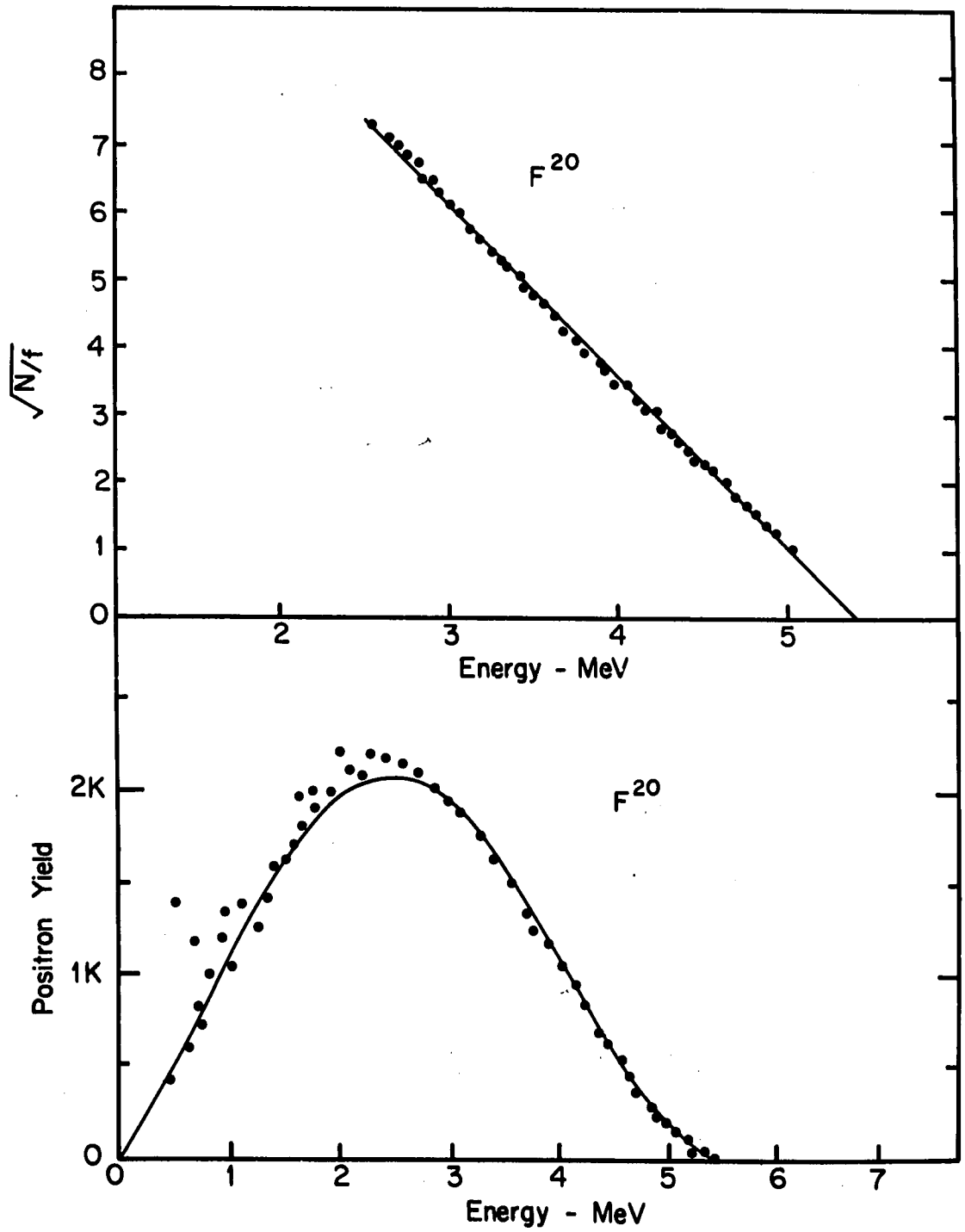
8
7
6
5
4
3
2
1
0
$\sqrt{N_{/f}}$
F^{20}
2
3
4
5
Energy - MeV
2K
1K
0
Positron Yield
F^{20}
0
1
2
3
4
5
6
7
Energy - MeV

Assuming isotropy of emission of the betas, the total yield after correction for the dead time of the analyzer (.7%) was obtained by dividing the yield obtained above by the fraction of 4π steradians subtended by the spectrometer.

A possibly important correction might ensue if the backscattering of betas by the 100 mg/cm^2 gold target backing were a large effect. Due to the high energy of the betas (3.0 to 5.5 MeV) in the region used for the yield determination, this is expected to be small. However the effect was studied by obtaining F^{20} beta spectra both with and without an additional 100 mg/cm^2 gold foil mounted on the source facing the detector. After correcting the energies for losses due to the additional thickness of gold, it was found that the attenuation of the beta yield by the insertion of this additional foil was less than 1% for betas between 3 and 5 MeV. No correction was made for this effect.

The F^{20} source, thus calibrated, was then used to determine the efficiency of the coincidence detectors utilized for the Sc^{41} measurements. The detector was retracted 3 cm. from the normal position in order to reduce gain shifts due to the large counting rates obtained with this source. The yield per unit charge of F^{20} beta measured with the coincidence detectors did not change when the beam current delivered to the target was varied a factor of 30.

Pulse height windows were set on both detectors, and the gain stabilized against changes in counting rate to be encountered by placing a Cs^{137} gamma ray source to establish a counting rate in both detectors much greater than that to be encountered during the measurement. The

energy scale was of importance only for the secondary corrections necessary to obtain the efficiency for Sc^{41} positrons from that measured for F^{20} electrons.

To obtain the efficiency of the detector system for Sc^{41} positrons a correction to the above had to be made due to the different character of the spectrum for positrons and electrons, caused by opposite coulomb effects near the nucleus, and for the 60 keV difference in end point energy. A third factor is the effective shift of the Sc^{41} spectrum up in energy due to occasional capture in the spectrometer of one of the positron annihilation quanta. The value of the latter correction (82 keV) obtained by Cramer[5] for his spectrometer, similar in size to this, was used here.

In order to correct for the difference in the F^{20} and Sc^{41} beta energy distributions, the assumption was made that the efficiency of the detector was the same for both F^{20} and Sc^{41} betas emanating from the target with such energy as to be detected within the region of the pulse height window. The window permitted detection of an electron leaving the target with an energy between 3.1 MeV and 5.7 MeV, or a positron between 3.0 MeV and 5.6 MeV.

Thirty-one per cent of the F^{20} electrons and 35% of the Sc^{41} positrons are emitted from the target with an energy in the detectable range. The total efficiency of the detector for Sc^{41} positrons is then a factor of 1.13 greater than for the F^{20} electrons. The efficiency ($f(\Omega,\varepsilon)$) for Sc^{41} betas emitted was 3.5%. When operating in the normal manner the efficiency is about 14%. The difference is due

to both the positioning of the detector with respect to the target and a lower setting of the pulse height window for the thick detector, set at a higher energy here to eliminate interference from the 1.6 MeV gamma ray associated with the F^{20} decay. The errors in the measurement are summarized in Table 1.

Immediately after the experimental determination of $f(\Omega,\varepsilon)$ as described above, a 40 keV thick calcium target was made in the target chamber and the plateau yield of the 1.842 MeV state was determined to serve as a secondary calibration for future runs.

The measured yield, 5.802/microcoulomb (Y_{obs}, Page (12)) is multiplied by the beam pulsing correction (2.28) determined as described earlier, and corrected by $f(\Omega,\varepsilon)$. The total yield of positrons for this resonance is 388.6 $\pm$ 71.2/microcoulomb.

TABLE 1

Uncertainties in Calibration Due to:

Beam Pulsing Correction	0.5%
Window Setting	0.5%
Solid Angle	2.5%
Integrator	3.0%
Statistics	2.1%
Backscatter	1.0%
k from Fermi fit	7.0%

3. Experimental Results

The data were taken in two distinct phases. In phase one the positron yield as a function of proton energy was measured using a thin target in order to locate the resonances and determine approximately their relative yields. In phase two thick targets were used to determine accurately the energies of the resonances, their radiative widths for the ground state transitions, and in a few cases their total widths.

a. Thin Target Measurements

The thin target (3-10 keV) excitation function, shown in Figure 6, was taken during 4 separate periods on the accelerator, which were needed to cover the entire range of energy. In each period, new data overlapping part of the region previously covered confirmed the reproduceability of the data from the previous run. The data presented here were taken after initial surveys of the entire energy region were completed to reveal the gross features of the data. For the present measurements the energy dispersion of the beam was approximately .03% of the beam energy, and the resonance energies were reproducible to ± 2 keV. The energy scale of the figure was obtained from the energies of the resonances calibrated as secondary standards.

Forty-six resonances in the region of bombarding energy between .60 and 5.20 MeV are attributed to Sc^{41} on the basis of the beta spectra recorded concurrently with the measurement of the excitation function. Beta spectra taken during the thick target yield measurements, to be

FIGURE 6

$Ca^{40}(p, \gamma)Sc^{41}$ excitation function. No background has been subtracted.

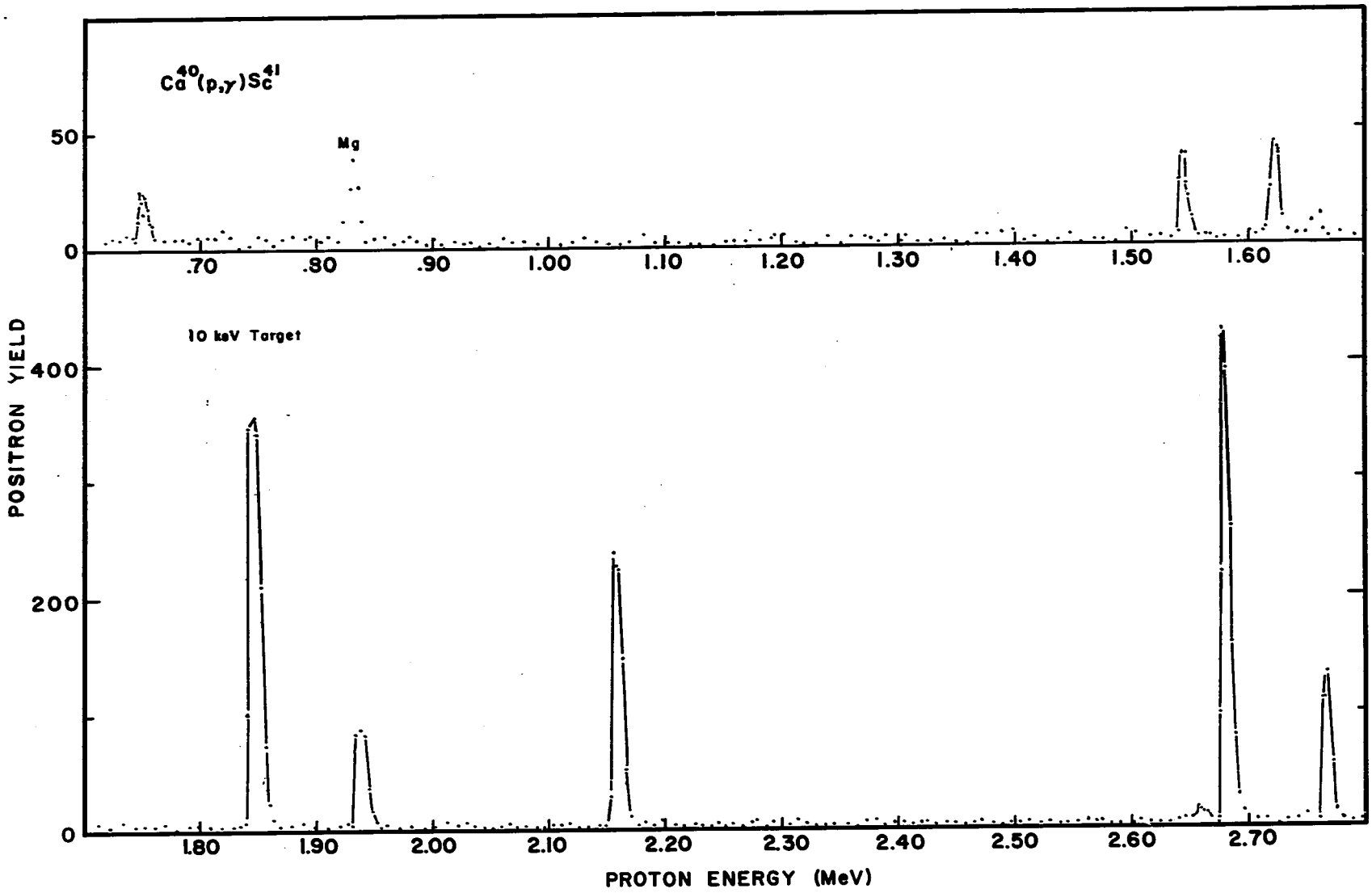
$Ca^{40}(p,\gamma)Sc^{41}$
Mg
10 keV Target
50
0
400
200
0
.70
.80
.90
1.00
1.10
1.20
1.30
1.40
1.50
1.60
1.80
1.90
2.00
2.10
2.20
2.30
2.40
2.50
2.60
2.70
POSITRON YIELD
PROTON ENERGY (MeV)

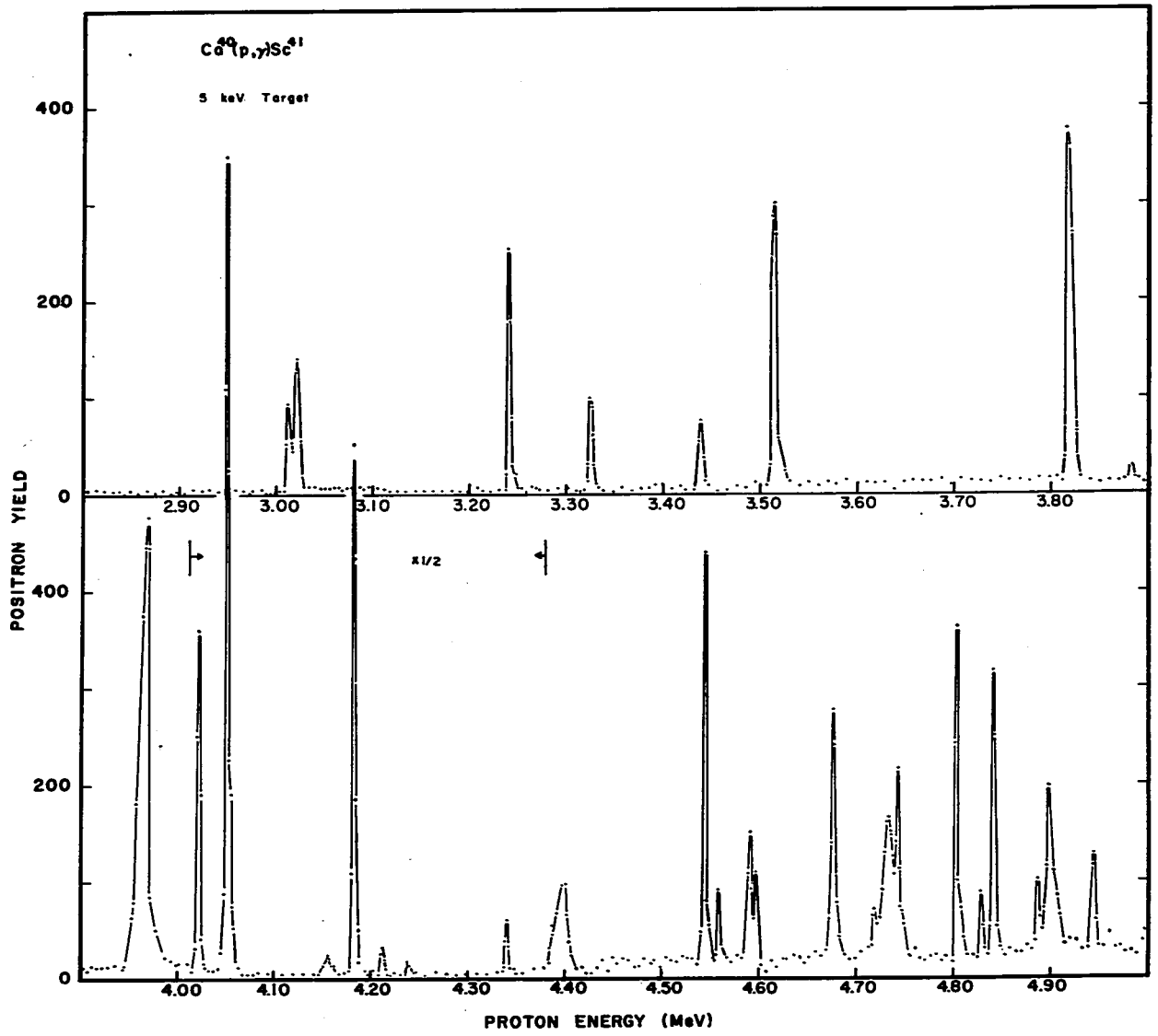
$Ca^{40}(p,\gamma)Sc^{41}$
5 keV Target
400
200
0
2.90
3.00
3.10
3.20
3.30
3.40
3.50
3.60
3.70
3.80
x1/2
400
200
0
4.00
4.10
4.20
4.30
4.40
4.50
4.60
4.70
4.80
4.90
POSITRON YIELD
PROTON ENERGY (MeV)

discussed below, provided additional confirmation. Several weak maxima in the cross section were attributed to target impurities. The resonances attributed to Sc^{41} are listed in Table 2, along with their relative yields obtained from the thick target measurements.

Two contaminants, magnesium and silicon, known to be present on the target, are possible sources of spurious resonances. The radiative capture of protons by Mg^{24} forms Al^{25}, a positron emitter[12] of 3.24 MeV end point and 7.3 sec. half life. Similarly proton capture by Si^{28} forms P^{29}, a positron emitter[12] of 3.95 MeV end point and 4.2 sec. half life. Two resonances observed at bombarding energies of 0.83 and 1.66 MeV in the present measurement, corresponding in energy to two known resonances of the Mg^{24} $(p,\gamma)Al^{25}$ reaction are attributed to this reaction on the basis of the crude beta spectra taken. In the region above E_p = 4.3 MeV betas of end point energy between 2.8 and 3.4 MeV were detected, attributed to Al^{25}, gradually increasing in yield as the bombarding energy increased. Only a few very weak maxima in the yield function were attributable to this source, which otherwise contributed less than half of the total off resonance yield present in this region. A typical spectrum containing both the Sc^{41} positron decay and the Al^{25} decay is shown in Figure 3 presented in the discussion of the detector system.

The remainder of the off resonance yield is attributable to several effects. A room background of 5-10 counts per data point (about 100 seconds) was present at all times with the voltage on both accelerators in the laboratory turned down. No increase in this background was noted with voltage on the terminal of the 5.5 MeV accelerator when the beam

TABLE 2

Levels Observed in $Ca^{40}(p,\gamma)Sc^{41}$

E_p (MeV)	Rel. Yield	Γ (keV)
0.648 ± 0.002	0.021 ± 0.001	
1.540 ± 0.003	0.070 ± 0.002	
1.621 ± 0.003	0.075 ± 0.003	
1.8417± 0.0015	1.0	
1.934 ± 0.003	0.206 ± 0.005	
2.153 ± 0.003	0.644 ± 0.019	
2.658 ± 0.003	0.012 ± 0.002	
2.6766± 0.0020	1.276 ± 0.016	
2.764 ± 0.003	0.342 ± 0.006	
3.010 ± 0.003	0.230 ± 0.007	
3.019 ± 0.004	0.451 ± 0.013	
3.240 ± 0.004	0.666 ± 0.009	
3.325 ± 0.004	0.335 ± 0.006	
3.440 ± 0.004	0.212 ± 0.006	
3.515 ± 0.004	1.050 ± 0.014	
3.8193± 0.0030	1.155 ± 0.014	
3.881 ± 0.006	0.088 ± 0.009	
3.965 ± 0.005	1.120 ± 0.030	2.4 ± 0.6
4.0246 ± 0.0030	2.053 ± 0.041	
4.054 ± 0.007	6.674 ± 0.134	
4.160 ± 0.009	0.04*	
4.1848± 0.0045	3.354 ± 0.167	

TABLE 2 CONTINUED

4.219 ± 0.007	0.169 ± 0.013	
4.244 ± 0.009	0.08*	
4.346 ± 0.007	0.407 ± 0.025	
4.402 ± 0.009	0.853 ± 0.152	9.5 ± 3.0
4.551 ± 0.007	1.537 ± 0.185	
4.564 ± 0.009	0.26*	
4.596 ± 0.009	0.48*	
4.602 ± 0.010	0.33*	
4.683 ± 0.007	0.95*	
4.724 ± 0.010	0.16*	
4.741 ± 0.010	3.66*	11.5 ± 3.0
4.748 ± 0.010	0.55*	
4.812 ± 0.008	2.460 ± 0.246	
4.835 ± 0.008	0.34*	
4.850 ± 0.008	0.944 ± 0.300	
4.894 ± 0.011	0.28*	
4.907 ± 0.011	3.55*	9.4 ± 2.0
4.952 ± 0.011	0.40*	
5.011 ± 0.011	1.05*	4.2 ± 2.0
5.098 ± 0.011	0.61*	3.9 ± 1.0
5.127 ± 0.011	0.15*	
5.154 ± 0.011	0.84*	
5.158 ± 0.011	1.81*	
5.191 ± 0.011	2.16*	

* ± a factor of 2

was deflected and stopped by a gold covered slit at bombarding energies below 4.2 MeV. However, a gradual increase in beam deflected background was noted above this energy, and by E_p = 5 MeV had reached 20-30 counts per data point. An additional background of 10-20 counts per 100 seconds was present when the tandem accelerator at the laboratory was accelerating high energy deuterons. Runs were scheduled only when the tandem was running lower energy protons to avoid this problem. The remainder of the yield present between resonances is attributed on the basis of the crude beta spectra taken to Sc^{41}, and may be due to very weak unresolved resonances or to continuum capture, discussed in a later section.

Maximum proton beam currents of 1-2 μa were utilized for the entire excitation function, with typical data points of 50 microcoulombs of charge delivered to the target. No noticeable target deterioration occurred with beam currents of this magnitude.

b. Thick Target Measurements

For the second phase of the investigation thick targets (20 keV) were used, enabling precise energies to be assigned to the resonances and accurate relative yields to be obtained.

By "thick target" is meant that the thickness of target in energy units is much greater than the intrinsic width of the resonance and the experimental resolution. When this condition is obeyed the yield as a function of energy rises rapidly to a plateau. The extent of the plateau is determined by the target thickness. Ideally the measurements should be carried out with targets of infinite thickness, but this is not practicable. However the yield from a target of finite thickness can be related to that of an infinite target by the following expression[13]:

$$Y_{max}(\xi)/Y_{max}(\infty) = \frac{2}{\pi} \text{Arctan}(\xi/\Gamma')$$

where Γ' is the experimentally observed width of the resonance (including beam spread), $Y_{max}(\xi)$ is the maximum yield obtained for a target of finite thickness, and $Y_{max}(\infty)$ is the thick target plateau yield.

In the region below 4.1 MeV the level density was sufficiently low to permit individual resonances to be resolved with a 30 keV thick target. In this region the correction to the yield necessary to account for the finite target thickness ranged from 1 to 3% for the most part. In the region above 4.1 MeV bombarding energy many resonances could not be resolved with a thick target. Furthermore the non-resonant yield increased in proportion to target thickness whereas the resonant yield did not, obscuring some of the weaker resonances. However, a 13 keV target, used for measurements above 4.1 MeV, permitted semi-thick target data on 7 resonances to be obtained. Corrections to the plateau yield obtained with the 13 keV target varied between 5% and 10%, depending on the observed width of the resonance.

Table 3 lists the different runs necessary to obtain the data over the entire range of energy, the target thicknesses at a proton energy corresponding to the mid-point of the particular region of interest and the energy calibration standards used in each region.

TABLE 3

Data	Energy Region Covered (MeV)	Target Thickness (keV)	Energy Calibration Resonance
3/23/63	1.84 - 4.06	30	1.8417 MeV 2.6766 MeV
9/29/63	3.81 - 4.86	13	3.8193 MeV 4.0246 MeV
10/5/63	4.02 - 5.20	2.5	4.0246 MeV 4.1848 MeV
1/7/64	0.600 -1.94	45	1.8417 MeV

The energies assigned to the resonances correspond to the mid-point of the rise of the thick target yield curve. Corrections to these energies to take into account the Lewis effect* and the lack of an infinite target were negligible with respect to the magnitude of the other uncertainties in the measurement.

---

*The "Lewis effect" was first predicted by H. W. Lewis[14] and later observed by Walters, et al.[15] in the thick target gamma ray yield curve for the $Al^{27}(p,\gamma)Si^{28}$ reaction. This effect is a result of the fact that protons traveling through a target material lose energy in discrete jumps due to collisions with electrons. Protons incident on a thick target with energy greater than the resonance energy of a narrow resonance may jump over the resonance, not contributing to the yield, whereas those incident at the resonant energy all have a chance to react. Thus for narrow resonances the thick target yield curve should show a peak just above the resonance energy. The resonance energy is also shifted slightly from the half maximum yield point.

During a given run, resonance energies repeated to better than 1.0 keV, the shift caused by retuning of the beam. No energy shift attributable to build-up of contaminants was noticed within this limit.

The energies of 5 prominent resonances served as secondary standards used for energy calibration purposes during each run. The energies of these resonances were obtained by careful thick target measurements immediately after calibration of the energy scale of the accelerator as described earlier. The targets were evaporated in situ just prior to measurement and were 10 to 50 keV thick.

The values obtained for the energies of the resonances are:

1.8417 ± 0.0015 MeV

2.6766 ± 0.0020 MeV

3.8193 ± 0.0030 MeV

4.0246 ± 0.0030 MeV

4.1848 ± 0.0045 MeV

The uncertainties listed are attributable to:

1.) The uncertainty in the primary calibration energies

2.) The uncertainty in determining the threshold frequency from the data (± 0.7 keV)

3.) The reproduceability of the threshold frequency due to tuning of the beam (± 0.5 keV) and the uncertainty in the location of the frequency of the resonance due to retuning of the beam (± 5 kc).

The energies of these resonances were determined in this manner on 3 separate occasions. The maximum deviation for the 3 measurements obtained was 1.4 keV for the higher resonances, and 0.8 keV for the lowest resonance. The results presented represent an average of the values obtained in the 3 runs.

Thick target plateau yields of the resonances were obtained and related to absolute positron yield by comparison with the thick target yield obtained for the resonance at 1.842 MeV which had been adopted as the standard of reference. The measurement of the total positron yield per microcoulomb for this resonance was described in Section 2.

Measurements on a few resonances required special procedures described below. In order to obtain a practicable yield during thick target measurements on the weak 648 keV resonance it was necessary to increase the beam current available at the low energy. The control of the accelerator voltage was changed to slits at the exit of the analyzing magnet, so that strong focusing electrostatic lenses could be used to focus all available beam onto the target. Also the beam defining slits were not clamped down for best energy resolution. In this manner peak beam currents of 3 microamperes were available on the target (resulting in an average pulsed beam of 1.5 microamperes), and data points of 200 microcoulombs accumulated charge were taken. When operating in this manner the beam spread measured at 1.84 MeV increased to 0.1% of the beam energy.

The doublet at 3.010 - 3.019 MeV, shown in Figure 7, also required special treatment. The thick target yield of the higher energy resonance

was determined by subtracting the yield of the lower energy resonance from the combined yield of the two states.

For 19 resonances above 4.1 MeV for which satisfactory data could not be obtained with the thick target, the data obtained with a 2.5 keV target, shown in Figure 6, was used to determine the energies and relative yields of the states. Due to the poor determination of the actual resonance maxima with the thin target an additional error of as much as a factor of 2 could be introduced into relative yields obtained in this way. The corrections for target thickness effects to the data obtained with the 2.5 keV target were between 30% and 40%, aside from the few wide states observed. The relative yields for the states are given in Table 2 and have been corrected for target thickness effects.

Total widths for the states could be obtained in only 6 cases, the experimental widths on the others being attributable solely to experimental resolution. For a thick target, the experimental width of the resonance is given by the interquartile distance (Γ') of the lower edge of the resonance curve[13].

A comparison of the rise of the lower edge of the thick target yield curves for the 3.965 MeV resonance and its neighbors at 3.515 and 4.025 MeV is shown in Figure 7. It is seen that the experimental width of the resonances at 3.515 and 4.025 MeV is about 1 keV, consistent with beam spread expected at this energy, whereas that of the 3.965 resonance is 2.5 keV, obviously greater than the other two. The experimental width Γ' is related to the resonance width Γ and the beam dispersion δ by the relation[13,17] $\Gamma'^2=\Gamma^2+\delta^2$. From this expression the actual width may be obtained.

FIGURE 7

Thick target yield curves. Note the exceptional width of the 3.965 MeV resonance, indicated by the slow rise of low energy edge for this resonance.

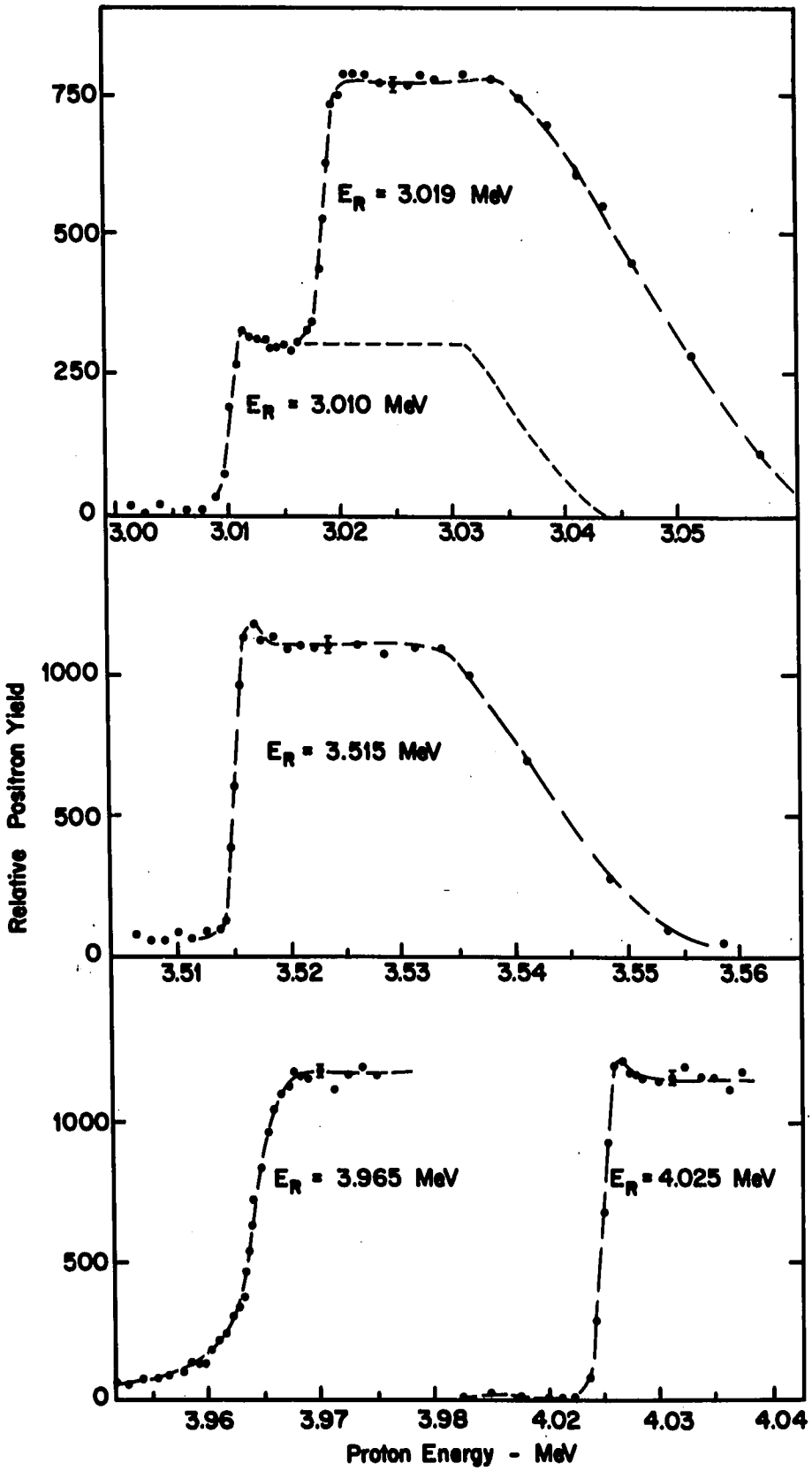
750
500
250
0
E_R = 3.019 MeV
E_R = 3.010 MeV
3.00
3.01
3.02
3.03
3.04
3.05
1000
500
0
E_R = 3.515 MeV
3.51
3.52
3.53
3.54
3.55
3.56
1000
500
0
E_R = 3.965 MeV
E_R = 4.025 MeV
3.96
3.97
3.98
4.02
4.03
4.04
Relative Positron Yield
Proton Energy - MeV

As mentioned earlier a thick target could not be used to study all the resonances above E_p = 4.1 MeV. Of those studied with a thin target, 5 resonances showing widths greater than experimental resolution were observed. These resonance line shapes are presented in Figure 8, along with line shapes of 2 resonances having widths due only to experimental resolution. The experimental width (Γ'') of resonances observed with a thin target may be related to the resonance width Γ, the beam dispersion δ , and the target thickness ξ in the following manner[13,17] $\Gamma''^2 = \Gamma^2 + \delta^2 + \xi^2$. The target thickness was obtained by an average over those resonances for which thick target measurements showed only a width attributable to beam spread. The resonance width, Γ , could then be obtained from the above expression. This method is of course not as sensitive a means for determining resonance widths as that using a thick target.

The four states observed at E_p = .648, 1.540, 1.621 and 1.842 MeV have been found previously by J. W. Butler[4] utilizing this reaction. The first and fourth states were definitely assigned to Sc^{41} on the basis of the gamma ray energy observed, whereas the second and third were only tentatively assigned to this nucleus by him. Both the energies and relative yields obtained by Butler for these states are in agreement with the present results.

FIGURE 8

Thin target (2.5 keV) yield curves for several states. The resonances at the left have a width attributable to experimental resolution only.

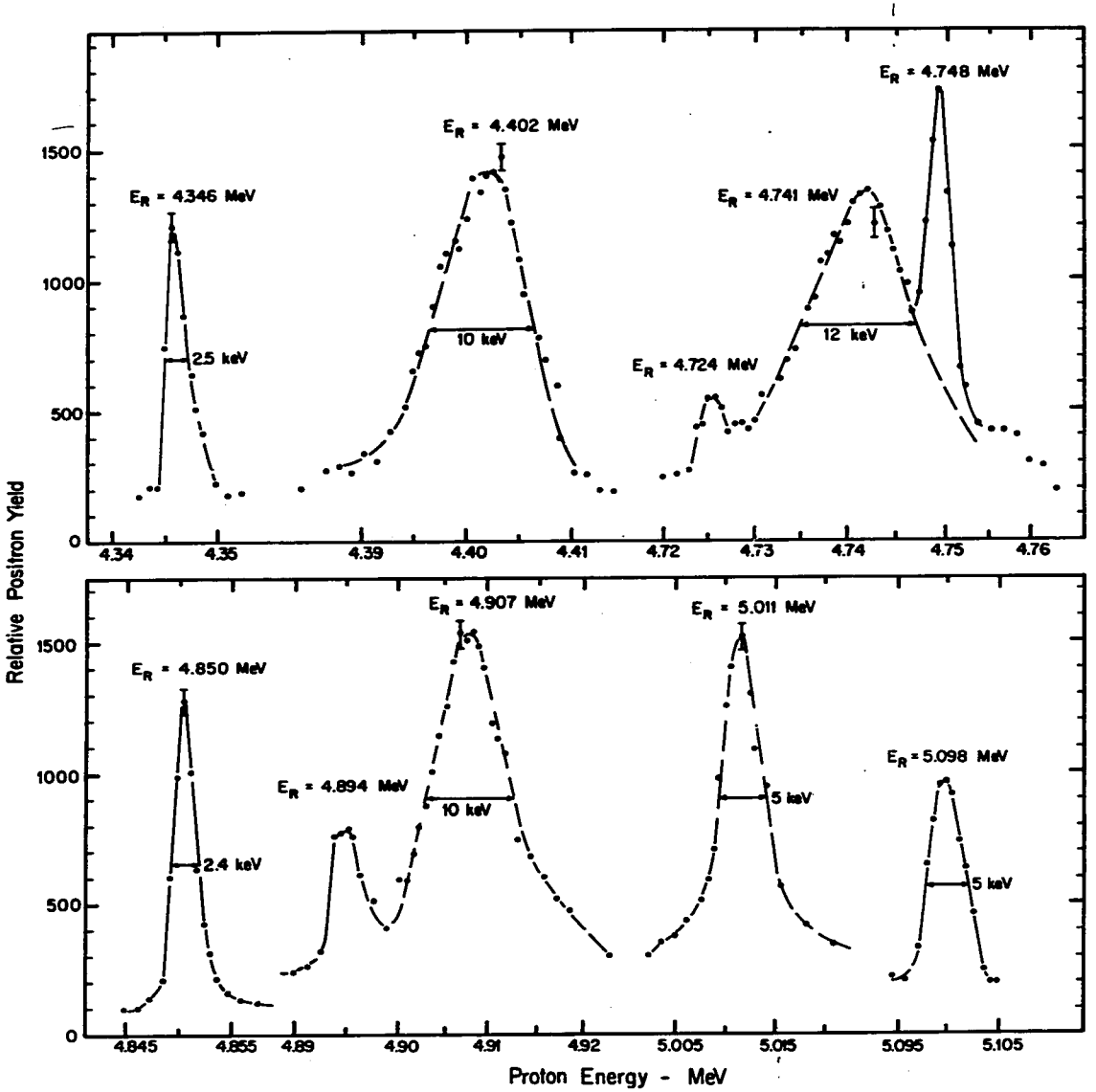
Relative Positron Yield
Proton Energy - MeV
E_R = 4.346 MeV
2.5 keV
E_R = 4.402 MeV
10 keV
E_R = 4.724 MeV
E_R = 4.741 MeV
12 keV
E_R = 4.748 MeV
E_R = 4.850 MeV
2.4 keV
E_R = 4.894 MeV
E_R = 4.907 MeV
10 keV
E_R = 5.011 MeV
5 keV
E_R = 5.098 MeV
5 keV

c. Extraction of Parameters

The integrated cross section for a resonance is obtained as follows[13]:

$$\int \sigma \, dE = \frac{eAS}{N} Y(\infty) = 2\pi^2 g \lambda^2 \Gamma_\gamma \Gamma_p / \Gamma$$

where S = stopping power of target

A = atomic number of the target

$Y(\infty)$ = plateau yield per unit charge

If the assumption is then made that $\Gamma_\gamma \ll \Gamma_p$, the radiative width, apart from a statistical factor, may then be determined by:

$$g\Gamma_\gamma = \frac{1}{2\pi^2 \lambda^2} \int \sigma \, dE$$

where $g = \frac{2J + 1}{(2I + 1)(2S + 1)}$

The absolute yield of positrons per unit charge delivered to the target for a given resonance is obtained from the product of its relative yield and the absolute positron yield of the 1.842 MeV resonance (388.6/microcoulomb), determined during the calibration of the detectors as discussed previously.

The integrated cross sections and radiative widths, aside from the statistical factor, obtained for the states are listed in Table 4. The uncertainties in these quantities are those of the relative yield, plus an uncertainty of 17% contributed by an uncertainty in the detector efficiency function, and 7% contributed by uncertainty in the stopping power of calcium. Also listed is the excitation energy of the level in Sc^{41}, assuming a Q value for the reaction of 1.082 MeV calculated from the tables of Konig, et al[16].

TABLE 4

Resonance Parameters Obtained in $Ca^{40}(p,\gamma)Sc^{41}$

E_p (MeV)	E_{exc} (MeV)	$\int \sigma dE$ (ev-barns)	$g\Gamma_\gamma$ g.s. (ev)
0.648	1.714	0.017	0.0025
1.540	2.584	0.035	0.013
1.621	2.663	0.037	0.014
1.842	2.879	0.450	0.193
1.934	2.969	0.090	0.040
2.153	3.182	0.262	0.131
2.658	3.675	0.004	0.003
2.677	3.692	0.448	0.279
2.764	3.778	0.117	0.075
3.010	4.018	0.092	0.064
3.019	4.027	0.143	0.100
3.240	4.242	0.205	0.154
3.325	4.325	0.101	0.078
3.440	4.437	0.062	0.050
3.515	4.511	0.305	0.249
3.819	4.808	0.316	0.280
3.881	4.868	0.024	0.021
3.965	4.950	0.287	0.265
4.025	5.008	0.541	0.506
4.054	5.036	1.749	1.648
4.160	5.140	0.010	0.010

TABLE 4 CONTINUED

4.185	5.164	0.859	0.836
4.219	5.197	0.043	0.042
4.244	5.222	0.020	0.020
4.346	5.321	0.101	0.102
4.402	5.376	0.211	0.215
4.551	5.521	0.370	0.392
4.564	5.534	0.063	0.066
4.596	5.565	0.115	0.123
4.602	5.571	0.079	0.084
4.683	5.650	0.224	0.244
4.724	5.690	0.038	0.041
4.741	5.706	0.856	0.943
4.748	5.713	0.129	0.142
4.812	5.776	0.569	0.637
4.835	5.798	0.078	0.088
4.850	5.813	0.217	0.245
4.894	5.856	0.064	0.073
4.907	5.868	0.810	0.923
4.952	5.912	0.091	0.104
5.011	5.970	0.236	0.275
5.098	5.055	0.135	0.160
5.127	6.083	0.033	0.039
5.154	6.109	0.185	0.221
5.158	6.113	0.398	0.477
5.191	6.145	0.473	0.570

The integrated cross section and $g\Gamma_\gamma$ obtained represent only that portion of the capture process which results in the formation of the ground state of Sc^{41}. Since all of the excited states of Sc^{41} are unstable to proton emission, gamma decay is competing with much faster particle emission, and a transition to the ground state involving an intermediate state through cascading would be extremely unlikely, since gamma emission would have to compete with particle emission for both radiating states. Thus it is expected that the integrated cross sections obtained above are primarily for direct ground state transitions, with little cascade contribution. Indeed, rough measurements of gamma ray decay intensities made during angular distribution measurements is in agreement with this assumption for most of the states below 4.2 MeV.

CHAPTER II

Lifetime of First Excited State of Sc^{41}

1. Introduction

Interest in the experimental determination of the lifetimes of the first excited states of the mirror nuclei Ca^{41} and Sc^{41} stems from the fact that these states can be described, to a first approximation, as states in which a single nucleon is in a $p_{3/2}$ shell model orbital about the doubly magic Ca^{40} core. On the basis of this description the lifetime of the states which decay by E2 transitions to the $f_{7/2}$ ground state then should be given by the single particle value. Knowledge of the experimental lifetimes makes possible a test of the adequacy of this simple description.

No interest in the measurement of the lifetime of the first excited states of Ca^{41} and Sc^{41} was displayed until recently when the lifetime of the state of Ca^{41} was measured by means of the Doppler shift technique[18]. The value obtained of 3.3×10^{-13} seconds, corresponds to an enhancement of the E2 transition probability to the ground state of about a factor of 10 over the single particle value. The information on these states relevant to the present discussion is summarized in Figure 9. There is abundant evidence indicating that the ground and first excited states of Ca^{41} are the chief components of the $f_{7/2}$ and $p_{3/2}$ shell model orbitals , respectively.

The information establishing the properties of the first excited state of Sc^{41} comes from a variety of sources. The state is rather

FIGURE 9

The lower levels of Ca^{41} and Sc^{41} are compared. The gamma ray transitions of interest are indicated.

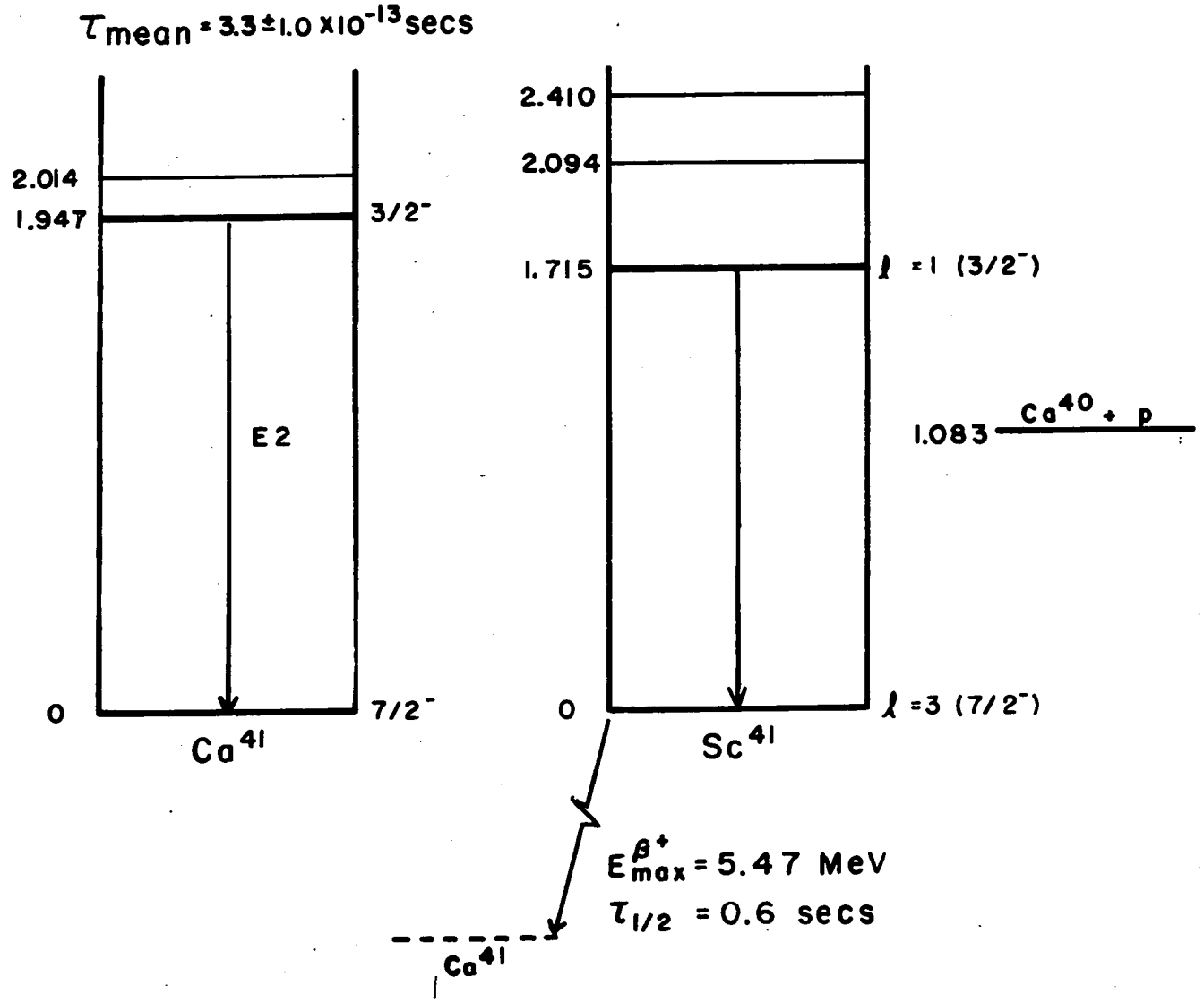
$\tau_{mean} = 3.3 \pm 1.0 \times 10^{-13}$ secs
2.014
1.947
3/2⁻
E2
0
7/2⁻
Ca41
2.410
2.094
1.715
l = 1 (3/2⁻)
1.083
Ca40 + p
0
l = 3 (7/2⁻)
Sc41
$E^{\beta^+}_{max} = 5.47$ MeV
$\tau_{1/2} = 0.6$ secs
Ca41

definitely located at an excitation energy of 1.72 MeV on the basis of measurements using the $Ca^{40}(p,\gamma)Sc^{41}$, $Ca^{40}(d,n)Sc^{41}$ and $Ca^{40}(He^3,d)Sc^{41}$ reaction[19,20,21]. Evidence from stripping studies with the latter two reactions shows that the state is formed by capture of $\ell = 1$ protons and has a spectroscopic factor of 1.2. Results from dispersion theory analysis of the angular distribution of protons elastically scattered from Ca^{40} in the range of bombarding energies between 2 and 5 MeV indicate a reduced width for the state on the order of 50% of the single particle limit. On basis of these data, the state is identified as the probable analog of the first excited state of the mirror nucleus Ca^{41}, which occurs at 1.95 MeV.

It was particularly convenient for the purpose of the present work that the 1.72 MeV state can be formed directly by resonance capture in the $Ca^{40}(p,\gamma)Sc^{41}$ reaction at a bombarding energy of 648 keV. This circumstance made it possible to determine the radiative lifetime of the state simply by measuring the Sc^{41} positron activity (E^{β}_{max} = 5.47 MeV, $T_{1/2}$ = 0.6 secs.) produced after the transition to the ground state. The experimental arrangement used for the measurement is described in Chapter I, and will not be discussed here.

2. Experimental Results

The positron yield curves obtained in the region of interest are shown in Figure 10. The upper curve was taken with a target approximately 10 keV thick and shows the region of bombarding energy from 600 to 800 keV. Repeated runs over this region revealed no resonances other than the one of interest. The next known state of Sc^{41}, not observed in the (p,γ) reaction, is at 1.08 MeV. To obtain the plateau yield indicated in the lower half of the figure a target 50 keV thick was used. The bars indicate the statistical uncertainty of the data. The beam spread when operating in the manner necessary to obtain the data was 2 keV at 1.84 MeV.

The plateau yield of this resonance was compared with that obtained for the calibration resonance at 1.842 MeV to obtain the absolute beta flux for this state.

The relationship between the integrated cross-section and the yield of an infinite target is:

$$\int \sigma \, dE = \frac{eAS}{N} Y(\infty)$$

Available evidence indicates that $\Gamma_\gamma \ll \Gamma_p$ so that the radiative width may be obtained:

$$g\Gamma_\gamma = \frac{1}{2\pi^2 \lambda^2} \int \sigma \, dE$$

In this manner we have obtained a value of 1.3×10^{-3} electron volts for the radiative width, which is indeed negligible with respect to a proton width expected to be 1-2 eV . This radiative width corresponds

FIGURE 10

Positron yield curves in neighborhood of 0.648 MeV resonance. The upper curve, taken with a 10 keV target, shows no indication of other resonances. The data of lower curve, taken with a 50 keV target, were used to obtain the lifetime of the state.

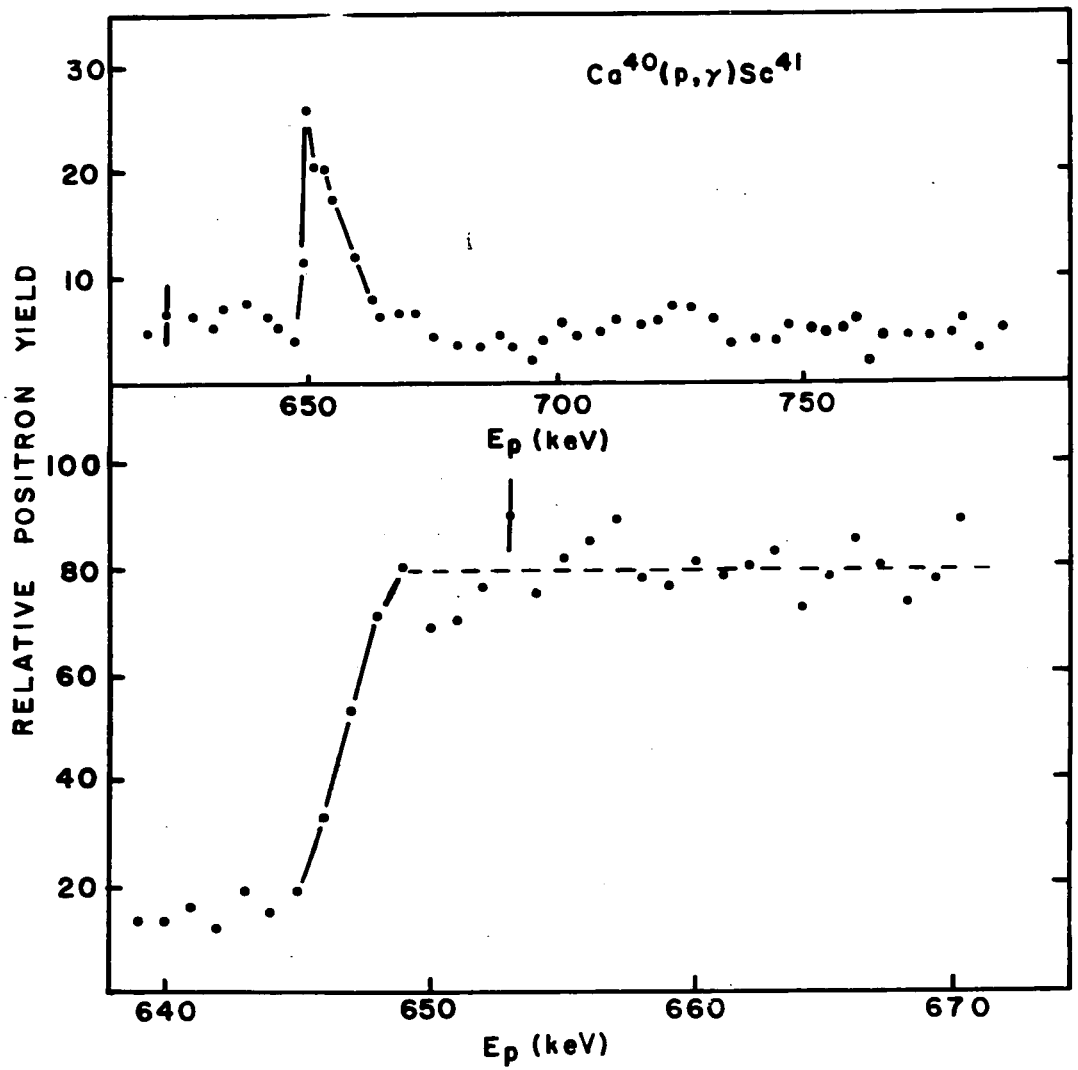
$Ca^{40}(p,\gamma)Sc^{41}$
RELATIVE POSITRON YIELD
30
20
10
650
700
750
E_p (keV)
100
80
60
40
20
640
650
660
670
E_p (keV)

to a lifetime for the state of $5.2 \pm 1.5 \times 10^{-13}$ seconds. The transition is thus an enhanced E2 transition, a factor of 13 faster than the Weisskopf estimate.

The uncertainty in the measurement of the lifetime is about 30%, of which 18% is contributed by an uncertainty in the calibration of the absolute yield, 3% by statistical uncertainty of the data and 7% by uncertainty in the stopping power of calcium.

In an earlier measurement, J.W. Butler[4], obtained a value for the integrated cross-section for this state of .02 ev - b accurate to a factor of 2. The lifetime we derive from this result is 4.3×10^{-13} seconds, which is in agreement with our results.

CHAPTER III

Non-Resonant Capture

1. Introduction

In many light nuclei, the proton radiative capture cross-section shows a smooth variation with proton energy. The resonances for the reaction are superimposed on this background radiation, the cross-section of which is on the order of 1 microbarn. In many cases the angular distribution of the radiation is a simple $\sin^2 \theta$ distribution, characteristic of a dipole oscillator oriented along the beam direction. The smooth non-resonant excitation function, along with the simple angular distribution, has led to the description of the process as direct capture. This is considered to be due to an electric dipole transition between an initial state in which there is essentially no nuclear interaction and a final state in which the proton is bound.

The total cross-section for the continuum capture may be expressed in the following form[23]:

$$\sigma(E_\lambda) \propto \sum_{l_i\, l_f\, J_i} |Z(l_i J_i l_f J_f I \lambda)|^2 \, |\langle l_f J_f | r^\lambda | l_i J_i \rangle|^2$$

where λ is the multipole order of the radiation, and i, f indicate initial and final states respectively. The radial matrix element may be written:

$$|\langle \ell_f J_f | r^\lambda | \ell_i J_i \rangle| = k_i^{-1} k_f^{-1} \left| \int_0^{R_o} u_{\ell_f J_f} r^\lambda u_{\ell_i J_i} \, dr + \int_{R_o}^{\infty} u'_{\ell_f J_f} r^\lambda u'_{\ell_i J_i} \, dr \right|$$

where R_o is the nuclear radius.

The case of capture into an unbound final state has been considered by Faessler[23]. For this case, he shows that the contribution of the second integral in the matrix element is negligible with respect to the first. This implies that the capture is occurring inside the nucleus. No calculations have been done for the $Ca^{40}(p,\gamma)Sc^{41}$ reaction.

Capture into a bound state has been considered by Christy and Duck[24] (hereafter referred to as CD). In this case the second integral in the matrix element is shown to be dominant, so that the primary capture is occurring outside of the nucleus. The initial wave function includes the nuclear phase shifts and is of the following form:

$$u_{\ell_i J_i} \sim \left(F_\ell(kr) \cos \delta_{\ell_i J_i} + G_\ell(kr) \sin \delta_{\ell_i J_i} \right)$$

The final state wave function used is a Whittaker function, normalized to the bound state amplitude at the nuclear radius. Thus the cross-section for this reaction depends on the amplitude of the final state

wave function in the region exterior to the nucleus as well as the nuclear phase shifts involved. CD obtain the cross-section for this process for several light nuclei and show reasonable agreement with available data.

The cross-section for this process may be expressed in terms of a parameter S(E) which is defined by:

$$\sigma = \frac{S(E)}{E} e^{-2\pi\eta} \qquad \eta = Z_1 Z_2 e^2 / \hbar v$$

where Z_1 and Z_2 are the atomic numbers of the beam particle and target respectively, E is their center of mass energy and v the relative velocity of the two nuclei. The parameter S(E) is nearly constant with energy, but the cross-section itself varies greatly because of the coulomb barrier. Thomas and Tanner[25] (hereafter referred to as TT) have calculated the cross-section for the direct radiative capture of protons to the ground state of Sc^{41} using the method of CD, but generating the final state wave function using a Saxon-Woods potential adjusted to give the correct binding energy and ignoring the nuclear phase shifts. The cross-sections they obtain for a transition from an incident d-wave to a final $1f_{7/2}$ orbit bound by 1.08 MeV are 0.23 and 0.50 microbarns at proton energies of 3.20 and 3.50 MeV respectively (S = 68 and 76 keV-barns).

2. Experimental Procedure

The measurement of the cross-section of non-resonant capture for Ca^{40} + p was undertaken detecting the positron decay of Sc^{41} with the equipment discussed in Chapter I. This equipment was designed to obtain as high a yield to background ratio as possible, while retaining reasonable efficiency, and thus was almost ideal for this measurement. The disadvantage is the lack of information on the character of the resultant gamma radiation and on its energy variation as the bombarding energy is changed.

Only two deviations from the experimental procedure already discussed were made. To reduce the possibility of interference by background radiation from the target the pulse height window was set to exclude betas of less than 2 MeV initial energy. The slits at the exit of the analyzing magnet were used to provide the feedback signal stabilizing the voltage of the accelerator. This procedure enabled most of the analyzed beam to be placed on the target with the aid of strong focusing electrostatic lenses. The targets used were made in a separate vacuum system, coated with a .3-.6 mg/cm^2 gold layer, and transferred to the target chamber. The techniques used in preparation of this type of target are discussed in Chapter IV. The absolute efficiency of the detector system was determined by measuring the thick target yield of the 1.842 MeV state, determined previously to be 388.6/microcoulomb.

The regions chosen to measure the non-resonant capture cross-section were those sufficiently far from any resonance observed in the

(p,γ) experiment so that only an insignificant yield would be contributed by capture at nearby states, and where possible isolated from any known levels of Sc^{41}. Figure 11 shows the known energy levels of Sc^{41} and indicates the regions of investigation. Below 3.6 MeV proton energy no known levels existed closer than 90 keV to the region of investigation in Sc^{41}. The region at 3.64 MeV proton energy is immediately below a 36 keV wide $\ell=1$ state observed in the elastic scattering, but unobserved in the (p,γ) reaction. The region at 3.76 MeV proton energy is about 20 keV below a 1 keV wide $\ell=2$ state observed only in the elastic scattering measurements. The region at 3.94 MeV proton energy is 20 keV below, and 50 keV above, states of 2-3 keV width observed in both the (p,p) and (p,γ) reactions.

FIGURE 11

The cross-hatched regions were investigated for continuum capture. All of the known levels of Ca^{41} and Sc^{41} from 2-5 MeV excitation energy are shown.

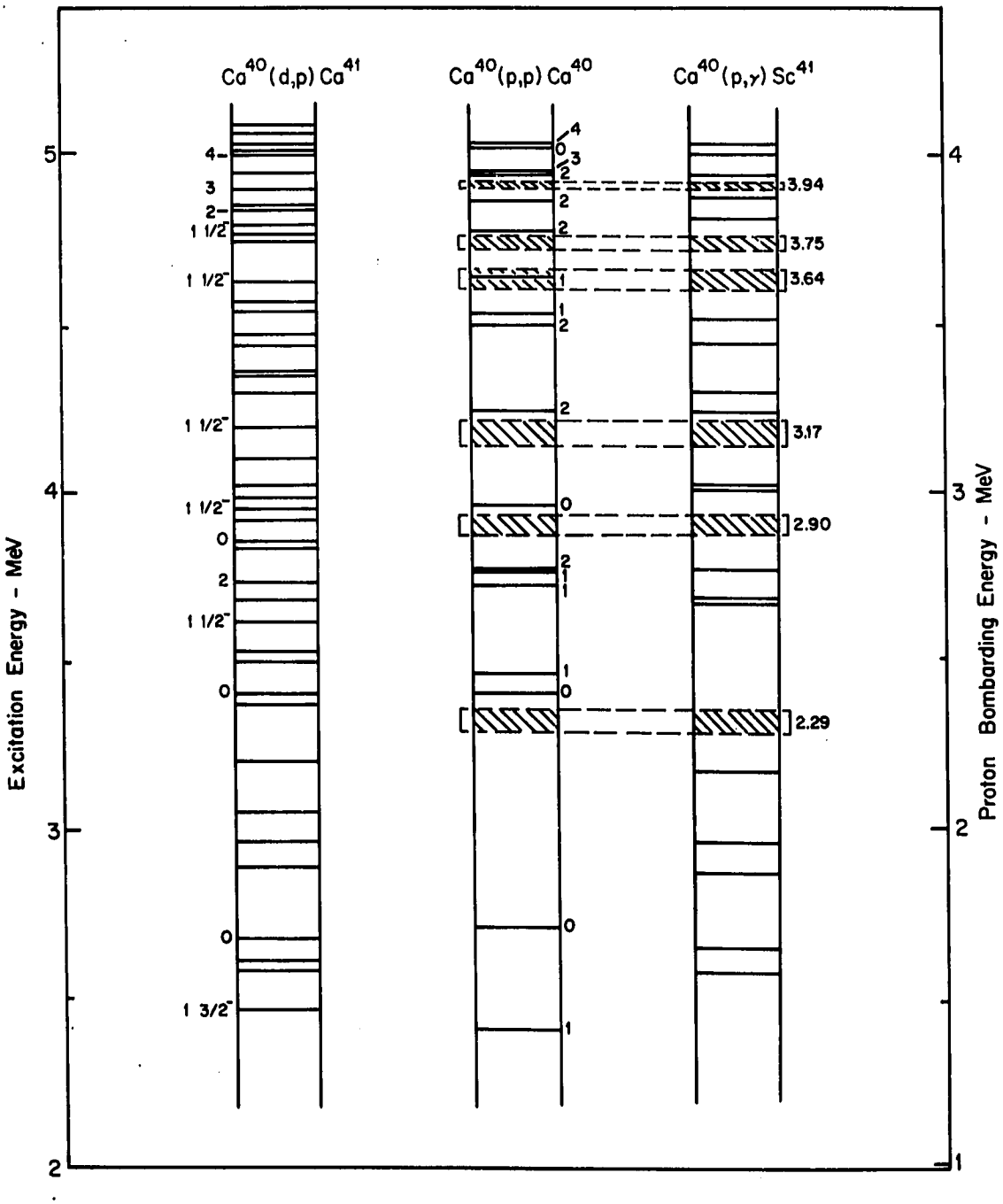
Ca40(d,p) Ca41
Ca40(p,p) Ca40
Ca40(p,γ) Sc41
Excitation Energy - MeV
Proton Bombarding Energy - MeV
5
4
3
2
4
3
2
1
4-
3
2-
1 1/2-
1 1/2-
1 1/2-
1 1/2-
0
2
1 1/2-
0
0
1 3/2-
4
0
3
2
2
2
1
2
2
1
2
1
1
0
0
1
3.94
3.75
3.64
3.17
2.90
2.29

3. Experimental Results and Conclusions

The yield for a given energy was obtained by averaging data taken in fine steps over regions 10 to 100 keV wide to ascertain that there were no resonances in the region which might have been missed in the measurements described in Chapter I. Background measured while the beam was deflected off the target was then subtracted from the yield.

The cross-section obtained for the process, varying from .03 to 1.3 microbarns, is shown in Figure 12. The data shown were obtained with a 63 keV target. The errors indicated are relative error only. An additional 30% error is present in the absolute cross-sections owing to the combined uncertainties of absolute calibration and target thickness. The portion of the yield attributable to the tails of the known states nearby is less than 2% of that observed. Some of the measured yield might also be attributable to weak, unresolved levels in Sc^{41}. There are 9 more levels known in Ca^{41} below E_{exc} = 5 MeV than are known in Sc^{41}, however it is unlikely that more than 1 or 2 would be located in each region of investigation. In order to ascertain if the yield observed is from these "missing" states the yield was measured in several regions with 4 targets varying in thickness from 5 to 60 keV. If the yield is indeed due to direct capture, it should increase linearly with target thickness. This is indicated by the results shown in Figure 12. However if the yield is due to unresolved weak resonances it should reach a plateau and not increase linearly as target thickness is increased.

FIGURE 12

A. The cross-section for the $Ca^{40}(p,\gamma)Sc^{41}$ reaction measured in the region free of known resonances is shown as a function of bombarding energy. The bars on the data indicate relative errors only. The solid curve is a fit calculated using the formula of Christy and Duck[24].

B. The yield obtained in each energy region for 3 targets of different thicknesses is shown normalized to that obtained with a 63 keV target. The lines indicate the ratios of the thickness of each target to the 63 keV target. The bars indicate the errors.

C. The S factor derived from the cross-section shown in (A) is plotted. The errors are relative errors only. The solid curve is a calculated fit using the formula of Christy and Duck[24]. The X's are values calculated by Thomas and Tanner[25].

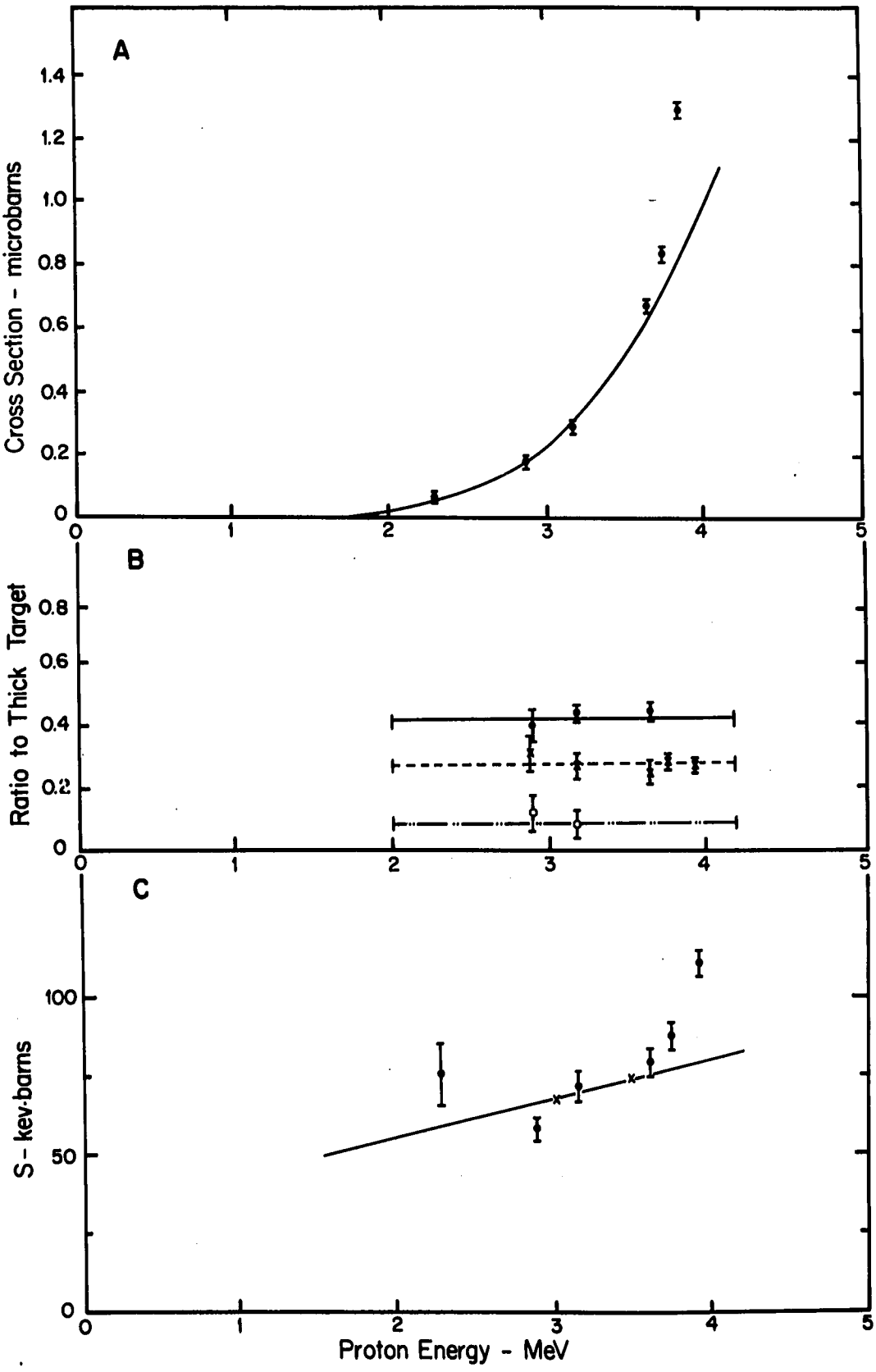
A
Cross Section - microbarns
1.4
1.2
1.0
0.8
0.6
0.4
0.2
0
0
1
2
3
4
5
B
Ratio to Thick Target
0.8
0.6
0.4
0.2
0
0
1
2
3
4
5
C
S - kev-barns
100
50
0
0
1
2
3
4
5
Proton Energy - MeV

The values of the cross-section obtained by TT are indicated in Figure 12 and are in good agreement with the measured value. The cross-section, calculated assuming the energy dependence given by CD, but normalized to the results of TT, is shown and reproduces the general trend of the data. The energy dependence of S obtained by CD was used for this calculation and for Ca^{40} is of the form:

$$S = A\left(\frac{E_B}{E_\gamma}\right)^{\frac{1}{3}} \exp\left(\frac{2(\ell_2^2-\ell_1^2)}{12^{\frac{1}{3}}\alpha^{2/3}}\left(\frac{E_\gamma}{E_B}\right)^{\frac{1}{3}}\right); \quad \alpha = \frac{Z_1 Z_2 e^2 \mu}{\hbar^2 (2\mu E_B)^{\frac{1}{2}}}$$

where A is a normalization constant determined from the results of TT, E_γ is the energy of the gamma decay, E_B is 1.082 MeV, the binding energy of the final proton in Sc^{41}, ℓ_1 is the initial orbital angular momentum of the proton and ℓ_2 the final orbital angular momentum of the proton. Also shown in the figure is a plot of the experimental S factor obtained, with the values calculated by TT and the energy dependence of CD indicated.

Although the value of S(E) obtained is in agreement with the calculated value, the apparent energy dependence of this factor is obviously much greater than the calculated value. This may be attributable to several sources. One possible source is a slight increase in background radiation of an energy above the 3 MeV window setting. An estimate of 5-10% for the upper limit of this contamination was made from the crude beta spectra taken which is not sufficient to account for the discrepancy.

In the elastic scattering experiments[2] on Ca^{40}, the presence of a $d_{5/2}$ phase shift was required in this region to obtain satisfactory fits to the angular distributions and the continuum cross-section. The presence of this phase shift may be required to obtain the experimentally measured energy dependence.

A third factor may be capture into an unbound state, as described by Faessler, which then decays to the ground state. In this case, however, the gamma decay to the ground state would be competing with much faster particle emission and thus would not be expected to be observed. A fourth possibility is the occurrence of many weak states unobserved in both Ca^{41} and Sc^{41}, which may be contributing to the yield.

In order to determine the cause of the above disagreement further experimental investigation needs to be undertaken. The extension of the measurements over a larger energy range, and a measurement of the gamma decay associated with this capture should be sufficient to resolve the problem.

CHAPTER IV

Gamma Ray Angular Distributions

1. Introduction

In the present chapter measurements of the angular distributions of gamma rays emitted in transitions to the ground state from capture resonances, located as described in Chapter I, will be discussed. The object of these measurements was to provide information to aid in assignments of spin and parities to the states of Sc^{41} involved. Attention was given chiefly to states below E_p = 4.1 MeV, corresponding to excitation energies in Sc^{41} of less than 5.1 MeV. This was done because the states were better resolved and there was less background to contend with, and because of the interest in comparison with analog states of Ca^{41} about which the most is known in detail in this region of excitation energy.

Sixteen resonances were investigated in this way and they fell into two categories. For the 4 states for which ℓ values were assigned by Brown, the angular distributions make possible a choice of J^{π} values. For the other 12 states for which no other information was available, the angular distributions together with the lifetimes of the states, obtained as described in Chapter I, should at least give a strong indication as to the preferred J values of the states. As it turned out, J values could be assigned with reasonable certainty in only 4 of these cases, and could be limited to only two choices in 7 other cases. The one remaining state could be limited only to 3 possible

J values. Correlation measurements on gamma rays associated with the decay of these states could provide additional information further limiting the choice of possible J values of the states for which uncertainty remains. However, as mentioned in Chapter I, all excited states of Sc^{41} are proton unstable and hence successive cascading to the lower lying states appears to be an improbable occurrence. In gamma ray spectra taken during these measurements no clear cut evidence was obtained for transitions other than those directly to the ground state. This does not imply that they do not occur, only that they are relatively weak.

2. Experimental Apparatus and Procedure

The target chamber and associated apparatus used for the gamma ray angular distribution measurements was the same as that described earlier in connection with the positron measurements, except for a modification of the target extension tube permitting the target to be mounted at an angle of 45° with respect to the beam. This was done to reduce the asymmetries due to attenuation of the gamma radiation measured between the angles of 0° and 90°. For these measurements, maximum beam currents compatible with target stability were required. Experience showed that currents up to 8 microamperes were acceptable. Such currents could be obtained only by using the strong focusing lenses installed in the beam tube, but at the expense of some loss of beam energy definition, since this mode of operation required that the stabilizing voltage of the accelerator be controlled by signals from slits at the exit of the analyzing magnet. Between 65% and 95% of the analyzed beam was focused on the target, depending on tuning conditions of the accelerator and the beam energy used.

Twenty mil tungsten and 5 mil gold blanks were used for target backings. The tungsten backing was used when beam currents as large as 5-7 microamperes were necessary and the thinner gold backing used for lower beams. Backings of these thicknesses gave adequate heat dissipation on the one hand and transparency to the Sc^{41} positrons on the other, the latter property being useful when locating a state of interest immediately prior to the gamma ray measurement.

The proton beam, after focusing by electrostatic lenses, passed through 1/2" square tantalum slits 8' from the target, a 3/8" round tantalum aperature 4 feet from the target, and was limited to a 1/8" wide by 1/4" high spot on the target by gold covered slits placed 8" before the target. The small lateral displacement of the beam permitted by this arrangement introduced a negligible uncertainty in the gamma ray yields at the detector distances used. All of the slits used to limit the beam before reaching the target were replaced with clean tantalum slits before each run.

The affinity of calcium for impurities and the very low cross-section for the capture process necessitated the use of special procedures to avoid target contamination and hence to reduce gamma ray background. In practice, it was found that oxygen, in particular O^{18}, was the most vexing of the contaminants present in any abundance. At proton energies above 3 MeV, the $O^{18}(p,\alpha\gamma)N^{15}$ reaction produces a prolific yield of 5.3 MeV gamma rays which interfere with gamma rays from several of the states in Sc^{41} under investigation. Accordingly the following procedure was adopted in preparing targets in order to minimize their oxygen contamination. First, the natural calcium metal, available in lump form at 99.5% purity, was scraped to produce a shiny surface and then inserted into a thoroughly outgassed tantalum evaporation boat. Next, at a vacuum of 2 to 3×10^{-6} mm Hg a preliminary evaporation of the calcium metal was made onto the walls of the bell jar while the target backing was shielded. This was done chiefly to outgas the calcium but had the additional benefit that the calcium

deposited on the walls of the bell jar acted as a "pump" to remove active gases from the vacuum system. The target was then made at a vacuum of about $1x10^{-6}$ mm Hg and protected from subsequent contamination by evaporation of a 0.3-0.6 mg/cm^2 layer of gold onto the fresh calcium surface. Studies by means of the elastic scattering of protons of targets prepared in this manner, after transfer to the accelerator vacuum system in air, revealed less than 2% oxygen contamination, with no noticeable change after 12 hours in the vacuum system. An additional advantage of the gold protective layer was to reduce target "burn-off," presumably due to the higher heat conductivity and higher melting point of gold as compared to calcium. Heat dissipations as high as 20 watts could be tolerated with no noticeable target evaporation, when a cooling jet of air was directed at the target backing. A disadvantage of the gold coating was that it increased the energy spread of the beam incident on the calcium target. In one case where this effect prevented resolution of two resonances a target was made in place using the evaporator in the target chamber.

The gamma rays were detected by two 5" x 5" NaI (Tl) crystals mounted on RCA 8055 photomultiplier tubes. Pulses from the photomultipliers were fed into suitable preamps and then into the low level inputs of the separate halves of a Nuclear Data 1024 channel analyzer operating in the multiplex mode. The analyzer was connected to an on-line IBM 1401 computer, programmed to plot the data and store it on magnetic tape for future analysis.

The pulse height scale was calibrated by measuring gamma rays of standard sources. The counters had a resolution of 8-1/2% fwhm for a Cs^{137} gamma ray line. Some standard shapes obtained with these crystals for various energy gamma rays are shown in Figure 13. The counters were encased in a lead annulus 2" thick in order to shield against background. Slight gain shifts were noted both with time and with counting rate, but were not more than 1 to 2 channels in 200 and were unimportant in the present application.

One of the counters was used to monitor the reaction and the other to obtain the angular distribution. The latter counter was placed on an arm which rotated about a vertical axis centered with respect to the center of the target to within 1/32". The zero position of the angular scale was determined by sighting through a pin hole in the center of the mount of the moveable detector to detect alignment with two plumbbobs, one suspended from the center of the target and one suspended from the center of the beam tube approximately 2 ft. from the target. In this manner angular alignment of the system could be accomplished to within $\pm$ 2°, with respect to the beam.

The angular symmetry of the system was checked by measuring the angular distribution of the gamma rays from the 3 MeV first excited state of C^{13} which was produced by the $C^{13}(p,p'\gamma)C^{13}$ reaction at a bombarding energy of 4 MeV. The angular distribution of this radiation is known to be isotropic[12]. Figure 14 shows the arrangement of the target extension tube with respect to the detectors and a representative $C^{13}(p,p'\gamma)$ angular distribution.

FIGURE 13

Line shapes measured with the 5" x 5" NaI (Tl) crystals for gamma rays from some standard sources.

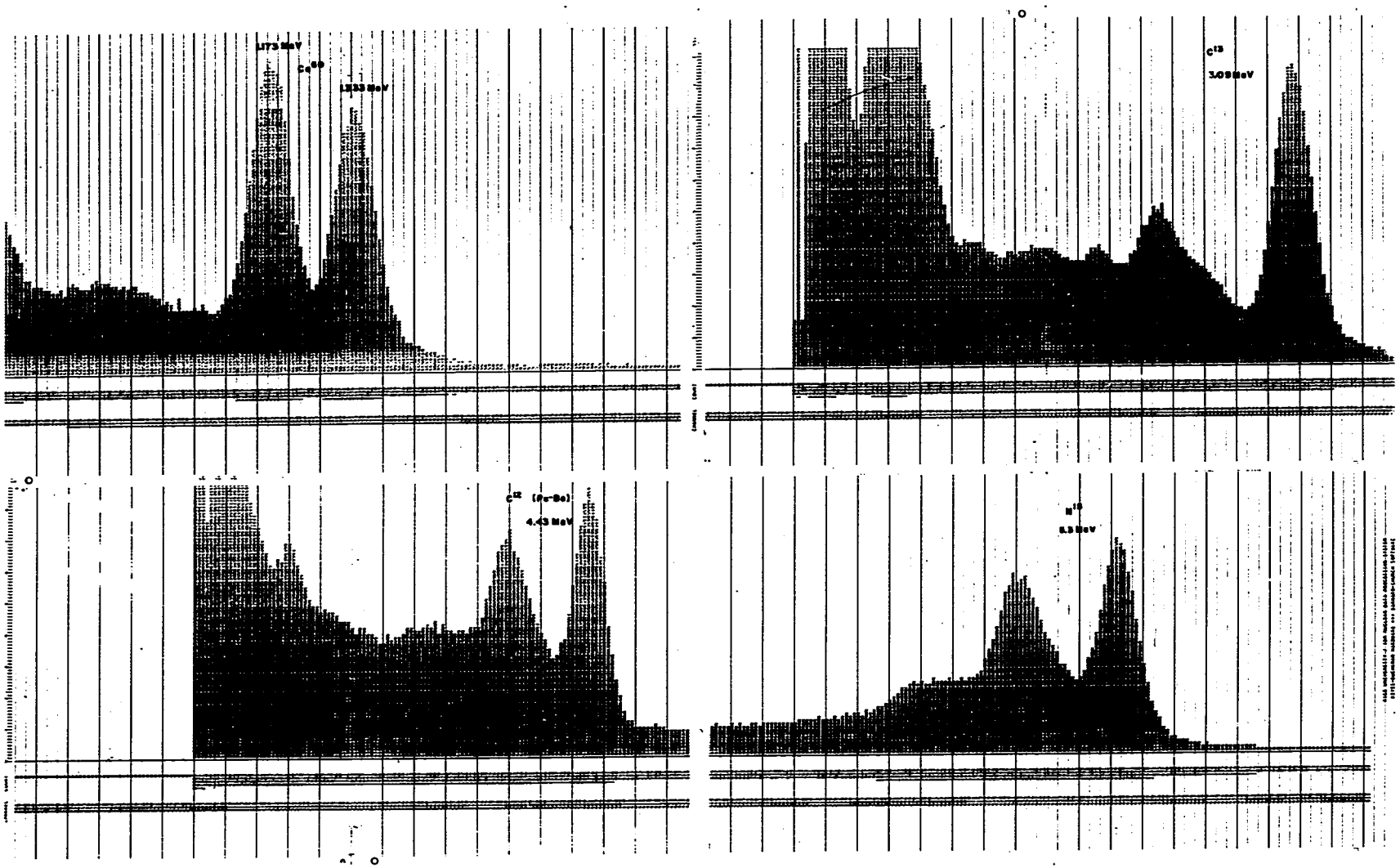
1.173 MeV
Co60
1.333 MeV
C13
3.09 MeV
C12 (p-Be)
4.43 MeV
N15
5.3 MeV

FIGURE 14

The arrangement used in the angular distribution measurements is illustrated. The insert shows the angular distribution obtained for the isotropic 3 MeV C^{13*} gamma ray.

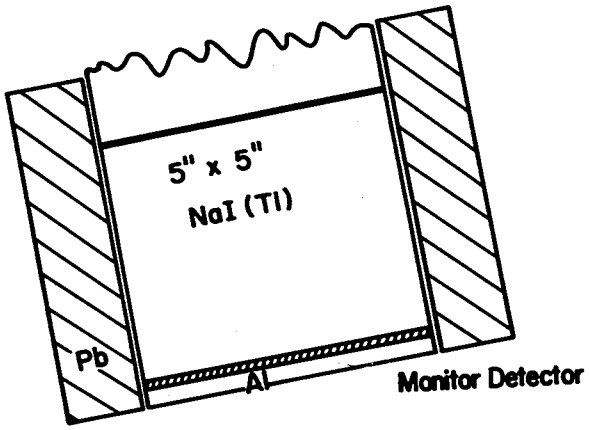
5" x 5"
NaI (Tl)
Pb
Al
Monitor Detector

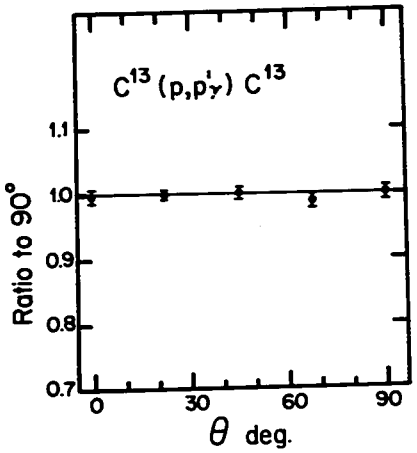
C13 (p,p'γ) C13
Ratio to 90°
1.1
1.0
0.9
0.8
0.7
0
30
60
90
θ deg.

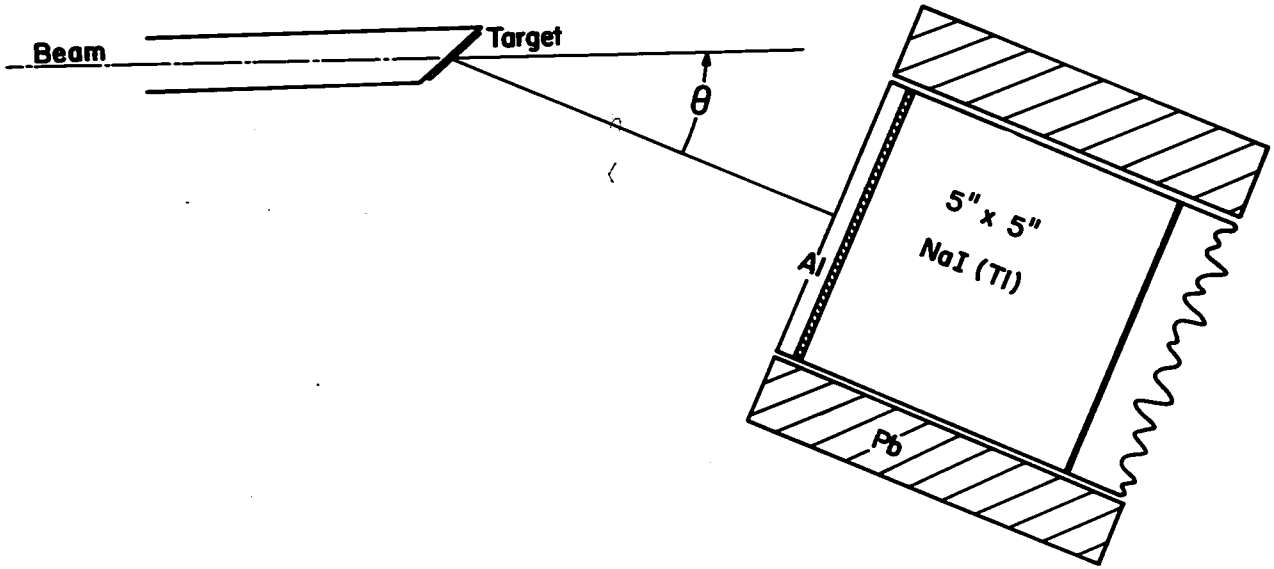
Beam
Target
θ
5" x 5"
NaI (Tl)
Al
Pb

Before the Sc^{41} gamma ray measurements could be made, the resonances of interest had to be located. For most cases, an excitation curve in the immediate meighborhood of each resonance was run to locate accurately the resonances and ascertain the target thickness. For the 4 resonances between 1.8 and 2.8 MeV, this was done by setting a pulse height window to integrate the full energy peak of the Sc^{41} gamma ray of interest. For the other resonances the Sc^{41} positron yield was measured as described in Chapter I. For several of the weak resonances above E_p = 3.2 MeV this was not practical due to attenuation of the positron yield by the 20 mil tungsten target backing used. For these resonances, for which targets 20-30 keV thick were used, the energy calibration of the accelerator by measurement at a strong nearby resonance was relied upon to insure location of the resonances in question.

The targets used for all but 2 of the resonances were from 15 to 40 keV thick. An 8 keV target was used for two of the resonances which could not be resolved with the thick targets.

The low yield of the resonances required that long data points be taken. Beam currents varied from 2 to 8 microamperes depending on the temper of the accelerator during the particular run. Due to the large number of resonances on which data was desired, the time spent per resonance was limited to 12-14 hours. For these measurements data were taken at either three or five equally spaced angles between 0° and 90° with the front face of the movable detector placed 3", 5", or 10" from the target depending upon the intensity of the

particular resonance. A background spectrum was also taken below resonance at one angle for each state. Table 5 lists the resonances on which angular distributions were obtained and indicates the number of angles at which data were taken, the charge accumulated per angle, and the distance of the movable detector from the target. The monitor counter was placed at 3-1/2" from the target at 100° with respect to the beam direction for all but the two weakest states observed for which it was placed at 2" and approximately 120°.

TABLE 5

E_p (MeV)	Detector Distance	Number of Angles	q (millicoul.)
1.540	3"	3	-
1.621	3"	3	-
1.842	10"	5	20
1.934	5"	3	20
2.153	5"	5	25
2.677	10"	5	20
2.764	5"	5	30
3.010	5"	5	15
3.019	5"	5	15
3.240	5"	3	20
3.440	5"	4	20
3.515	10"	5	15
3.819	10"	5	20
3.965	10"	5	25
4.025	10"	5	25
4.054	10"	5	11

3. Measurements of Spectra and Angular Distributions

A selection of spectra representative of those obtained both on and off resonance in three different energy regions is shown in Figure 15 and Figure 16. It is evident there is in each spectrum a strong continuous background on which the Sc^{41} peak resides. The quality of the spectra shown is that obtainable by a careful application of routine procedures involving proper beam collimation, careful target preparation procedures, and shielding of the crystals to reduce extraneous background. While improvement of the Sc^{41} lines with respect to background could doubtless be achieved, it was believed that a major effort would be required to identify and eliminate contaminants believed to be the source of the difficulty. This was not thought to be necessary to obtain data of sufficient quality to establish the character of most of the angular distributions. However, the relative weakness of the Sc^{41} lines with respect to the background was indeed a problem when determining the yield of the Sc^{41} gamma rays in the spectrum. A discussion of the background is given in the next section.

a. The Background Problem

The background which interferes with the measurement of the Sc^{41} gamma rays comes from three sources. The first source, of importance only at bombarding energies below 2.5 MeV, is the residual background present when the accelerators are off. A spectrum taken under this condition for 2 hours is shown in Figure 17. The spectrum is very similar to those obtained by Raboy and Traul[26] who identified the

FIGURE 15

Typical on (top) and off (bottom) resonance gamma ray spectra. On the left is that taken at the 2.677 MeV resonance and on the right for the 3.819 MeV resonance.

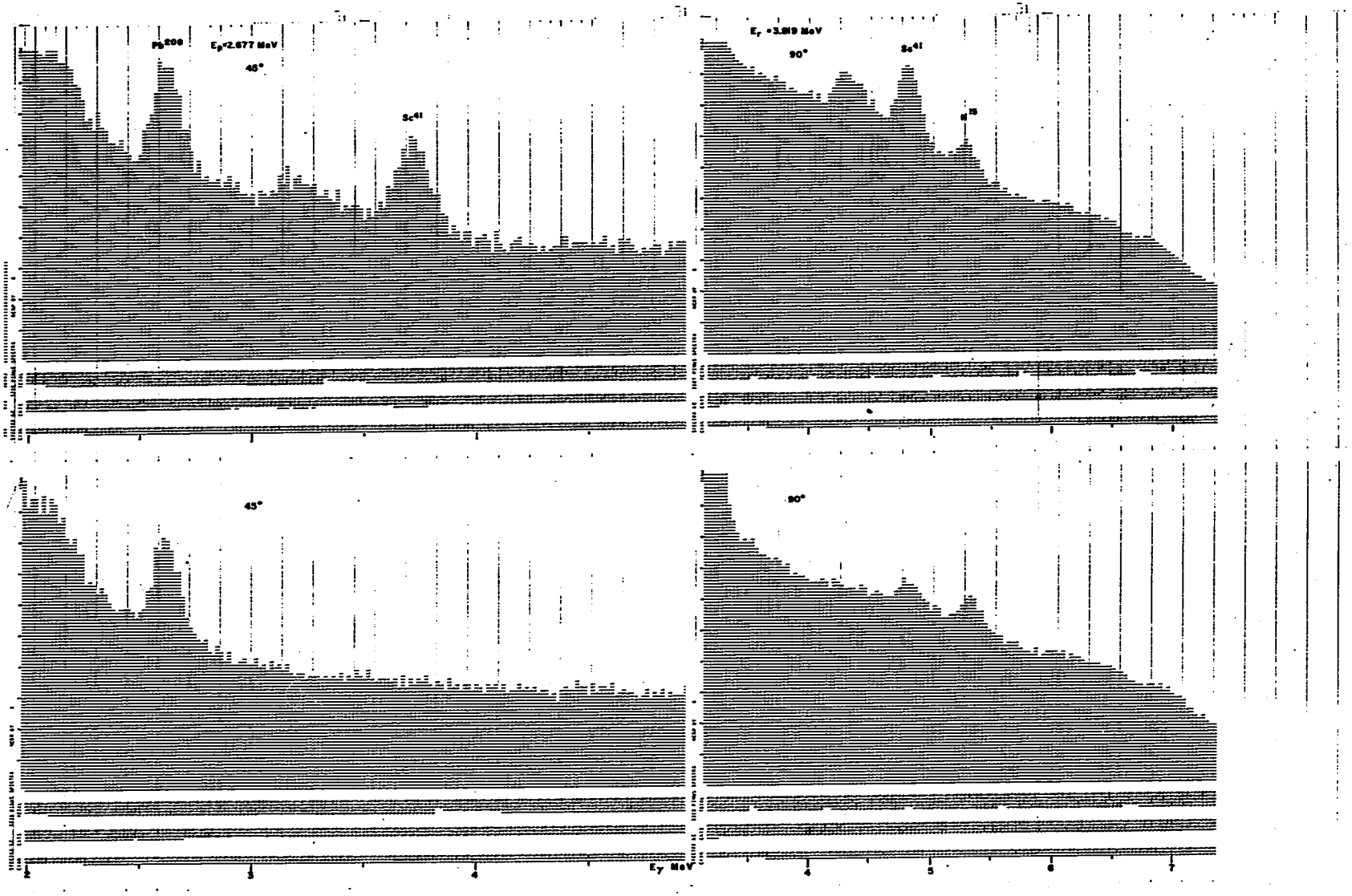
Pb208
Ep=2.677 MeV
45°
Sc41
Er =3.869 MeV
90°
Sc41
N15
45°
90°
Ey MeV
2
3
4
4
5
6
7

FIGURE 16

In the upper portion of the figure on (left) and off (right) resonance spectra taken at the 1.842 MeV resonance are shown. The spectra in the lower half of the figure are those resulting from a subtraction of room background from the upper two.

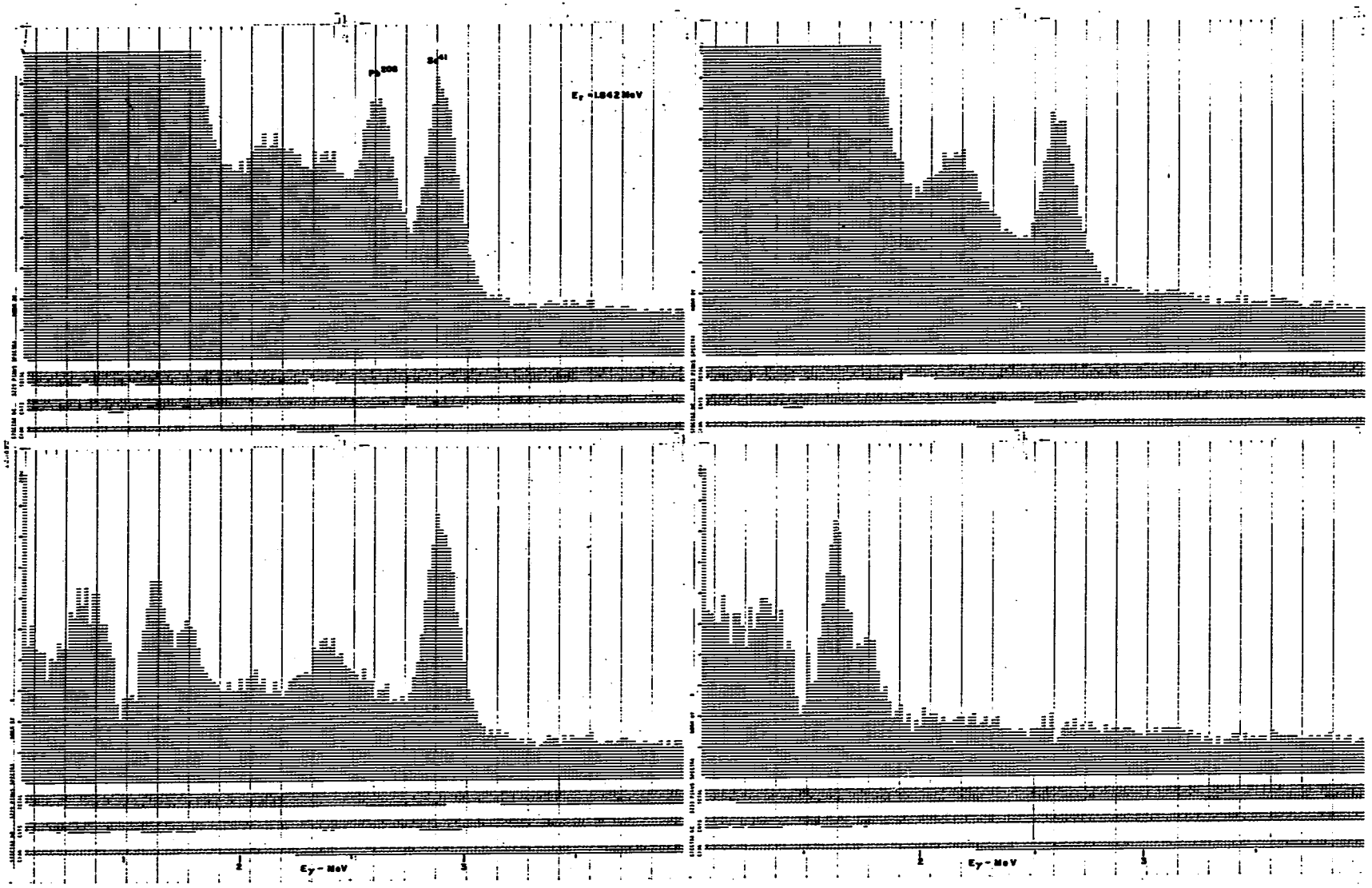
E_γ = 1.842 MeV
E_γ - MeV
E_γ - MeV

FIGURE 17

A gamma ray spectrum taken with a 5" x 5" NaI (Tl) crystal for two hours with the accelerator voltage down.

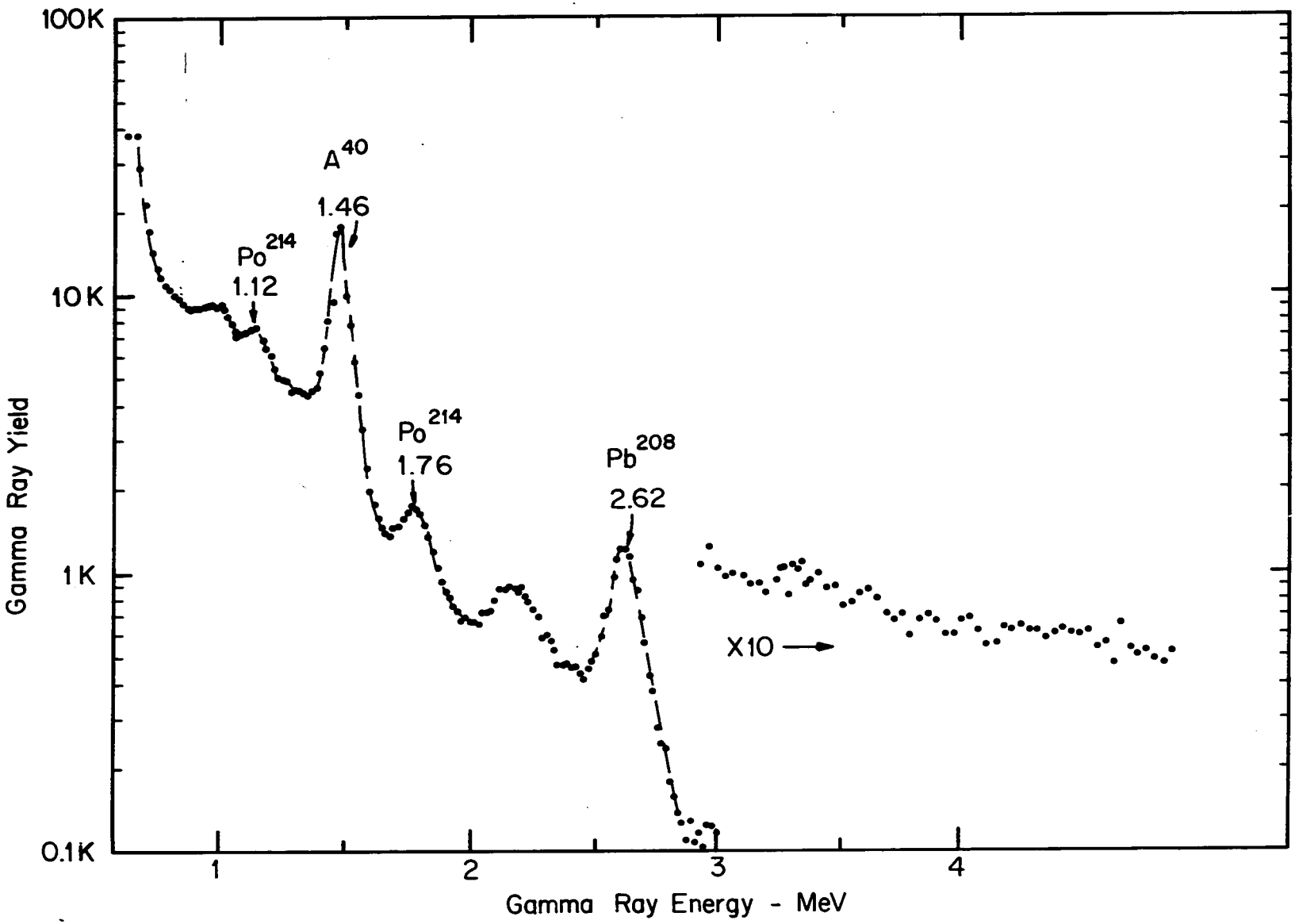
100K
10K
1K
0.1K
Gamma Ray Yield
A40
1.46
Po214
1.12
Po214
1.76
Pb208
2.62
X10
1
2
3
4
Gamma Ray Energy - MeV

peaks found in the residual background spectrum of a NaI crystal as due to the characteristic radiations from K^{40} and various members of the decay series of Th^{232} and U^{238}. The sources of the lines indicated on the spectra are from their work, and the energies are in agreement with our energy calibration.

The target backing, in which the protons were stopped, is the second major source of background. High intensity lines at low energies are due to coulomb excitation but could be severely attenuated by insertion of a 1/8" thick lead absorber between the detectors and the target. A spectrum taken at 3.96 MeV bombarding energy with a gold backing is shown in Figure 18. The gamma ray backgrounds from both the tungsten and gold target backings are quite similar. There are no lines in either spectrum above E_γ = 3.2 MeV, but only a strong continuum. Below 3.2 MeV lines appear in both cases which have not been identified, and the background begins to rise more abruptly below 2.6 MeV. It is worth remarking here, that the 6.14 MeV gamma ray from the first excited state of O^{16}, formed through the $F^{19}(p,\alpha\gamma)O^{16}$ reaction, one of the most troublesome contaminants for many (p,γ) reactions, was not detectable above the continuous background for the target backings used. However, in one case, a sheet of 2 mil thick 99.95% pure fine gold obtained for this experiment was found to have considerable fluorine contamination and had to be discarded.

The third source of background is the target material itself. High resolution proton elastic scattering measurements on targets made utilizing the 99.5% pure calcium metal from the same source as used in

FIGURE 18

Spectra of the gamma rays emitted when a 3.95 MeV proton beam is incident on a gold backing, both with and without a 25 keV thick layer of calcium present, are shown. The cross-hatched area represents magnitude of the Sc^{41} line obtained at the 3.965 MeV resonance. Most of the peaks below 3 MeV are attributable to the backing. Above this energy the backing contributes only a continuum yield.

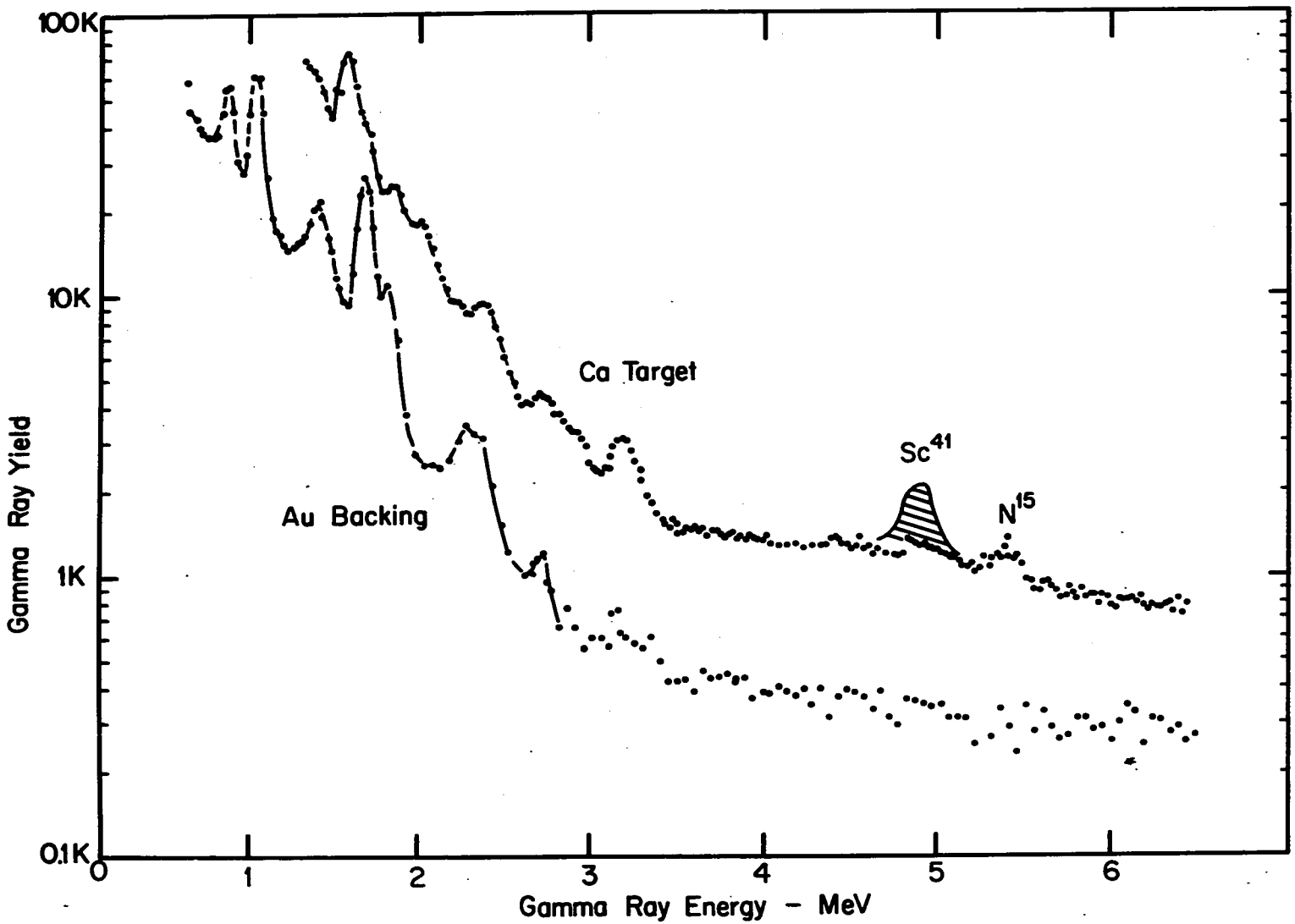
100K
10K
1K
0.1K
Gamma Ray Yield
Ca Target
Au Backing
Sc41
N15
0
1
2
3
4
5
6
Gamma Ray Energy – MeV

this experiment revealed the presence of carbon, nitrogen, oxygen, and magnesium contaminants as well as traces of silicon and fluorine[27]. A sample off resonance background spectrum taken at E_p = 3.96 MeV with a gold backed 25 keV thick target is shown in Figure 18, together with the spectrum due to gold alone. There are recognizable peaks in most of the spectra (Figures 15, 19, and 20) taken above 3.2 MeV bombarding energy, corresponding to gamma ray energies of 6.90 $\pm$ .20 MeV, 6.40 $\pm$ .20 MeV, 6.12 $\pm$ .20 MeV, 5.60 $\pm$ .15 MeV, 5.30 $\pm$ .15 MeV and 4.80 $\pm$ .15 MeV. The peaks at 5.30 MeV and 4.80 MeV are definitely attributable to the full energy and first escape peaks of gamma rays produced in the $O^{18}(p,\alpha\gamma)N^{15}$ reaction due to the O^{18} impurity mentioned earlier. These peaks are the most difficult to contend with because their energies are comparable to those of gamma rays produced in transitions to the ground state of Sc^{41} from capture resonances in the range of bombarding energies between 3.8 and 4.1 MeV. The 6.12 MeV gamma ray and possibly also the 6.9 MeV gamma ray are probably due to the $F^{19}(p,\alpha\gamma)O^{16}$ reaction. These gamma rays do not interfere seriously with the Sc^{41} line because they only contribute to the continuum present in that region. The spectrum in the region of gamma ray energy below 3.2 MeV is complex, and no identifications were made in this region although most of the known contaminants could be contributing. A portion of the background radiation present in all regions could be due to the other isotopes of calcium, the next most abundant of which is Ca^{44} (2%).

Spectra taken at 1.842 MeV bombarding energy with the crystal at the 0° position and 10" from the target are shown in Figure 16. Also shown are the on and off resonance spectra after subtraction of the room background. The relative magnitude of the different backgrounds is apparent.

b. Data Reduction

General Procedure

The general procedures described below were used to extract the Sc^{41} gamma ray yields from the pulse-height spectra. As mentioned earlier the data were stored on magnetic tapes. Special programs were constructed to perform the normalization, subtraction, and gain shift functions necessary in the data processing, and to plot the results of the analysis.

Excessive time would have been required to obtain off resonance spectra at all angles, so an off-resonance spectrum taken at one angle was used to characterize the shape of the background. This spectrum was then normalized to the on-resonance spectra, at each angle, in the region above the Sc^{41} line. Figure 19 illustrates the procedure used to obtain the net Sc^{41} yield. Two regions, (1) and (2), above the Sc^{41} line were chosen for this normalization. A third region (3) was chosen to correspond to the region of the Sc^{41} peak. The net Sc^{41} yield is then obtained by:

FIGURE 19

On and off resonance spectra taken at the 3.515 MeV resonance are shown. The resultant Sc^{41} line, after subtraction of the lower spectrum from the upper is shown in the lower righthand corner. This line shape may be compared with that of the 4.43 MeV C^{12*} gamma ray from a Pu-Be source.

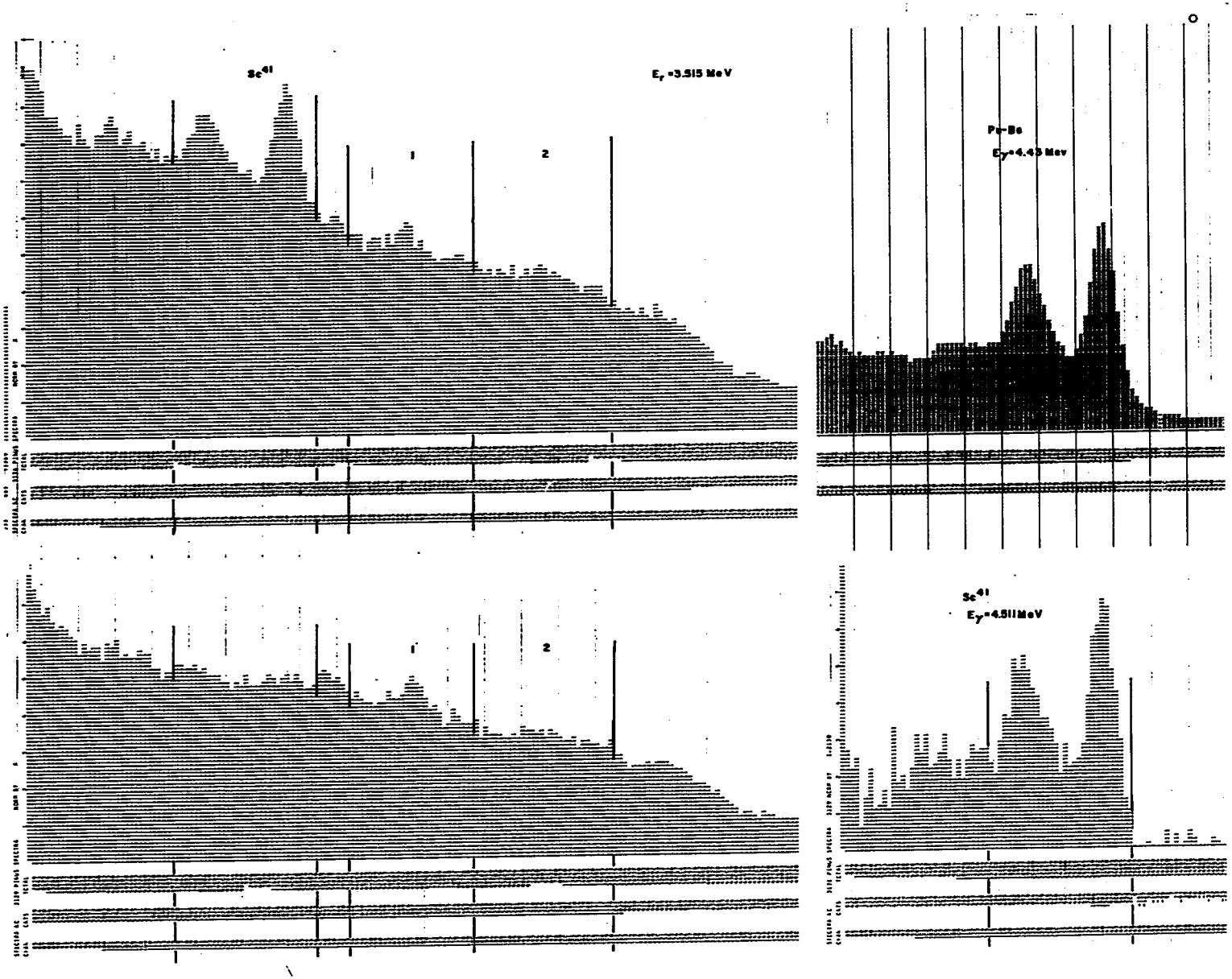
Sc⁴¹
E_r =3.515 MeV
1
2
Pu-Be
E_γ=4.43 Mev
Sc⁴¹
E_γ=4.511MeV

$$Y_1(\theta) = Y_{ON}(3) - Y_{off}^{(3)}\, Y_{ON}^{(1)} / Y_{off}^{(1)}$$

$$Y_2(\theta) = Y_{ON}(3) - Y_{off}^{(3)}\, Y_{ON}^{(2)} / Y_{off}^{(2)}$$

corresponding to a choice of two possible background normalizations. In a corresponding manner yields were obtained for the monitor detector. The data were then expressed as the ratio:

$$R_L(\theta) = Y_L(\theta) / Y_{MON}$$

for all of the angles. These ratios were then normalized to either the 90° or 0° ratio, whichever was larger. Although both $Y(\theta)$ and $R(\theta)$ depend quite strongly on the particular background normalization chosen, the resultant normalized angular distributions depend only slightly on it when the same criteria are applied for all angles at a given resonance.

The uncertainty in the Sc^{41} yield at each angle is of two types, that strictly due to statistics, which were relatively poor owing to the subtraction of the large numbers, ranging between 1% and 10% for the various resonances, and that which is a result of the particular background analysis performed. To obtain an estimate of the latter, the results obtained using different normalization regions were compared. The resultant uncertainties ranged between 3% and 20%.

The net Sc^{41} yield obtained for the 3.515 MeV resonance (E_γ = 4.511 MeV) is shown also in Figure 19. The line shape may be compared

with that of the C^{12} 4.432 MeV gamma ray from a Pu-Be source. Comparisons of the Sc^{41} line shapes obtained from the above procedure with standard line shapes provide an additional indication of the quality of the background subtraction.

Specific Problems

The procedures used for reduction of the gamma ray data differ from resonance to resonance, as required by the nature of the background radiation present in the pulse height spectrum. In the lower energy region, for the 4 states observed between 1.54 and 1.94 MeV bombarding energy, the natural room background was an important factor. The 2.613 MeV Pb^{208} gamma ray present in the room background is not resolved from the ground state gamma rays emitted in the decay of the states in Sc^{41} at 1.54 and 1.62 MeV (E_γ = 2.59 MeV and 2.67 MeV respectively), and presents a problem for the states located at 1.84 and 1.93 MeV (E_γ = 2.89 and 2.98 MeV respectively). This background which is accurately known was subtracted from the spectrum before the above analysis was performed. Above a bombarding energy of 2.6 MeV the natural room background contributed a negligible portion of the spectrum in the region of interest and was ignored in the analysis of the results.

In the region of bombarding energy above E_p = 3.8 MeV the gamma decay of the 5.276 and 5.304 states of N^{15} formed in the $O^{18}(p,\alpha\gamma)N^{15}$ reaction was of sufficient intensity to present an added problem for the analysis of the spectra for the four states of Sc^{41} investigated.

The lower state, located at a proton energy of 3.819 MeV, lies on a broad resonance in the $O^{18}(p,\alpha\gamma)N^{15}$ reaction, and the contamination was most severe for this resonance. Here the energy of the ground state gamma ray corresponds roughly to the first escape peak of the N^{15} gamma ray. For the other three states the Sc^{41} peak is located between the first escape and full energy peaks of the N^{15} radiation. Gamma spectra taken at the 3.819 MeV resonance are shown in Figure 15. The background problem for the upper states is illustrated by spectra taken at the 4.025 MeV resonance in Figure 20. In order that the offending gamma ray might be properly removed from the spectra, a rough excitation function for the $O^{18}(p,\alpha\gamma)N^{15}$ reaction was obtained, and angular distributions of the resultant gamma rays were measured at selected energies in the region of bombarding energy from 3.8 to 4.1 MeV.

For the Sc^{41} resonance located at E_p = 3.82 MeV, off resonance spectra were obtained at 0°, 45° and 90° and subtracted from the corresponding on resonance spectra, after normalization using a region of the spectra above the N^{15} gamma rays. Corrections to the resulting Sc^{41} yields were then made to account for the change in yield of the N^{15} gamma rays associated with the slight difference in off and on resonance bombarding energies. Slight corrections to the data at 22-1/2° and 67-1/2° were made for the angular distribution of the N^{15} gamma rays. The N^{15} yield was obtained from the full energy peak, which was resolved from the Sc^{41} peak at this energy, by assuming a linear background under the peak.

FIGURE 20

Off-resonance and on-resonance spectra taken at the 4.025 MeV resonance are shown. The Sc^{41} line obscures the 5.3 MeV N^{15} line, preventing accurate determination of its effect on the Sc^{41} angular distribution.

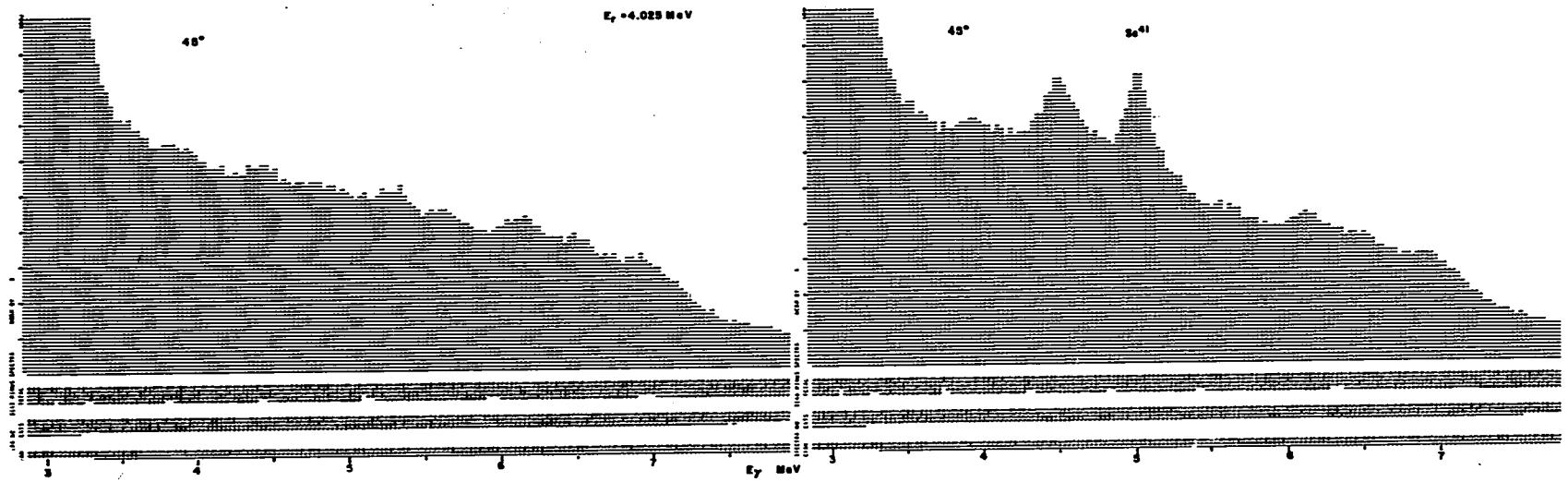
E_γ = 4.025 MeV
45°
45°
Sc^{41}
3
4
5
6
7
E_γ MeV

For the 3 remaining resonances at E_p = 3.965, 4.025 and 4.054 MeV for which N^{15} was also a problem the yield in the N^{15} gamma ray line was obtained from the off resonance background spectrum by assuming a linear background under the N^{15} gamma ray. The N^{15} yield was corrected for the bombarding energy change necessary to obtain the off resonance spectra and for angular distribution effects. The yield in the region of the Sc^{41} line was then corrected for the effects of the N^{15} line. This correction was as much as 50% at one angle at the 3.965 MeV resonance, but was no more than 15% for the other two resonances. The uncertainties in the points of the angular distributions for these states are those already mentioned of statistics and of analysis procedure, and an additional 5-15% caused by the necessary treatment of the N^{15} contaminations, estimated by changing this correction within reasonable limits.

c. Gamma Ray Angular Distributions

Angular distributions of the ground state gamma decays of 16 resonances were obtained comprising all but 4 of those occurring below E_p = 4.1 MeV, the region of primary interest in this phase of the investigation.

The distributions were fitted with a legendre polynomial expansion of the following form:

$$W(\theta) = 1 + a_2 P_2(\cos\theta) + a_4 P_4(\cos\theta)$$

The legendre polynomial coefficients a_2 and a_4, as well as their deviations, were obtained by least square fits to the data with the aid of a computer and were corrected for the finite solid angle subtended by the detectors by the method of Rose[28]. The distributions resulting from the least square fits are shown by the lines through the data Figure 21. The bars indicate the error on the data points obtained as discussed earlier. For the 3 point distributions a least square fit was unnecessary as the coefficients could be calculated directly from the data points. Table 6 lists the experimental coefficients obtained, and the coefficients after the solid angle correction, which are to be compared with theoretical coefficients. The states for which the coefficients exhibit the largest error are those for which only 3 point angular distributions were obtained, due to the low yields of the resonances in question. This was the case for the resonances located at bombarding energies of 1.541, 1.620, 1.934 and 3.240 MeV. Only 4 points were obtained for the weak resonance at 3.440 MeV, due to a failure of the accelerator during the course of the measurement. For the resonance at 3.019 MeV, one of the two measured using a target not coated with gold, evaporation of the target by the beam reduced the yield substantially at one of the five angles taken. Consequently one angle had to be discarded and only a four point distribution was obtained.

FIGURE 21

The angular distributions obtained for gamma decay to the Sc^{41} ground state of the resonances investigated are shown. The bombarding energy of each resonance is indicated. The data was normalized to either 0° or 90°, whichever was the greater. The curves are least square fits to the data. The bars indicate the errors.

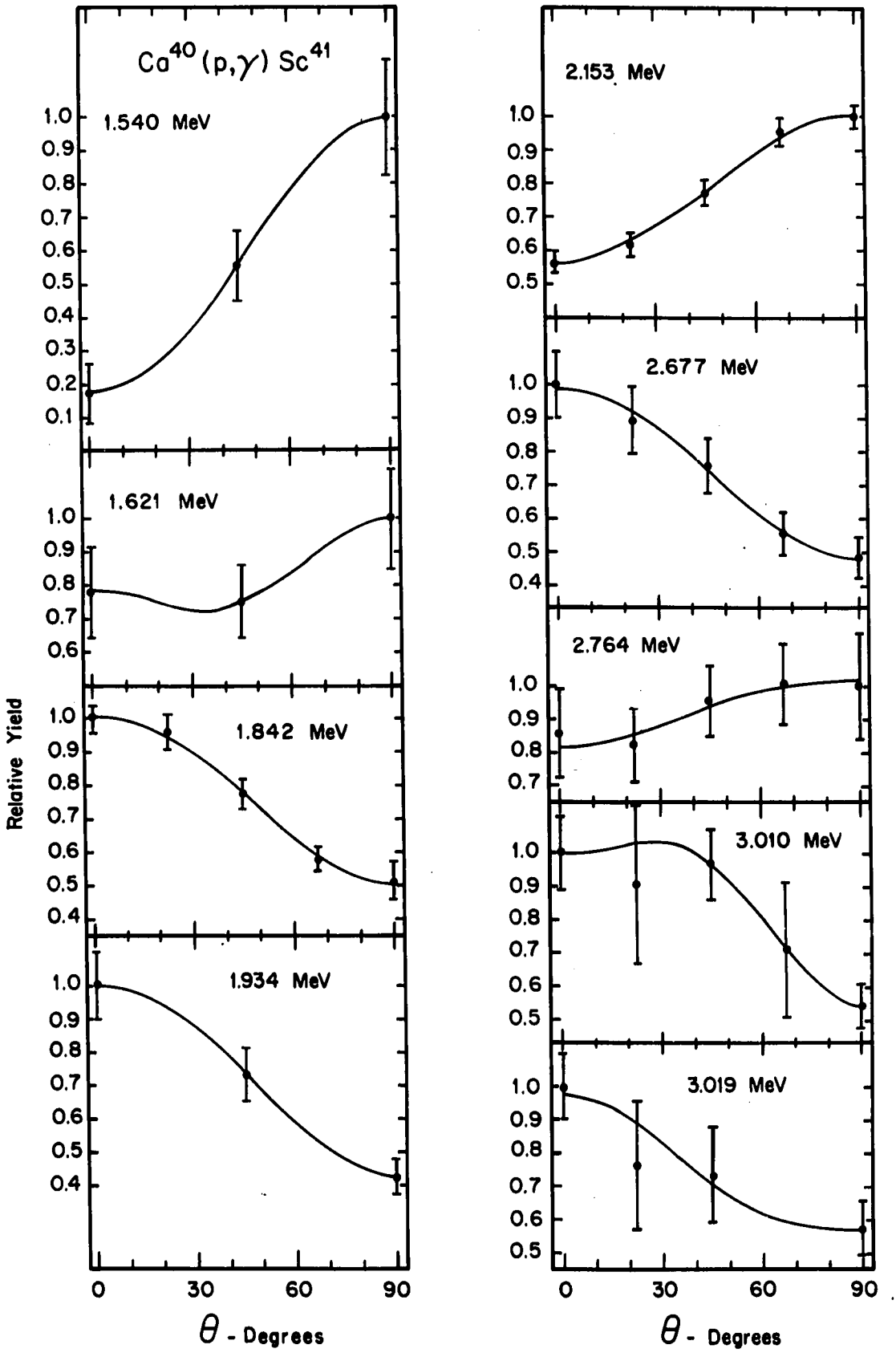
$Ca^{40}(p,\gamma)\ Sc^{41}$
1.540 MeV
1.621 MeV
1.842 MeV
1.934 MeV
2.153 MeV
2.677 MeV
2.764 MeV
3.010 MeV
3.019 MeV
Relative Yield
θ - Degrees
θ - Degrees

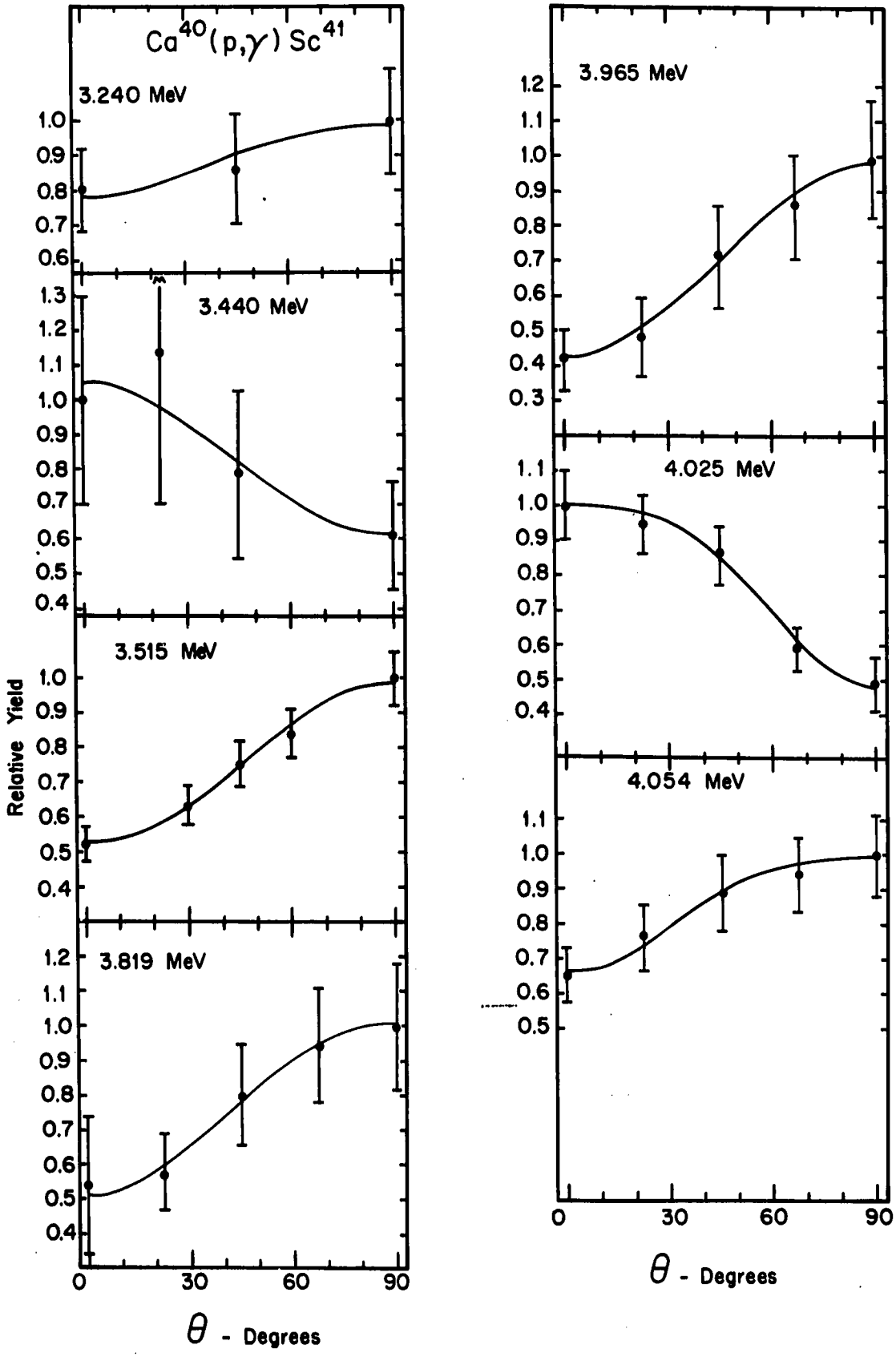
$Ca^{40}(p,\gamma)Sc^{41}$
3.240 MeV
3.440 MeV
3.515 MeV
3.819 MeV
3.965 MeV
4.025 MeV
4.054 MeV
Relative Yield
θ - Degrees
θ - Degrees

TABLE 6

Legendre Polynomial Coefficients Obtained

E_r (MeV)	Experimental		Corrected	
	a_2	a_4	a_2	a_4
1.540	-0.793	0.046	-1.02±0.34	0.12±0.51
1.621	-0.233	0.152	-0.30±0.28	0.39±0.47
1.842	0.502	-0.029	0.52±0.03	-0.03±0.03
1.934	0.616	-0.031	0.69±0.21	-0.04±0.25
2.153	-0.349	+0.011	-0.39±0.02	0.02±0.03
2.677	0.521	0.028	0.54±0.03	0.03±0.04
2.764	-0.126	-0.019	-0.14±0.05	-0.03±0.08
3.010	+0.466	-0.229	0.52±0.03	-0.34±0.05
3.019	+0.360	0.099	0.40±0.14	0.15±0.24
3.240	-0.161	0.041	-0.18±0.20	0.06±0.30
3.440	0.377	0.016	0.42±0.15	0.02±0.25
3.515	-0.378	0.011	-0.39±0.03	0.01±0.03
3.819	-0.381	-0.024	-0.39±0.04	-0.03±0.05
3.965	-0.479	0.005	-0.50±0.04	+0.01±0.05
4.025	0.545	-0.140	0.56±0.04	-0.16±0.06
4.054	-0.205	-0.071	-0.21±0.03	-0.08±0.04

4. Analysis and Discussion of Results

a. Introduction

The angular momentum of the states of the compound nucleus Sc^{41} can take on only the values $\ell \pm 1/2$, where ℓ is the angular momentum in units of $\hbar$ of the incoming proton, as a result of 0 spin of the target nucleus Ca^{40}. In the elastic scattering experiments by Brown, no orbital angular momentum higher than 4 was observed and thus guided by this result we will, in this discussion, assume the range of ℓ-values to be similarly limited. This leads to a maximum spin of $9/2^+$ for the Sc^{41} states formed in the proton capture reaction. Transitions to the $f_{7/2}$ ground state can then be expected from initial states having all spins from J = 3/2 to J = 9/2. In each case we will consider only the lowest multipole orders, except where natural mixing (M1 + E2) may occur it has been taken into account. Transitions from states of J = 1/2 may be excluded due both to the fact that higher multipolarities are necessary for the ground state transition and the fact that intermediate states are available through which they may decay by lower multipolarities.

The theory which describes the angular distributions of these transitions is well known and has been used to calculate the angular distributions for the various possible cases. The results are listed in Table 7. The distributions are given by[29]:

$$W(\Theta) = \sum_{tt'} S_t S_{t'}^* W_{tt'}$$

where S_t are "matrix elements" and t and t' are labels for interfering transitions.

TABLE 7

Angular Distributions for Gamma Ray Transition to a $7/2^-$ Final State from an Initial State of Spin and Parity J^π :

Pure Transitions

$$W(\Theta) = 1 + a_2 P_2(\cos\Theta) + a_4 P_4(\cos\Theta)$$

J^π	Type of Transition	a_2	a_4
$3/2^-$	E2	+.143	0
$5/2^+$	E1	-.143	0
$7/2^+$	E1	+.476	0
$9/2^+$	E1	-.333	0

Mixed Transitions

$$W(\Theta) = W_1 + x^2 W_2 + xW_{12}, \quad x = \left|\frac{S_E}{S_M}\right|$$

$$W_1 = A_0 + A_2 P_2(\cos\Theta) + A_4 P_4(\cos\Theta)$$

$$W_{12} = A_2 P_2(\cos\Theta)$$

J^π	Type of Transition	W_1 A_0	W_1 A_2	W_1 A_4	W_2 A_0	W_2 A_2	W_2 A_4	W_{12} A_2
$3/2^+$	M2 + E3	1.0	0.14	0	1.0	-0.50	0	-0.46
$5/2^-$	M1 + E2	1.0	-0.14	0	1.0	-0.35	0.11	-0.74
$7/2^-$	M1 + E2	1.0	0.47	0	1.0	-0.27	-0.49	-0.41

For a (p,γ) reaction $W_{tt'}$ is of the form:

$$W_{tt'} = \sum_k (-1)^{s-I} Z(\ell J \ell' J' s k)\, Z_1(LJL'J'Ik)\, P_k(\cos\theta)$$

where $\text{MAX}(|\ell-\ell'|, |L-L'|, |J-J'|) \le k \le \text{MIN}(\ell+\ell', L+L', J+J')$

$P_k(\cos\theta)$ are the legendre polynomials

Z and Z_1 are angular momentum coupling coefficients

ℓ is the orbital angular momentum of the incoming proton

J is the spin of the compound state

s is the channel spin

L is the multipole order of the gamma decay

I is the spin of the final state.

Conservation of parity requires that both $\ell+\ell'+k$ and $L+\pi+L'+\pi'+k$ be even. Note that in the absence of interference between two levels of opposite parity this implies that only even order legendre polynomial terms are present in the distribution. If we consider interference between two possible types of radiation only, then the distribution may be written in the form:

$$W(\theta) = W_M + x^2 W_E + x W_{ME}$$

where the subscripts refer to the type of transition and the mixing ratio x is defined as:

$$x = \left|\frac{S_E}{S_M}\right|$$

and may assume any value. It is seen that this is the amplitude ratio

of the electric to the magnetic transition, as used above. Figure 22 shows the legendre coefficients for each J plotted as a function of the mixing ratio x.

Experimental distributions in many cases could accommodate 2 or more J values for each state. In the interest of narrowing the range of choices, use was made of the quantity $g\Gamma_{\gamma_{g.s.}}$ obtained for each state in the manner described in Chapter I. Rough gamma ray yield determinations for each of the resonances confirmed the conjecture mentioned earlier that most of the positron yield measured on these resonances is attributable to a gamma ray transition directly to the ground state. Hence the value of $g\Gamma_{\gamma_{g.s.}}$ obtained via the positron measurement may indeed be used to estimate the lifetimes of the states.

A useful way of expressing a transition strength is in terms of the strength of a transition of the same energy and type calculated assuming the extreme one-particle model. The values of transition probability obtained with this model are called the Weisskopf[30,31] units (Γ_{γ_W}). If the observed radiative width is Γ_γ, the transition is said to have a strength of $|M|^2 = \Gamma_\gamma/\Gamma_{\gamma_W}$ Weisskopf units. $|M|^2$ is a measure of the square of the matrix element of the actual transition relative to that of the extreme one-particle transition. The range of $|M|^2$ to be expected for transitions of various multipole orders has been investigated empirically following procedures introduced by Wilkinson[31] and is shown in Figure 23. The data were taken from the tabulation of Booth, et al.[32], and from the tabulation of nuclear lifetimes in Appendix 3 of Siegbahn[33]. The data tabulated

FIGURE 22

The legendre coefficient A_2/A_0 and A_4/A_0 are shown for initial states of 3 different J^{π} values as a function of the mixing ratio for transitions to a $7/2^-$ ground state. The transition types are indicated.

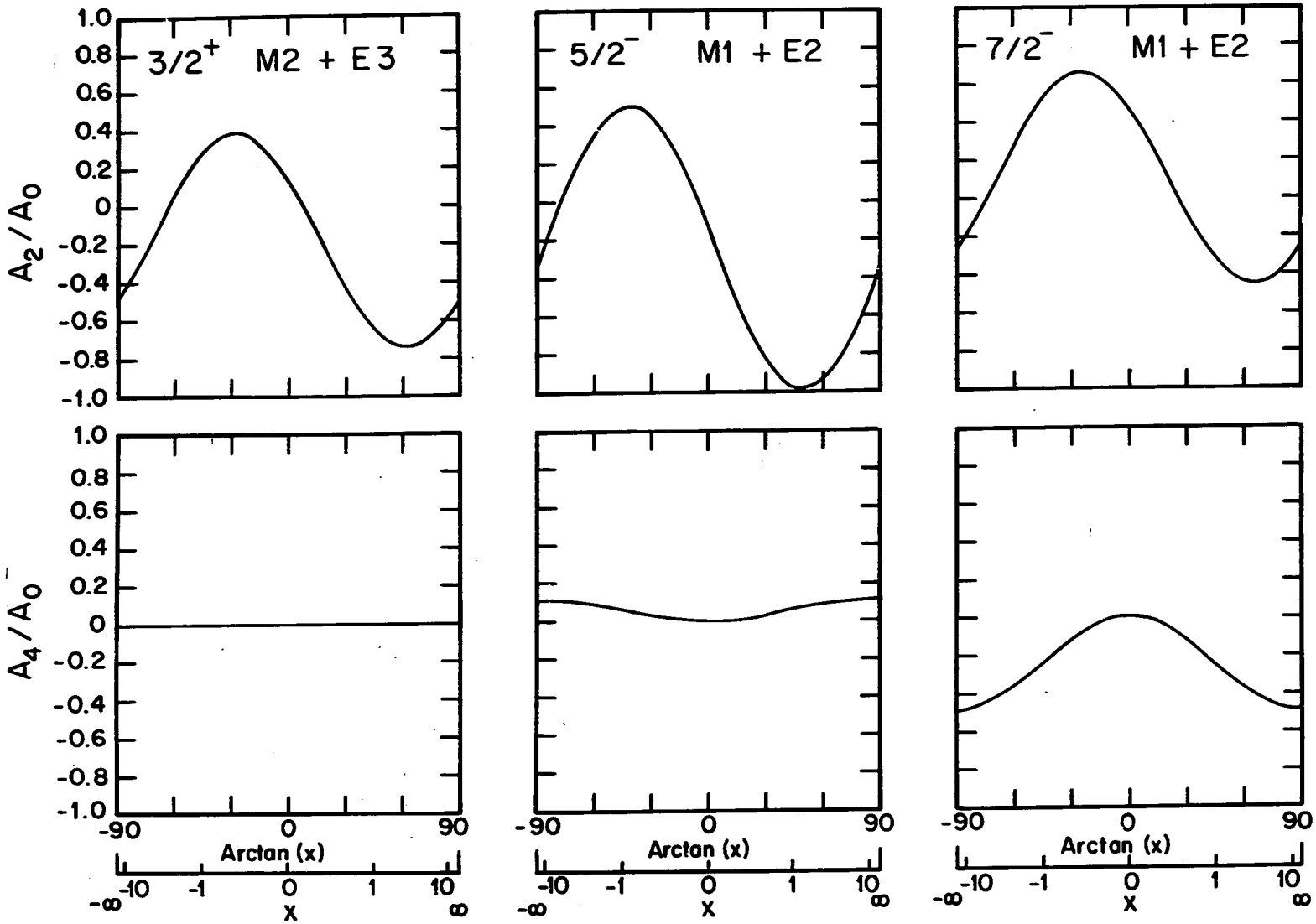
3/2+ M2 + E3
5/2− M1 + E2
7/2− M1 + E2
A2 / A0
A4 / A0
1.0
0.8
0.6
0.4
0.2
0
-0.2
-0.4
-0.6
-0.8
-1.0
-90
0
90
Arctan (x)
-∞
-10
-1
0
1
10
∞
X

FIGURE 23

The number of observed examples of each case is plotted as a function of $|M|^2 = \Gamma_\gamma / \Gamma_{\gamma_W}$ for various multipole orders. The numbers in each block represent the atomic number of the nucleus for which the transition was observed. The transitions indicated by the dotted lines were observed in this measurement.

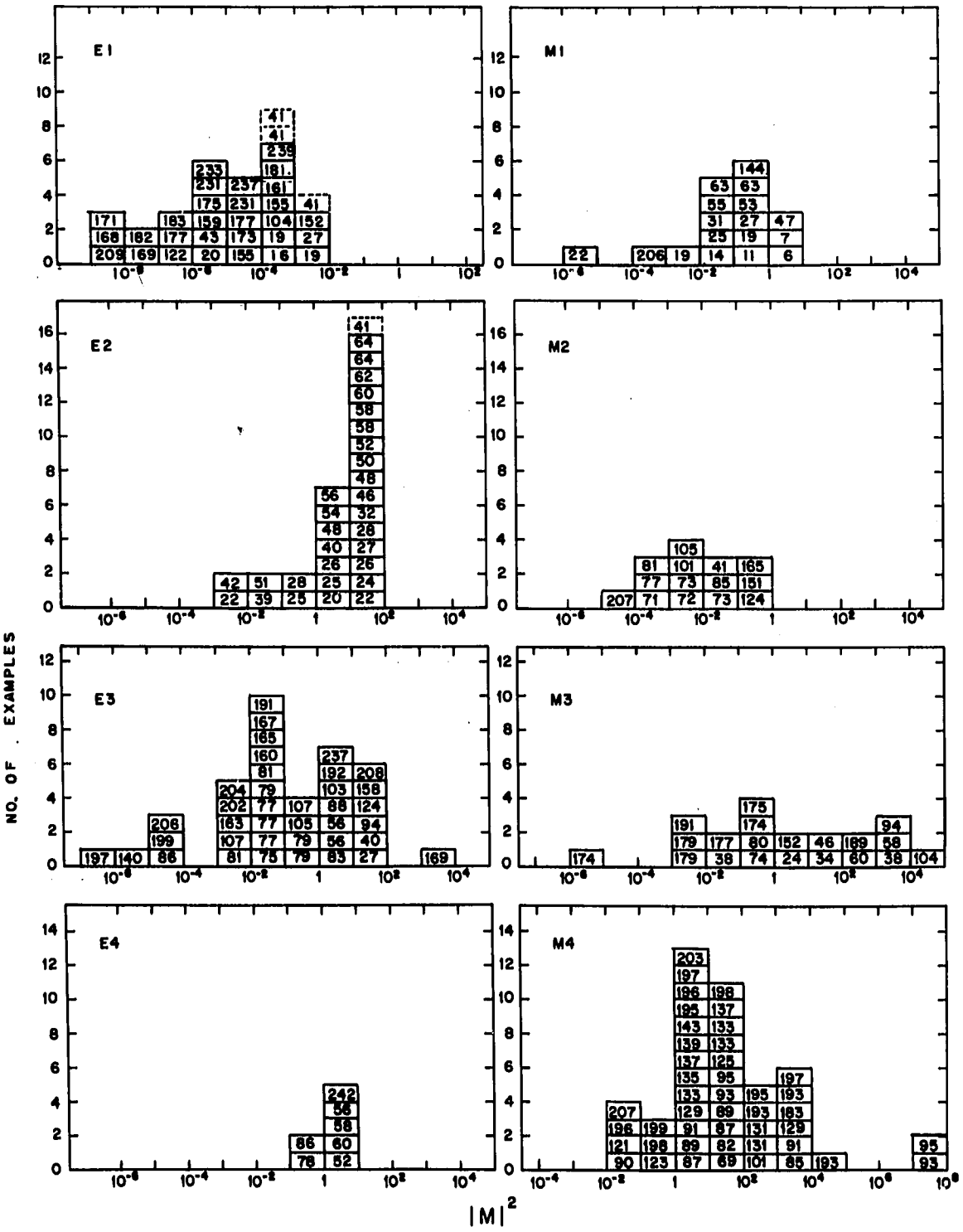
E1
M1
E2
M2
E3
M3
E4
M4
NO. OF EXAMPLES
|M|²

in Siegbahn listed the nuclear lifetime and the multipole order and type of transition, but did not include the ratio to the Weisskopf units. These were calculated using the form given by Wilkinson. The atomic number of the nucleus involved in indicated for each transition.

b. Assignments

On the basis of lifetime alone, states of total spin 1/2 are excluded. These would be either E3 or M3 transitions, and for the gamma decays observed would require transition speeds greater than 10^5 Weisskopf units, much faster than any known transitions of this type.

States of total spin 3/2 must be broken into 2 groups according to their parity. The $3/2^-$ states would be E2 transitions, expected to be enhanced, but would require a pure E2 gamma ray angular distribution. Angular distributions compatible with this pure multipole were not obtained for any of the states observed. (However as discussed in Chapter II the first excited state of Sc^{41} has a lifetime in good agreement with that expected for these transitions and for this reason as well as others mentioned earlier is assigned $3/2^-$.) If the states observed are $3/2^+$ states, the resultant M2 radiation would have a radiative width of 10^2-10^3 Weisskopf units. E3 decay of these states would require a width of 10^5-10^6 Weisskopf units. Both of these are outside of the range of known transitions of these types. Thus none of the states for which ground state gamma ray transitions are observed should be $3/2^+$ states.

J = 5/2 and J = 7/2 states may decay to the ground state of Sc^{41} by either an E1 transition ($5/2^+$, $7/2^+$) or an M1 + E2 transition ($5/2^-$, $7/2^-$). The radiative widths for these types overlap greatly so that no discrimination is possible on this basis. If, however, mixing is required, then states of negative parity are favored. The $9/2^+$ case is also a pure E1 transition.

In Figure 24 the coefficients obtained for each of the states observed are superimposed on the plots of a_2, a_4 as a function of the mixing ratio for the possible J values of the state. The figure for the 1.621 MeV resonance shows the a_2 and a_4 values for all possible spins. In Table 8 the possible spins and corresponding radiative widths (in Weisskopf units) derived from the positron results are indicated for the states for which angular distribution measurements were obtained. A discussion of the factors influencing the spin assignment for individual resonances is given below. Only those spins indicated possible by the legendre coefficients are discussed.

The data on the 1.540 MeV state is consistent with a $5/2^-$ assignment and an M1-E2 mixing ratio of .25. $J^\pi = 3/2^+$ is excluded on the basis of lifetime only.

The 1.621 MeV state could be either 5/2 or $9/2^+$ with correspondingly pure transitions (E1 or M1). A $3/2^+$ assignment is excluded on the basis of lifetime. It could also be $7/2^-$ with an M1-E2 mixing ratio for the transition of .55.

The 1.842 state is definitely J = 7/2, the transition requiring only a small quadrupole admixture. Odd parity is slightly favored

FIGURE 24

The legendre coefficients $a_2(=A_2/A_0)$ and $a_4(=A_4/A_0)$ obtained for each resonance are indicated by the cross-hatched regions. The curves are the theoretical coefficients for the various spins as indicated:

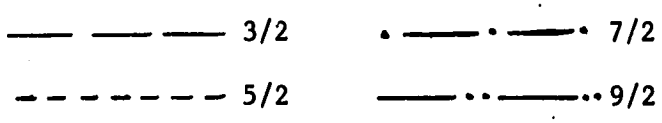

A spin value is possible for a given state only if the theoretical curves for both a_2 and a_4 overlap the experimental coefficients at the same value of x, the mixing ratio. Those theoretical curves for which this condition is obviously not met are not shown. For a pure transition this overlap should occur at x = 0 as it does for example in the case of the $5/2^+$, 2.764 MeV state which decays by E1 emission.

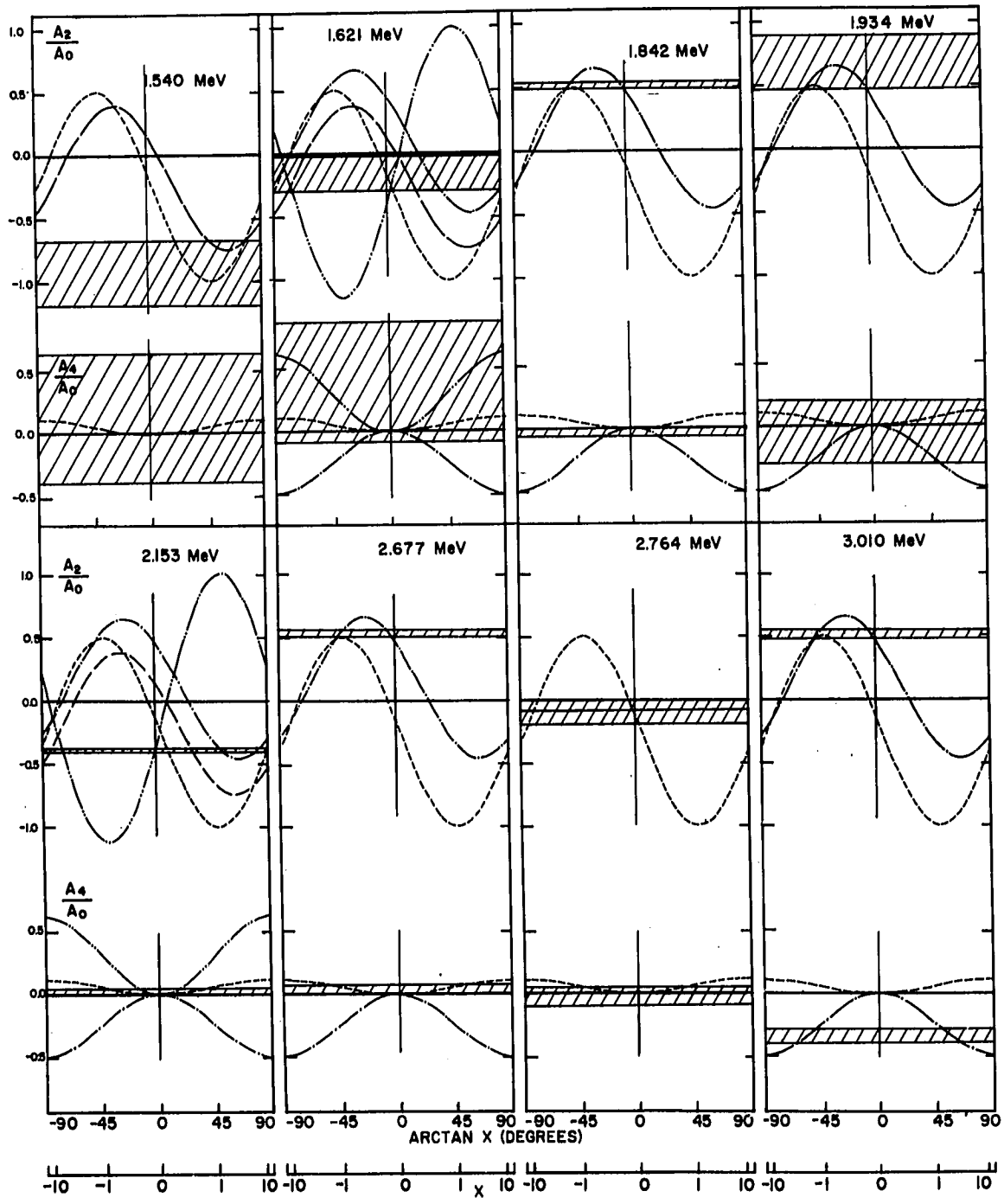
1.540 MeV
1.621 MeV
1.842 MeV
1.934 MeV
2.153 MeV
2.677 MeV
2.764 MeV
3.010 MeV
A2/A0
A4/A0
ARCTAN X (DEGREES)
X

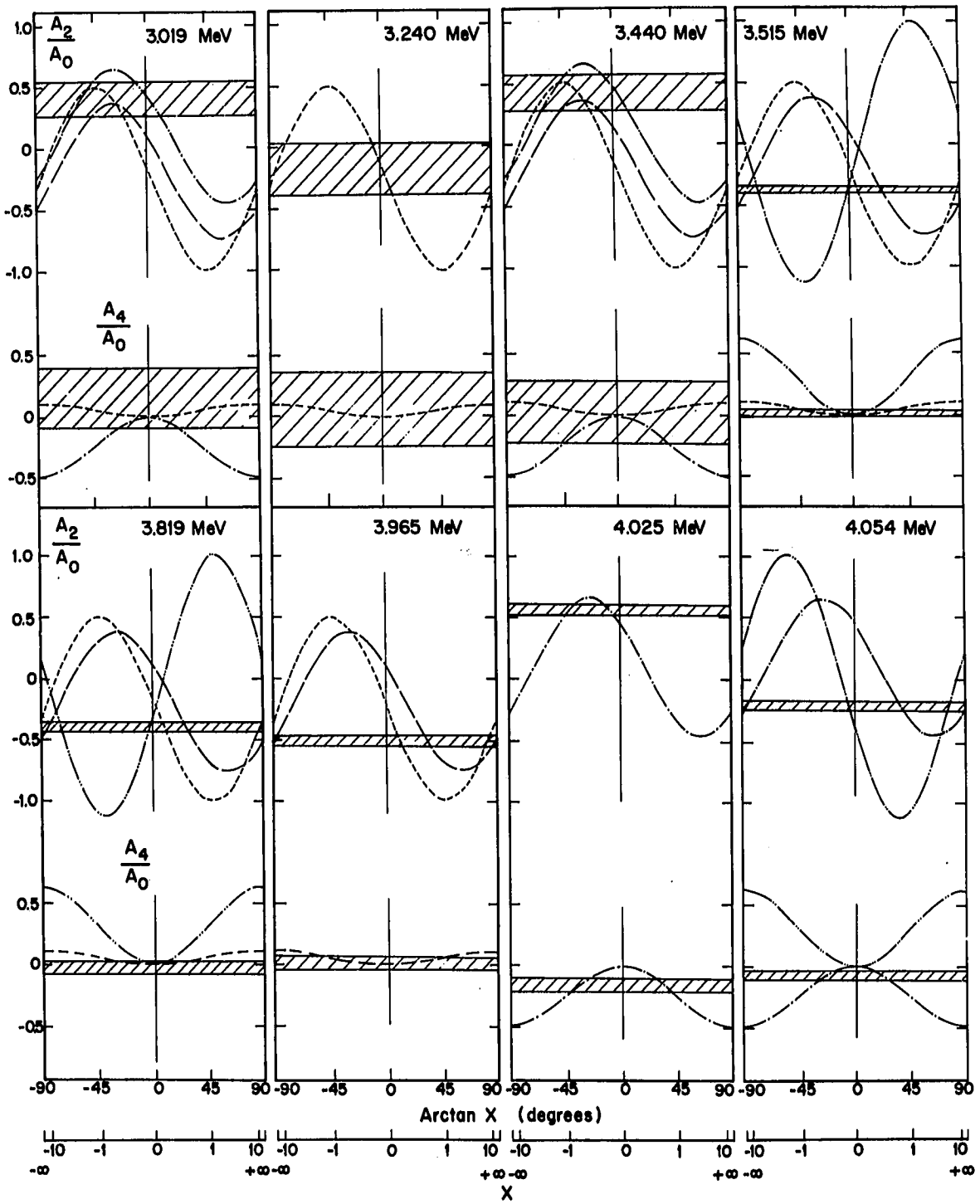
A2/A0
3.019 MeV
3.240 MeV
3.440 MeV
3.515 MeV
A4/A0
3.819 MeV
3.965 MeV
4.025 MeV
4.054 MeV
1.0
0.5
0
-0.5
-1.0
-90 -45 0 45 90
Arctan X (degrees)
-10 -1 0 1 10
-∞ +∞
X

TABLE 8

E_p (MeV)	E_{exc} (MeV)	Possible J	Transition Type	$g\Gamma_\gamma$ (ev)	$\|M\|^2$
1.540	2.584	$5/2^-$	M1 + E2	.013	1.1×10^{-2}
1.621	2.663	5/2	E1	.014	3.0×10^{-4}
			M1		1.1×10^{-2}
		$9/2^+$	E1		1.8×10^{-4}
		$7/2^-$	M1 + E2		8.8×10^{-3}
1.842	2.879	7/2	E1	.193	2.5×10^{-3}
			M1		9.6×10^{-2}
1.934	2.969	$5/2^-$	M1 + E2	.040	2.4×10^{-2}
		7/2	E1		4.7×10^{-4}
			M1		1.8×10^{-2}
2.153	3.182	$5/2^-$	M1 + E2	.131	6.5×10^{-2}
		$9/2^+$	E1		1.0×10^{-3}
2.677	3.693	7/2	E1	.279	1.7×10^{-3}
			M1		6.6×10^{-2}
		$(5/2^-)$	M1 + E2		8.8×10^{-2}
2.764	3.778	$5/2^+$	E1	.075	5.7×10^{-4}
3.010	4.018	$7/2^-$	M1 + E2	.064	1.1×10^{-2}
3.019	4.027	$5/2^-$	M1 + E2	.100	2.4×10^{-2}
		7/2	E1		4.7×10^{-4}
			M1		1.8×10^{-2}
3.240	4.242	$5/2^+$	E1	.154	8.5×10^{-4}
3.440	4.437	$5/2^-$	M1 + E2	.050	9.1×10^{-3}
		7/2	E1		1.8×10^{-4}
			M1		6.8×10^{-3}
3.515	4.511	$5/2^-$	M1 + E2	.249	4.3×10^{-2}
		$9/2^+$	E1		6.7×10^{-4}
3.819	4.808	$5/2^-$	M1 + E2	.280	4.0×10^{-2}
		$9/2^+$	E1		6.3×10^{-4}
3.965	4.950	$5/2^-$	M1 + E2	.275	3.6×10^{-2}
4.025	5.008	$7/2^-$	M1 + E2	.506	4.7×10^{-2}
4.054	5.036	$9/2^+$	E1	1.648	3.2×10^{-3}

The value of $|M|^2$ assumes pure E1 or M1 radiation.

within the margins of known experimental error, but could become positive if small undetected errors were present. A distinction of parities on the basis of lifetime is impossible, since it is within the expected range for both M1 and E1 transitions.

The 1.934 MeV state may be $J = 5/2^-$, the transition requiring an M1-E2 mixing ratio of .8, or 7/2 with no mixing.

The 2.153 MeV state may be $J = 9/2^+$, requiring only small mixing of M2 with E1, possibly due to slight undetected experimental errors. The lifetime is consistent with that expected for an E1 transition. A J^π of $3/2^+$ is possible, but ruled out on the basis of lifetime. A J^π of $5/2^-$ requiring an M1-E2 mixing ratio of .16 is also possible. A $5/2^-$ assignment, requiring formation by $\ell = 3$ protons might perhaps be favored in preference to the $9/2^+$ assignment, requiring formation by $\ell = 4$ protons, at this low bombarding energy.

The 2.677 MeV state is most likely $J = 7/2$. As in the case of the 1.842 MeV state, negative parity is favored but with reservations. An assignment of $5/2^-$ may not be disregarded entirely, as this coefficient is only slightly outside the error, but for this case both a_2 and a_4 would have to be at the extreme of error. The lifetime of the state is of no assistance.

The 2.764 MeV state has been observed in the elastic scattering results and assigned $\ell = 2$ by Brown. The distribution we obtain is compatible with a $5/2^+$ state decaying by a pure E1 transition. The $3/2^+$ case may be eliminated on the basis of lifetime. The lifetime is within the expected range and is shown dotted in Figure 23.

The only assignment possible for 3.010 state is $7/2^-$ with an M1-E2 mixing ratio of 1.1. This is due to the large a_4 obtained, ruling out any other possibilities.

The 3.019 MeV state may be $J = 5/2^-$ with an M1-E2 mixing ratio for the transition of about 1.3, or $J = 7/2$, the transition being either pure E1 or M1 radiation. $3/2^+$ is ruled out only by the lifetime of the state.

The 3.240 MeV state has been assigned $\ell = 2$ by Brown and the distribution obtained is compatible with a $5/2^+$ assignment. The lifetime is within the expected range and is shown in Figure 23.

The 3.440 MeV state may be either $J = 5/2^-$ with an M1-E2 mixing ratio for the transition of between 0.4 and 1.4, or $J = 7/2$, the transition being either pure E1 or M1 radiation. $3/2^+$ is ruled out only by the lifetime of the state.

The 3.515 MeV state may be either $J = 5/2^-$ with M1-E2 mixing ratio for the transition of .08 to .16, or $J = 9/2^+$ decaying by E1 radiation. No distinction is possible on the basis of the lifetime of the state.

The 3.819 MeV state might also be $J = 5/2^-$, with an M1-E2 mixing ratio for the transition of about 1.6 or $J = 9/2^+$ if a small undetected error is present.

The 3.965 state is a more difficult problem. Brown has observed an $\ell = 2$ state at 3.959 MeV and an $\ell = 3$ state at 3.962 MeV and it is not known whether the state observed in the (p,γ) is one or both of these. A comparison of energies obtained for states observed in

both experiments favors the $\ell = 3$ however. If we assume it is one or the other, then from the angular distributions obtained only $5/2^-$ (M1 + E2) and $3/2^+$ (M2 + E3) are possible since mixing is required to obtain a_2. The $3/2^+$ may be rejected because the width of the state, expressed in Weisskopf units, is much greater than has been observed for M2 or E3 transitions. Thus it appears that the state observed in the (p,γ) is the $\ell = 3$, $5/2^-$ state. The data is insufficient to tell whether there are any odd order legendre polynomial terms, which should be present if there is significant interference between the $\ell = 2$ and $\ell = 3$ states. This could also cause a_2 and a_4 to be in error. Thus if we are seeing only one of the resonances, then it is the $\ell = 3$, and if not no assignment is possible with the present data.

The 4.025 state is a $7/2^-$ state with an M1-E2 mixing ratio for the transition of 0.8 required to satisfy both the a_2 and a_4 coefficients obtained.

The 4.054 MeV state, assigned $\ell = 4$ by Brown, appears to be a $9/2^+$ state. a_2 obtained for this state is smaller than the theoretical value, and the a_4 coefficient is slightly negative, whereas it should be zero for a pure E1 or positive if there is any E1 + M2 mixture. However the N^{15} gamma ray background on which the gamma ray from this state resides in the spectra taken has $a_2 = +.33$, $a_4 = -.05$, so that if the amount of N^{15} gamma radiation present were underestimated the coefficients obtained for the Sc^{41} resonance would be in error in the direction noted. If we were to consider this state a $7/2^+$ state, an E1-M2 mixing ratio of .36 to .50 is required to obtain

a_4 while from .60 to .80 is required to obtain a_2. Due to this discrepancy and the necessity of invoking E1 + M2 mixture to obtain the coefficients using the $7/2^+$ assignment, this is discarded. The lifetime of this state, also indicated by one of the dashed boxes in Figure 23, is as expected for an E1 transition.

CHAPTER V

The Half Life and Mass of Sc^{41}†

Abstract

The half life and mass of Sc^{41} have been determined by measurements utilizing resonances of the $Ca^{40}(p,\gamma)Sc^{41}$ reaction. A value of 0.596 ± 0.006 seconds was obtained for the half life. The Q-value of the reaction was determined to be 1.083 ± 0.006 MeV, corresponding to a Sc^{41} mass excess of $-28,640 \pm 10$ keV on the C^{12} mass scale. These results lead to a log ft value of 3.443 for the Sc^{41} positron decay.

---

† This chapter represents a paper submitted for publication and is completely self-contained.

I. Introduction

The $Ca^{40}(p,\gamma)Sc^{41}$ reaction, recently investigated in the range of bombarding energy between 0.6 and 5.0 MeV, shows numerous resonances for radiative capture to the ground state[1]. In the present work, the mass of Sc^{41} was determined by measuring the Q-value for the reaction at two of the most prominent resonances. At resonance, the reaction also provides a unique means of producing a source of Sc^{41} positron activity uncontaminated by radioactive products caused by competing reactions. This circumstance has made possible the measurement of the half life of Sc^{41} for the first time without interference from an extraneous activity of comparable half life and endpoint energy.

In previous determinations of the half life, the activity has been produced by the $Ca^{40}(d,n)Sc^{41}$ reaction in all cases except one in which the $Ca^{40}(p,\gamma_0)Sc^{41}$ reaction was used at a bombarding energy of 30 MeV[2,3]. The Sc^{41} activity produced in either way is accompanied by positron activity from a potassium isotope formed in a competing (d,α) or (p,α) reaction. The occurrence of the extraneous activity generally has been overlooked. Recently, several measurements have been reported, using the $Ca^{40}(d,n)Sc^{41}$[4,5] reaction, in which the effect of the interfering activity was taken into account. These measurements yielded a value for the half life of about 0.6 sec, as compared to the previous value of 0.87 sec, but with an uncertainty of 2 to 5% because of the nature of the procedures used to deal with the extraneous component.

The mass of Sc^{41} has been determined once before by measurement of the $Ca^{40}(p,\gamma)Sc^{41}$ reaction Q-value[6]. The value obtained in the present work, using somewhat improved experimental techniques, agrees with the previous result but lies within narrower limits of error. Both values agree well with those derived from Q-value measurements of other reactions[7].

II. Measurements and Results

a) The half life of the Sc^{41} positron decay. The Sc^{41} activity was produced by bombarding a calcium target about 70 keV thick with 4.05 MeV protons to excite two of the strongest known capture resonances. The bombardment was interrupted cyclicly by electrostatically deflecting the beam for periods of 6 sec, during which time the decay of the activity was measured. The target was made by evaporating natural calcium metal onto a 100 mg/cm^2 thick gold foil which terminated the beam tube. The foil absorbed the proton beam but transmitted positrons with negligible energy loss.

The β-radiation from the source was detected by a low-resolution β-ray spectrometer consisting of two nested plastic scintillators arranged, as shown in the insert to Figure 1, to subtend a solid angle at the target approaching 2π steradians. Positrons having an energy of about 5.5 MeV -- corresponding to the endpoint energy of the Sc^{41} spectrum -- sustained an energy loss of 900 keV in traversing the thin forward detector, and were absorbed by the thick detector behind. Each scintillator was coupled optically to a Dumont 6363 photomultiplier

tube whose output, after amplification, was sent to a coincidence circuit set to operate as a resolving time of 60 nano-seconds. The coincidence output pulses from this circuit were counted as a function of time by a TMC 400 channel analyzer operating in the "multiscaler" mode. In this mode, the analyzer counts all input pulses in one channel, but advances that channel at regular intervals (10 milliseconds in the present work) until all 400 channels have been used, at which time it automatically stops. Data was accumulated during many consecutive sweeps through the 400 channels, each sweep being triggered by a signal from the switching circuitry controlling the deflection of the beam. The elapsed time scale of the analyzer was calibrated by measuring both 100 kcps and 1 kcps signals supplied by crystal controlled oscillators.

The contribution of background to the counting rate during measurements of the activity was very much reduced by counting in coincidence. It was reduced further by setting a discriminator on the amplified output of the large counter so as to pass only those pulses corresponding to energies greater than about 3 MeV, thereby eliminating interference from a number of possible low energy β-activities arising from light element target contaminants. Background never contributed more than 5% of the counts in the 400^{th} channel during the actual measurements.

The measurement of the decay of the Sc^{41} activity was followed immediately by a measurement of the decay of Li^{8}, produced by the $Li^{7}(d,p)Li^{8}$ reaction, in order to check the reliability of the

experimental procedures. The half life of Li^8 is comparable to that of Sc^{41} and its value is among those most accurately known[8]. The data obtained in these measurements are shown in Fig. 1. The lines shown are those given by a least squares analysis of the lagarithm of the counting rate versus time for data obtained in the first 3 seconds of decay. The values obtained for the half lives are 0.596 ± 0.006 seconds and 0.840 ± 0.012 seconds for Sc^{41} and Li^8, respectively. The errors quoted are the "standard deviations" due to the statistical scatter of the data, all other errors being negligible in comparison. The value for Sc^{41} compares with other recent values of 0.628 ± 0.014[4] and 0.55 ± 0.03 seconds[5]. The value given for the Li^8 half life by Ajzenberg and Lauritsen is $.848 \pm 0.004$[8].

b) The mass of Sc^{41}. The Q-value of the $Ca^{40}(p,\gamma)Sc^{41}$ reaction was determined from measurements made at two strong resonances occurring at bombarding energies of 1.84 and 2.68 MeV[1]. The thin target yield function of the reaction in the neighborhood of these resonances is shown in Fig. 2. It was obtained by measuring the Sc^{41} positron activity using the same experimental procedures as described above except that the coincidence yield was determined as a function of bombarding energy and the period of the bombarding-counting cycle was reduced to 0.2 seconds. As can be seen the resonance at the lower energy is well isolated and is located only 40 keV below the threshold of the $Li^7(p,n)Be^7$ reaction, one of the reactions used to calibrate the proton energy scale. The resonance at the upper energy, while not so well isolated, gives a yield a factor of approximately 150 greater than its nearest neighbor 20 keV away.

Figure 1

The decay curves for Sc^{41} and Li^{8}. The insert shows the arrangement of target and counters.

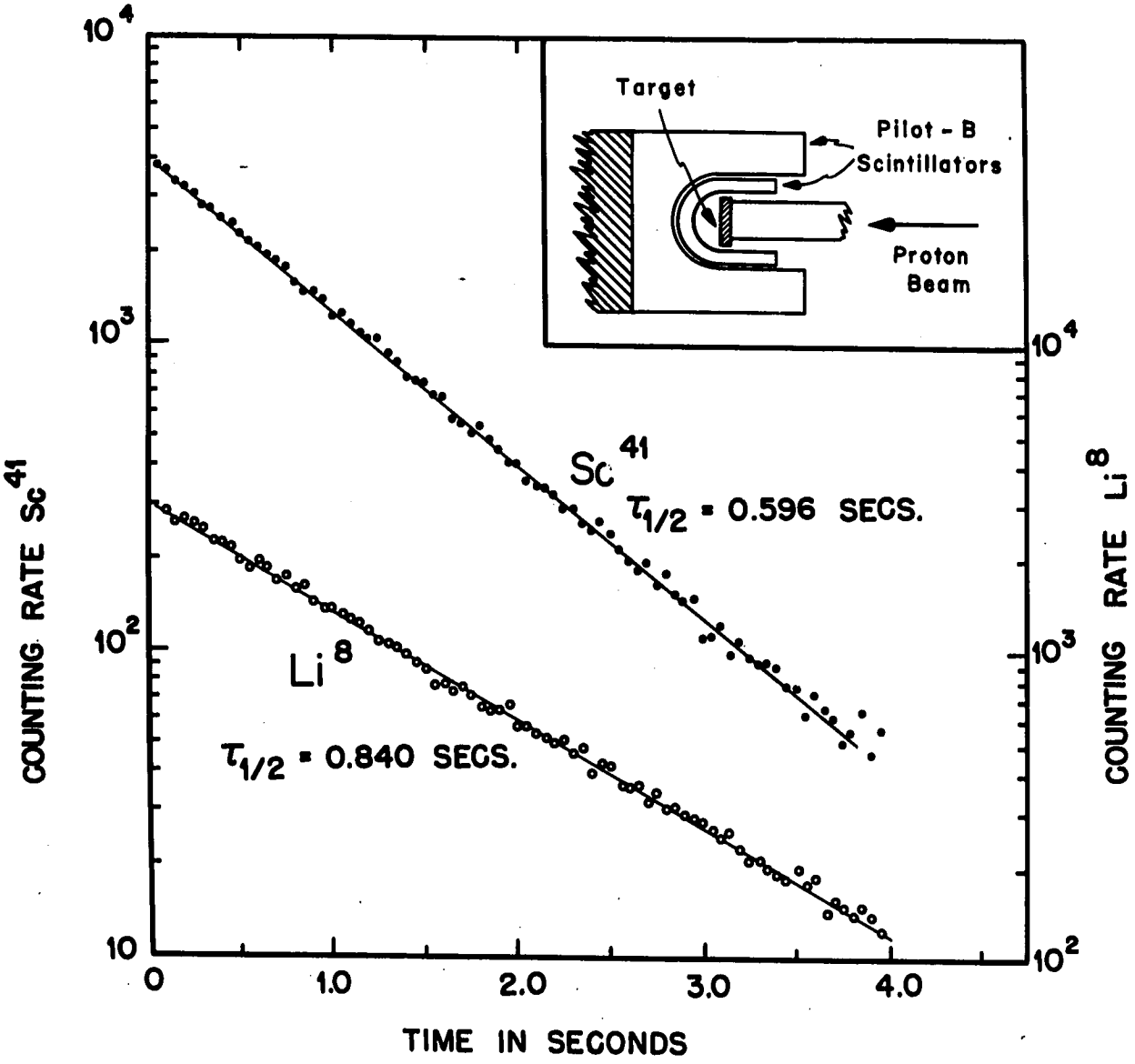
Target
Pilot - B
Scintillators
Proton
Beam
10^4
10^3
10^2
10
0
1.0
2.0
3.0
4.0
TIME IN SECONDS
COUNTING RATE Sc^{41}
COUNTING RATE Li^8
Sc^{41}
$\tau_{1/2}$ = 0.596 SECS.
Li^8
$\tau_{1/2}$ = 0.840 SECS.

Figure 2

Upper: The yield functions in the neighborhood of the two resonances of interest, measured with a 10 keV thick target.

Middle: The thick target yields at the resonances used for the Q-value measurements. The numbers labelling the data for the resonance at 2.677 MeV indicate the sequence in which the measurements were made.

Lower: The pulse height distributions of the 0.661 MeV Cs^{137} calibration γ-ray and the 2.880 MeV Sc^{41} γ-ray. The solid lines give the best Gaussian fits to the data. Dashed lines show the effect of a displacement of the Gaussian fits by 0.5 (3 keV) and 1.0 channels (6 keV), respectively, for the Cs^{137} and Sc^{41} γ-rays.

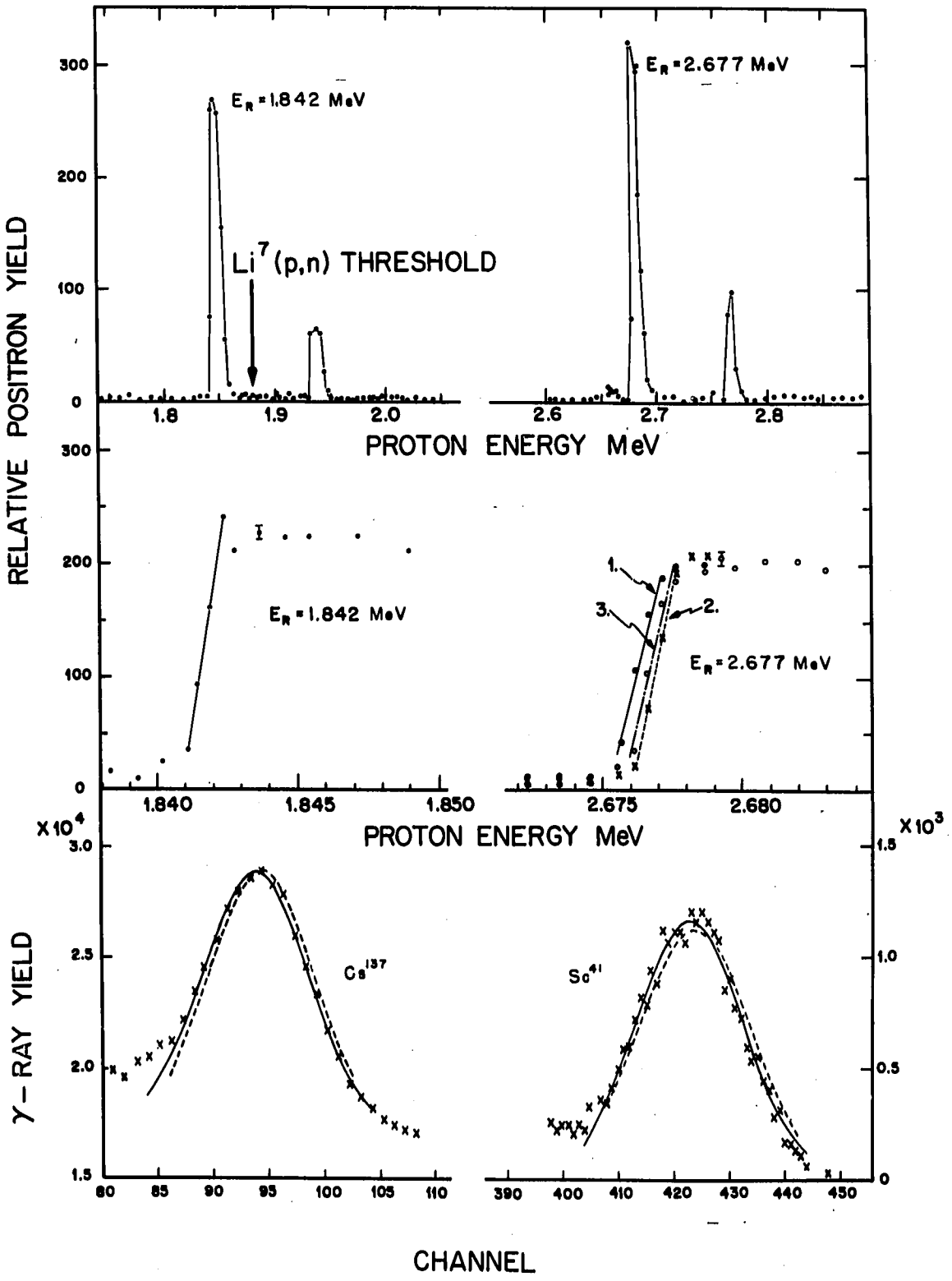
RELATIVE POSITRON YIELD
E_R = 1.842 MeV
E_R = 2.677 MeV
Li^7(p,n) THRESHOLD
PROTON ENERGY MeV
E_R = 1.842 MeV
E_R = 2.677 MeV
1.
2.
3.
PROTON ENERGY MeV
X 10^4
X 10^3
γ - RAY YIELD
Cs^{137}
Sc^{41}
CHANNEL

The energies assigned to the resonances were obtained from thick target yield measurements, representative results of which also are shown in Fig. 2. Three independent determinations of these energies were made. The targets were evaporated in situ just prior to measurement and were 10 to 50 keV thick. A section of the beam tube 30 inches long encased in a liquid air bath served as a trap to reduce buildup of target contaminants. Repeated measurements of the yield in the region of rise to the plateau reproduced to within $\pm$ 0.5 keV, as can be seen in the figure. The energies assigned to the resonances correspond to the midpoint of the rise of the yield curve. Corrections to these energies to take into account the Lewis effect[9] and the finite target thickness were negligible with respect to the magnitude of the other uncertainties in the measurement.

The proton bombarding energy was determined from the frequency of a nuclear magnetic resonance magnetometer having its probe located in the field of the 90° analyzing magnet of the accelerator[10]. The frequency scale of the magnetometer was calibrated in terms of energy by measuring the thresholds for the reactions[11]

$$Li^7(p,n)Be^7,\ E_{thr.} = 1.8807 \pm 0.0004 \text{ MeV}$$

and

$$C^{13}(p,n)N^{13},\ E_{thr.} = 3.2358 \pm 0.0011 \text{ MeV}.$$

Freshly prepared targets of Li^7 and C^{13} on gold backings were used. The threshold frequencies were determined using standard experimental procedures[12]. Repeated determinations of these frequencies for the two reactions fell, in each case, within a frequency interval corresponding to $\pm$ 0.5 keV.

The spectra of the capture radiations were obtained using a 3" x 3" NaI (Tl) crystal scintillation spectrometer. A combination of aluminum and lead absorbers shielded the crystal from the positron and low energy gamma radiations emanating from the target located about one inch away. The amplified output from the spectrometer was recorded by means of a 1024 channel pulse height analyzer. The energy calibration of the pulse height scale was accomplished by recording the spectra of γ-rays given by Cs^{137}, Co^{60}, Na^{24} and Pu-Be sources. Simultaneous calibrations using the cesium and cobalt sources were made first, at a counting rate large in comparison to those given by the Sc^{41} capture radiations. Both sources were left in place during all subsequent measurements in order to stabilize the gain of the system and also to provide internal reference lines of known energy in each spectrum. Calibrations with the Na^{24} and Pu-Be sources then were made at counting rates comparable to those encountered in the capture measurements. To check for long term drifts in the gain, spectra from all sources were recorded both before and after measurement of the capture radiation. A shift of one channel ($\sim$ 6 keV) was detected in one case during a run extending over a period of 5 hours.

The channel numbers to be associated with the energies of the γ-ray lines were specified by the maxima of gaussian distributions fitted to the data in the neighborhood of the full energy peaks. The fitting was done with the aid of a computer, programmed to calculate the "best" gaussian distributions as a function of the channel number specifying the maximum. The optimum position of the maximum was

determined when an error function proportional to the deviation of the calculated values from the data was minimized. The channel number specifying the optimum position was found to be uncertain to within about $\pm$ 1/4 channel for the calibration lines depending upon the particular shape assumed for the background underlying the peak. The energies of the six calibration lines were related to their positions on the pulse height scale by both linear and quadratic functions fitted to the data on the basis of a least squares criterion. The energies of the calibration lines recalculated using either of these functions agreed with the stated values to within $\pm$ 1 keV.

The spectra of the γ-rays from Sc^{41} were obtained by subtracting spectra recorded a few keV below resonance from those taken on resonance. Because of the subtraction of background and the relatively low yield of the gamma rays of interest, the statistical accuracy of the data describing the full energy peaks was considerably less than in the case of the calibration lines, and led to an uncertainty of $\pm$ 1/2 channel (3keV) and $\pm$ 1 channel (6 keV) in the location of the peaks associated with the resonances at E_p = 1.84 and 2.68 MeV, respectively.

The energies assigned to the gamma rays occurring in the transitions to the ground state are 2.880 $\pm$ 0.005 MeV and 3.694 $\pm$ 0.008 MeV for the resonances located at bombarding energies of 1.8417 $\pm$ 0.0015 MeV and 2.6766 $\pm$ 0.0020 MeV, respectively. The Q-values derived from these results are 1.0830 $\pm$ 0.006 and 1.0828 $\pm$ 0.009 MeV, respectively. Using a Q-value of 1.083 $\pm$ 0.006 MeV leads to a mass excess of Sc^{41} of

-28,640 ± 10 keV. An earlier determination of the Q-value of the $Ca^{40}(p,\gamma)Sc^{41}$ reaction gave 1.09 ± 0.02 MeV[6]. The value calculated from the tables of Konig, et al., is 1.082 ± 0.010[13].

The mass value of Konig[13] corresponds to an endpoint energy for the Sc^{41} positron spectrum of 5.474 MeV. This value together with the value of the half life determined by this experiment, leads to log ft = 3.443. The value of f was obtained by numerical evaluation of the integral of equation (19) in the National Bureau of Standards "Tables for the Analysis of Beta Spectra"[15].

References

1. J.P. Aldridge, III, N.A. Brown, C.M. Class and D. Youngblood, Bull. Am. Phys. Soc. Ser. II 9, 456 (1964).
2. D.R. Elliott and L.D.P. King, Phys. Rev. 60,489 (1941); R. Wallace and J.A. Welch. Phys. Rev. 117, 1297 (1960).
3. W.M. Martin and S.W. Breckon, Can. J. Phys. 30, 643 (1952).
4. J. Janecke, Z. Naturforsch, 15a, 593 (1960).
5. J.G. Cramer, Jr., and C.M. Class, Nuclear Physics 34, 580 (1962).
6. J.W. Butler, Phys. Rev. 123, 873 (1961).
7. H.E. Wegner and W.S. Hall, Phys. Rev. 119, 1654 (1960); B.E.F. Macefield, J.H. Towle and W.B. Bilboy, Proc. Phys. Soc. A77, 1050 (1961); S. Hinds and R. Middleton, see B.E.F. Macefield and J.H. Towle, Proc. Phys. Soc. 76, 56 (1960); G.F. Knoll, J.S. King and W.C. Parkinson, Phys. Rev. 131, 331 (1963).
8. F. Ajzenberg-Selove and T. Lauritsen, Nuclear Physics 11, 1 (1959).
9. H.W. Lewis, Phys. Rev. 125, 937 (1962); D.W. Palmer, J.G. Skofronick, D.G. Costello, A.L. Morsell, W.E. Kane and R.G. Herb, Phys. Rev. 130, 1153 (1963); D.G. Costello, J.G. Skofronick, A.L. Morsell, D.W. Palmer and R.G. Herb, Nuclear Physics 51, 113 (1964).
10. See, e.g. Nuclear Data Tables, Part 3, edited by J.B. Marion, p. 176 (1960).

11. J.B. Marion, Rev. Mod. Phys. 33, 139, 623 (1961).

12. J.B. Marion and T.W. Bonner, Fast Neutron Physics, Part II, edited by J.B. Marion and J.L. Fowler (Interscience Publishers, 1963), p. 1865.

13. L.A. Konig, J.H.E. Mattauch and A.H. Wapstra, Nuclear Physics 31, 18 (1962).

14. Y. Beers, Introduction to the Theory of Error (Addison-Wesley Publishing Co., Reading, Mass., 1957), Chaps. 4,5.

15. Table for the Analysis of Beta Spectra, National Bureau of Standards Applied Mathematics Series 13 (1952)(U.S. Government Printing Office, Washington, D.C.).

CHAPTER VI

Discussion

1. Comparison of Levels Seen in $Ca^{40}(p,p)Ca^{40}$ and in $Ca^{40}(p,\gamma)Sc^{41}$

The levels of Sc^{41} to be discussed in this section are shown in Figure 25 and listed in Table 9. The table includes preferred J values for those states for which the data are sufficient to support an assignment, and total widths and ℓ-values for those states seen in the elastic scattering measurements. $g\Gamma_{\gamma_{g.s.}}$ is also given for states seen in the (p,γ) measurements.

The discussion of the levels is presented in 3 sections; First, those seen in both experiments for which angular distributions were obtained on the gamma ray transition to the ground state, second, those observed in both experiments for which only positron decay data is available from the (p,γ), third, some $\ell = 2$ states observed only in the elastic scattering measurements, but for which spin values may be inferred. For 4 resonances observed in both reactions for which gamma ray angular distributions were obtained, definite J^{π} assignments could be made. The resonances in this category have been discussed in Chapter IV.

For 12 other resonances observed in both reactions for which no gamma ray angular distributions were obtained but where the ℓ values have been assigned by Brown[2], possible J^{π} values might be inferred by the radiative lifetimes of the states. However, the possibility of competing deexcitation by cascade transitions ending in the ground

FIGURE 25

The states of Sc^{41} obtained by the $Ca^{40}(p,p)Ca^{40}$ reaction and by the $Ca^{40}(p,\gamma)Sc^{41}$ reaction are compared up to an excitation energy of 6 MeV. The levels of Ca^{41} are compared with those of Sc^{41} below 5.0 MeV. Definite and tentative associations of the levels between the mirror nuclei are shown by the solid and dotted lines, respectively. The level indicated by the dot-dash line at 2.05 MeV in Sc^{41} was observed only in the $Ca^{40}(He^3,d)Sc^{41}$ reaction[20].

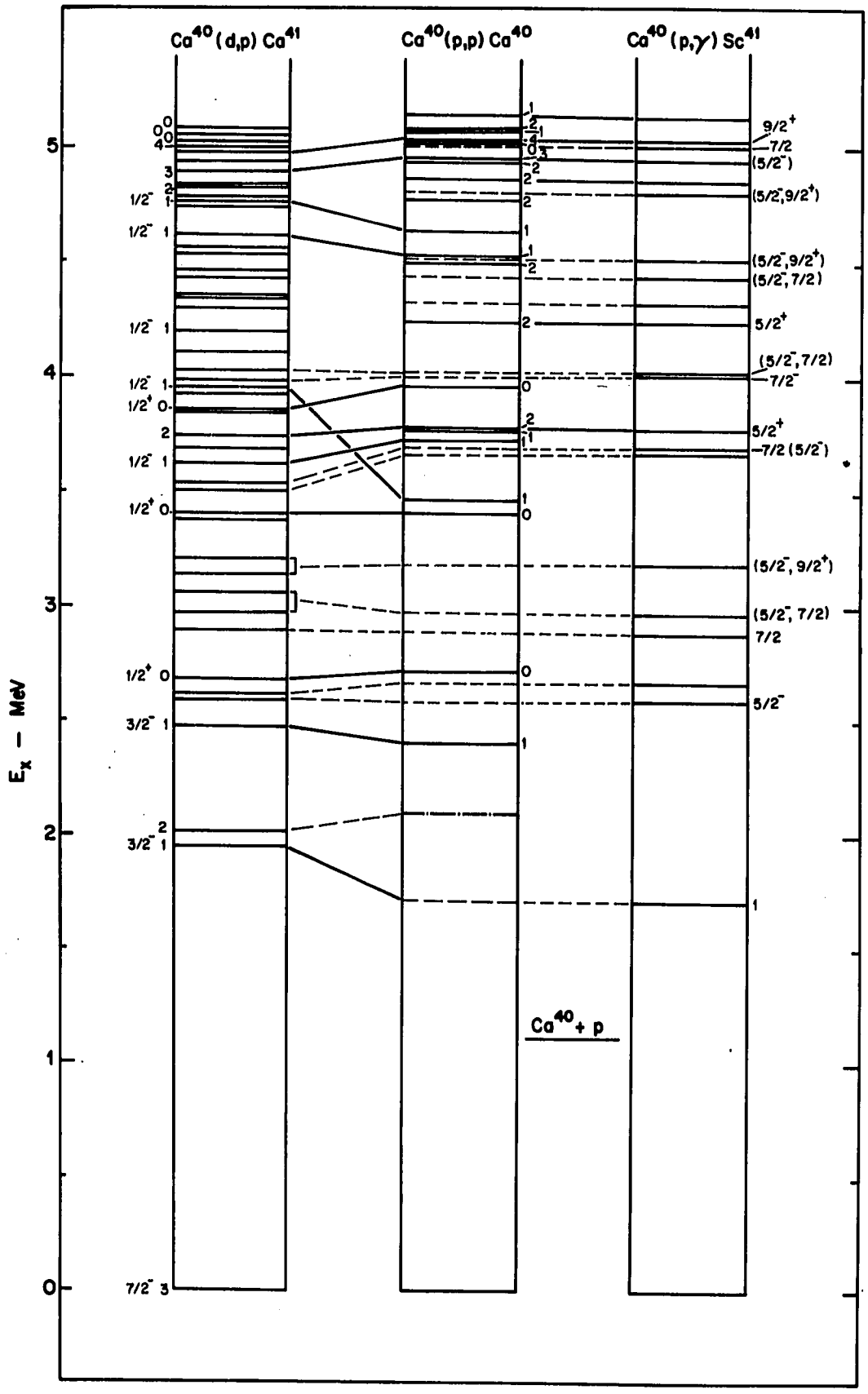
Ca40 (d,p) Ca41
Ca40(p,p) Ca40
Ca40 (p,γ) Sc41
Ex – MeV
Ca40 + p
9/2+
7/2
(5/2-)
(5/2-,9/2+)
(5/2-,9/2+)
(5/2-,7/2)
5/2+
(5/2-,7/2)
7/2-
5/2+
7/2 (5/2-)
(5/2-, 9/2+)
(5/2-, 7/2)
7/2
5/2-
1/2- 1
1/2- 1
1/2- 1
1/2- 1
1/2+ 0
1/2- 1
1/2+ 0
1/2+ 0
3/2- 1
3/2- 1
7/2- 3

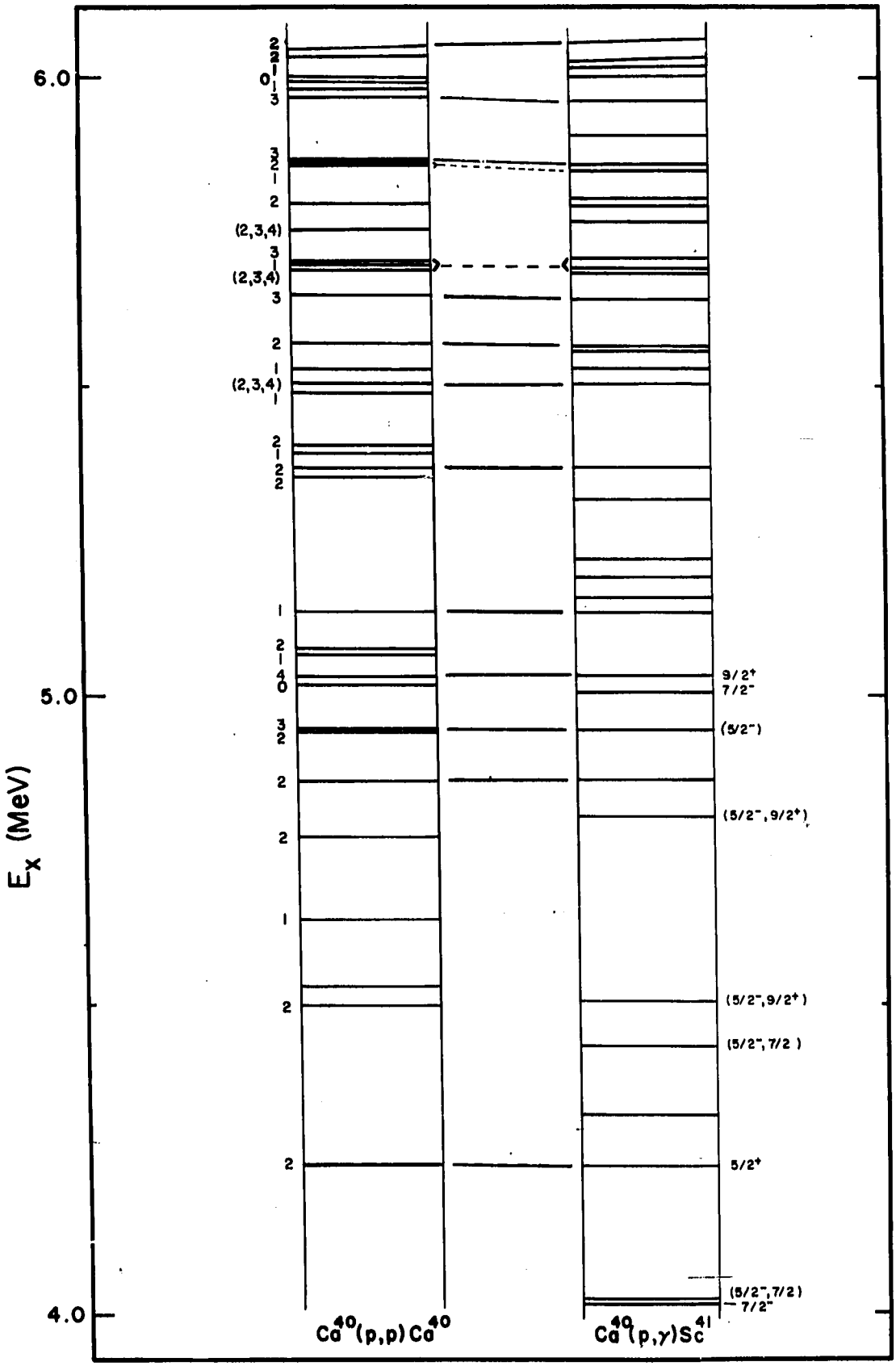
6.0
5.0
4.0
E_x (MeV)
(2,3,4)
(2,3,4)
(2,3,4)
9/2⁺
7/2⁻
(5/2⁻)
(5/2⁻, 9/2⁺)
(5/2⁻, 9/2⁺)
(5/2⁻, 7/2)
5/2⁺
(5/2⁻, 7/2)
7/2⁻
$Ca^{40}(p,p)Ca^{40}$
$Ca^{40}(p,\gamma)Sc^{41}$

TABLE 9

Comparison to $Ca^{40}(p,p)Ca^{40}$

$Ca^{40}(p,\gamma)Sc^{41}$			$Ca^{40}(p,p)Ca^{40}$			
E_p (MeV)	$g\Gamma_{\gamma g.s.}$	Γ_{lab} (keV)	E_p (MeV)		Γ_{lab} (keV)	J^π
2.764	0.08		2.765	2	0.2	$5/2^+$
3.240	0.15		3.242	2	0.1	$5/2^+$
			3.505	2	0.6	$(3/2^+)$
			3.785	2	1.4	$(3/2^+)$
3.881	0.02		3.877	2	2.0	
			3.959	2	3.0	$(3/2^+)$
3.965	0.28	2.4	3.962	3	1.0	$5/2^-$
4.054	1.65		4.049	4	0.4	$9/2^+$
			4.097	2	0.6	$(3/2^+)$
4.160	0.01		4.159	1	2.0	
			4.379	2	0.6	$(3/2^+)$
4.402	0.22	9.5	4.397	2	7.0	$(5/2^+)$
4.551	0.39		4.546	(2,3,4)	0.6	
4.602	0.08		4.602	2	2.0	$(5/2^+)$
4.683	0.24		4.681	3	1.0	
4.724	0.04		4.724	(2,3,4)	0.1	
			4.732	1	6.0	
4.741	0.94	11.5	4.738	3	7.0	
4.748	0.14					
4.835	0.09		4.833	(2,3,4)	0.1	
			4.872	2	0.6	$(3/2^+)$
4.894	0.07		4.895	1	2.0	
			4.899	2	2.6	$(3/2^+)$
4.907	0.92	9.4	4.905	3	5.0	
5.011	0.28		5.008	3	2.0	
			5.171	2	0.2	$(3/2^+)$
5.191	0.57		5.187	2	0.5	$(5/2^+)$

state, particularly for the weaker resonances, increases the uncertainty of $\Gamma_{\gamma\,g.s.}$ and hence weakens the reliability of such a procedure used as a tool to obtain J^{π} values. These resonances are presented below in increasing order of excitation.

E_p = 3.881 MeV, E_{exc} = 4.868 MeV: This weak resonance is identified with the 3.877 MeV ℓ = 2 observed in the (p,p). $\Gamma_{\gamma_{g.s.}}$ for this state is consistent with an E1 assignment, hence favoring J^{π} = $5/2^+$, but the possibility of important cascade contributions to the weak yield observed makes an assignment hazardous. The low yield prevented an accurate measurement of the total width of the state to confirm its identification with the (p,p) resonance.

E_p = 4.160 MeV, E_{exc} = 5.140 MeV: This weak transition probably corresponds to the 4.159 MeV, ℓ = 1 state observed in the (p,p), but the low yield prevented a measurement of the total width to confirm this association. $\Gamma_{\gamma\ g.s.}$ for this state is consistent only with a $3/2^-$ assignment. The possibility that a majority of the yield observed is due to cascade contributions casts doubt on the value of $\Gamma_{\gamma g.s.}$ obtained and makes an assignment on this basis very hazardous.

E_p = 4.402 MeV, E_{exc} = 5.376 MeV: This state is matched with the ℓ = 2 state at 4.397 MeV in the (p,p) results both by energy and total width. $\Gamma_{\gamma_{g.s.}}$ is consistent only with an E1 transition and thus the state is most likely J^{π} = $5/2^+$.

E_p = 4.551 MeV, E_{exc} = 5.521 MeV: This is identified with the (p,p) resonance at 4.546 MeV for which no definite ℓ value is given precluding a spin assignment. The value of $g\Gamma_{\gamma_{g.s.}}$ is consistent with either an E1 or M1 transition.

E_p = 4.602 MeV, E_{exc} = 5.571 MeV: The resonance at 4.602 MeV (ℓ = 2) in the (p,p) is identified with this resonance. The value of $\Gamma_{\gamma_{g.s.}}$ is consistent only with the E1 transition and thus a spin of $5/2^+$ is favored.

E_p = 4.683 MeV, E_{exc} = 5.650 MeV: This resonance corresponds to the ℓ = 3, 4.681 MeV resonance observed in the (p,p) but no discrimination of spin is possible based on $\Gamma_{\gamma_{g.s.}}$ although $5/2^-$ is favored by shell model considerations.

E_p = 4.724 MeV, E_{exc} = 5.690 MeV:
E_p = 4.741 MeV, E_{exc} = 5.706 MeV:
E_p = 4.748 MeV, E_{exc} = 5.713 MeV:
Two of the trio of states observed at 4.724, 4.741 and 4.748 MeV are identified with two of the three observed at 4.724, 4.732 and 4.738 MeV in the (p,p). The states located at 4.724-MeV in both experiments probably correspond, both being narrow. $g\Gamma_{\gamma_{g.s.}}$ for this state is consistent with either an E1 or M1 transition but the lack of a definite parity assignment prevents any spin determination. The wide 4.741 MeV resonance probably corresponds to the wide 4.738 MeV ℓ = 3 resonance observed in the (p,p). $g\Gamma_{\gamma_{g.s.}}$ for this state is consistent with either possible spin.

E_p = 4.835 MeV, E_{exc} = 5.798 MeV: This resonance probably corresponds to the 4.833 (p,p) resonance for which the ℓ value is indefinite. The value of $g\Gamma_{\gamma g.s.}$ is consistent with either an E1 or M1 transition.

E_p = 4.894 MeV, E_{exc} = 5.856 MeV: This resonance probably corresponds to the ℓ = 1, 4.895 MeV (p,p) resonance, although it may correspond to the ℓ = 2, 4.899 MeV (p,p) resonance. This latter comparison is discounted because the (p,γ) energies obtained tend to be slightly higher than those obtained for the corresponding (p,p) resonances. The value of $\Gamma_{\gamma\ g.s.}$ obtained is consistent with $J^{\pi} = 3/2^-$, however the possibility of significant cascade contributions to the yield makes this assignment hazardous.

E_p = 4.907 MeV, E_{exc} = 5.868 MeV: This resonance corresponds to the wide ℓ = 3, 4.905 MeV resonance in the (p,p). The value of $g\Gamma_{\gamma g.s.}$ obtained is consistent with either spin choice.

E_p = 5.011 MeV, E_{exc} = 5.970 MeV: This resonance is matched with the ℓ = 3, 5.008 MeV resonance in the (p,p) both by energy and width. The value of $g\Gamma_{\gamma g.s.}$ is consistent with either spin choice.

E_p = 5.191 MeV, E_{exc} = 6.145 MeV: This strong resonance corresponds to the narrow ℓ = 2 resonance at 5.187 MeV in the (p,p). The value of $\Gamma_{\gamma g.s.}$ is consistent only with $J = 5/2^+$.

In the third category are 7 $\ell = 2$ resonances of small proton width observed in the elastic scattering which are not observed in the radiative capture experiment. For these states this absence may infer higher multipolarities for the transitions, and thus indicate a spin of $3/2^+$ rather than $5/2^+$. These states are discussed below.

The narrow $\ell = 2$ level observed at $E_p = 3.505$ MeV by Brown was not observed in the (p,γ), although states of similar width and parity were observed just below it. Thus this state is most likely a $3/2^+$ state. A (p,γ) resonance at 3.515 MeV ($J^\pi = 5/2^-, 9/2^+$) is not believed to correspond to this state. The energy discrepancy (10 keV) is much greater than that observed for other, definite comparisons. There are two resonances located at 3.959 MeV ($\ell = 2$) and 3.962 MeV ($\ell = 3$) respectively for which one correspondence is seen in the (p,γ). As discussed earlier, a $5/2^-$ assignment is provisionally given to the (p,γ) resonance and thus the $\ell = 2$, 3.959 MeV state was not observed and is probably $3/2^+$. Narrow $\ell = 2$ resonances observed in the (p,p) at 4.097, 4.379, 4.872 and 5.171 MeV are also most likely $3/2^+$ states. Wider $\ell = 2$ states at 3.785 and 4.899 MeV are also unobserved and probably $3/2^+$.

2. Comparison of Ca^{41} and Sc^{41}

In Table 10 and Figure 25 a comparison is given of the levels up to excitations of 5 MeV seen in Sc^{41} in the present work and that of Brown[2] with those in Ca^{41} seen by Belote[1]. The ground states of both nuclei are known to be $\ell = 1$, $J^{\pi} = 7/2^-$. The level at 1.714 MeV has been seen by Macefield, et al.[21], in $Ca^{40}(d,n)Sc^{41}$, by Wegner[19] and by Sheppard, et al.[20], in $Ca^{40}(He^3,d)Sc^{41}$, and was assigned $\ell = 1$ by Wegner and Sheppard. A spectroscopic factor of 1.2, obtained by Sheppard, is evidence of its single particle character. This is identified with the $J^{\pi} = 3/2^-$ level at 1.949 MeV in Ca^{41} and is thought to be the major component of the $2p_{3/2}$ single-particle strength.

A level at 2.094 MeV has been observed by Sheppard and probably corresponds to the $\ell = 2$, 2.017 MeV level in Ca^{41}. The 2.409 MeV level was seen by Johnson[34] and by Rich[35] who assigned $\ell = 1$, as well as by Macefield and Sheppard. This is believed to correspond to the $\ell = 1$, $J^{\pi} = 3/2^-$ state at 2.471 MeV in Ca^{41}. The next two states at 2.584 and 2.663 MeV are seen only weakly in the present experiment and probably correspond to the 2.587 and 2.615 MeV states in Ca^{41}. The 2.713 MeV $\ell = 0$ state observed in elastic scattering corresponds to the 2.680 MeV $\ell = 0$ state in Ca^{41}. The $J = 7/2$, 2.879 MeV level probably corresponds to the 2.893 MeV level in Ca^{41} for which the ℓ value is unknown. The next 2 states in Sc^{41} have 5 possible analogs in Ca^{41} and no meaningful choice can be made. The $\ell = 0$, 3.411 MeV state observed by Brown corresponds to the 3.408 MeV, $\ell = 0$, state in Ca^{41}. The $\ell = 1$, 3.467 MeV state observed by Brown, apparently

TABLE 10

Comparison of Levels in Ca^{41} and Sc^{41}

Ca^{41} E_{exc} (MeV)	ℓ	J^{π}	Sc^{41} E_{exc} (MeV)
1.949	1	$3/2^-$	1.714
2.017	2		2.094
2.471	1	$3/2^-$	2.409
2.587	3	$5/2^-$	2.584
2.615			2.663
2.680	0	$1/2^+$	2.713
2.893		7/2	2.879
3.408	0	$1/2^+$	3.411
3.954	1	$1/2^-$	3.467
3.623	1	$1/2^-$	3.729
3.740	2	$5/2^+$	3.778
3.859	0	$1/2^+$	3.966
4.618	1	$1/2^+$	4.618
4.765	1	$1/2^-$	4.639
4.894	3	$5/2^-$	4.947
4.983	4	$9/2^+$	5.036

Only reasonably definite analog states are listed in this Table.

representing the principal part of the $2p_{1/2}$ single particle strength, must surely compare with $\ell = 1$, $J^{\pi} = 1/2^-$, 3.954 MeV state in Ca^{41} which possesses a large portion of the single particle strength. The pair of states at 3.673 and 3.692 MeV may compare with a pair of similar spacing at 3.504 and 3.536 MeV in Ca^{41}. The $\ell = 1$, 3.729 MeV state observed by Brown corresponds to the $\ell = 1$, $J^{\pi} = 1/2^-$, 3.623 MeV state in Ca^{41}, being roughly of the same single particle strength. The weak $\ell = 1$, 3.769 MeV level observed by Brown might correspond to the weak 3.686 MeV level in Ca^{41} for which no ℓ value is known. The $\ell = 2$, $J^{\pi} = 5/2^+$, at 3.778 MeV observed both in this experiment and by Brown corresponds to the 3.740 MeV, $\ell = 2$, state in Ca^{41}. The $\ell = 0$, 3.966 MeV state observed by Brown corresponds to the 3.859 MeV, $\ell = 0$, state in Ca^{41}.

Above this energy only 4 definite comparisons may be made. The $\ell = 1$, 4.532 MeV state observed by Brown has about the same single particle strength as that of the $J^{\pi} = 1/2^-$, 4.618 MeV level in Ca^{41}. A similar comparison between the $\ell = 1$, 4.639 MeV level in Sc^{41} and the 4.765 MeV, $J^{\pi} = 1/2^-$, level in Ca^{41} is valid. The $\ell = 3$, 4.947 MeV level observed by Brown corresponds to the $\ell = 3$, 4.894 MeV level in Ca^{41}. The $\ell = 4$, $J^{\pi} = 9/2^+$ level at 5.036 MeV corresponds to the $\ell = 4$, 4.983 MeV level in Ca^{41}.

The region above 5 MeV is not shown, but available data indicates extreme complexity for both nuclei, with few fruitful comparisons possible.

Several problems in matching levels are quite obvious in the region from 4 to 5 MeV. There is no apparent analog for the weak $\ell = 1$, $J^{\pi} = 1/2^-$, 4.198 MeV level in Ca^{41} observed in Sc^{41}. There are 6 $\ell = 2$ levels observed in Sc^{41} in this region, but only one in Ca^{41}, so that a definite match cannot be made. There are 3 $\ell = 0$ states observed in this region in Ca^{41}, but only one in Sc^{41}, again raising the question of correspondence.

It is apparent that the principle shell model states of $2p_{3/2}$ and $2p_{1/2}$ are displaced downward by 235 keV and 487 keV respectively while the weaker states are displaced usually less than 150 keV and shifted in either direction.

SUMMARY

Forty-six levels in Sc^{41} were located via the $Ca^{40}(p,\gamma)Sc^{41}$ reaction. Of these 21 had been previously identified by other experiments. Total widths were obtained for 6 of the levels, $g\Gamma_{\gamma g.s.}$ was obtained for all 46, assuming decay principally to the ground state. J values were assigned to 8 of the levels, while J values for 7 more were limited to two possibilities. In addition tentative J^{π} values were assigned to 11 resonances in $Ca^{40}(p,p)Ca^{40}$ by their absence or presence in the radiative capture channel.

The cross-section for non-resonant capture was measured and found to agree in magnitude with that calculated by Thomas and Tanner[25] for capture directly to the ground state of Sc^{41}. However, the energy dependence observed is greater than predicted.

The half life of Sc^{41} was determined to be $0.596 \pm .006$ seconds.

The Q value for the $Ca^{40}(p,\gamma)Sc^{41}$ reaction was determined to be 1.083 ± 0.006 MeV, corresponding to a Sc^{41} mass excess of $-28,640 \pm 10$ keV on the C^{12} mass scale.

A value of $5.1 \pm 1.5 \times 10^{-13}$ seconds was obtained for the lifetime of the first excited state of Sc^{41}, an enhancement of a factor of 12 over the single particle value.

ACKNOWLEDGMENT

I would like to thank Dr. C.M. Class for his guidance in this project. I would also like to express my gratitude to Mr. J.P. Aldridge, Dr. B.H. Wildenthal, and Mr. W.F. Rich for their assistance in obtaining the data.

I would like to thank the Rice University Physics Shop, and particularly Mr. J.F. Van der Henst, for constructing the apparatus necessary for the successful completion of this project.

I especially would like to acknowledge the aid and assistance given this project by my wife, Kay.

BIBLIOGRAPHY

1. T.A. Belote, A. Sperduto, and W.W. Buechner, Phys. Rev. (submitted for publication).
2. N.A. Brown and C.M. Class (to be published); N.A. Brown, Ph.D. Thesis, Rice University (1963).
3. W.M. Martin and S.W. Breckon, Can. J. Phys. 30, 642 (1952).
4. J.W. Butler, Phys. Rev. 123, 139 (1961).
5. J.G. Cramer, Jr., B.J. Farmer, and C.M. Class, Nuc. Inst. and Methods 16, 289 (1962); J.G. Cramer, Jr., Ph.D. Thesis, Rice University (1961).
6. U. Farinelli and R. Malvano, Rev. Sci. Instr. 29, 699 (1958).
7. J.P. Aldridge, III, M.A. Thesis, Rice University (1962).
8. See, e.g. Nuclear Data Tables, Part 3, edited by J.B. Marion, p. 176 (1960).
9. J.B. Marion, Rev. Mod Phys. 33, 139, 623 (1961).
10. J.B. Marion and T.W. Bonner, Fast Neutron Physics, Part II, edited by J.B. Marion and J.L. Fowler (Interscience Publishers, 1963), p. 1865.
11. Tables for the Analysis of Beta Spectra, National Bureau of Standards Applied Mathematics Series 13 (1952) (U.S. Government Printing Office, Washington, D.C.).
12. F. Ajzenberg-Selove and T. Lauritsen, Nuc. Phys. 11, 1 (1959).
13. Fowler, Lauritsen and Lauritsen, Revs. Mod. Phys. 20, 236 (1948).
14. H.W. Lewis, Phys. Rev. 125, 937 (1962).
15. W.L. Walters, D.G. Costello, J.G. Skofronick, D.W. Palmer, W.E. Kane, and R.G. Herb, Phys. Rev. Letters 7, 284 (1961).
16. L.A. Konig, J.H.E. Mattauch, and A.H. Wapstra, Nuc. Phys. 31, 18 (1962).

17. N.H. Gale, J.B. Gargond, and J.M. Calvert, Nuc. Phys. 38, 222 (1962).

18. C.M. Class, private communication.

19. H.E. Wegner and W.S. Hall, Phys. Rev. 119, 1654 (1960).

20. D.M. Sheppard, H.A. Enge, and H.Y. Chan, Bull. Am. Phys. Soc. 10, 25 (1965); H.A. Enge, private communication.

21. B.E.F. Macefield, J.H. Towle, and W.B. Gelbay, Proc. Phys. Soc. (London) 77, 1050 (1961).

22. V.P. Adyosevich, L.V. Groshev, A.M. Demidov, and B.N. Lutsenko, Journal of Atomic Energy 3, 325 (1956).

23. A. Faessler, Nuc. Phys. 65, 329 (1965).

24. R.F. Christy and Ian Duck, Nuc. Phys. 24, 89 (1961).

25. G.C. Thomas and N.W. Tanner, Nuc. Phys. 44, 647 (1963).

26. S. Raboy and C.C. Traul, Nuc. Inst. and Methods 9, 145 (1960).

27. N.A. Brown, private communication.

28. M.E. Rose, Phys. Rev. 91, 610 (1953).

29. W.T. Sharp, J.M. Kennedy, B.J. Sears, and M.G. Hoyle, AECL No. 97, CRT-556 (1954).

30. V.F. Weisskopf, Phys. Rev. 83, 1073 (1951).

31. D.H. Wilkinson, in Nuclear Spectroscopy, Fay Ajzenberg-Selove ed., Academic Press, New York (1960).

32. E.C. Booth, B. Chasan, and K.A. Wright, Nuc. Phys. 57, 403 (1964).

33. J. Lind Skog, T. Sundstrom and P. Sparrman, in $\alpha\beta\gamma$ Ray Spectroscopy, K. Siegbahn, ed., North Holland Publishing Co., Amsterdam (1965).

34. J. Johnson, Ph.D. Thesis, Rice University (1957).

35. W.F. Rich, M.A. Thesis, Rice University (1965).